

STATIONARY STATES OF DISSIPATIVE MANY-BODY
QUANTUM SYSTEMS VIA MATRIX PRODUCT OPERATORS

by

Oliver Thomson Brown

Submitted in conformity with the requirements
for the degree of Doctor of Philosophy in Physics



School of Engineering & Physical Sciences

Submitted April, 2018

The copyright in this thesis is owned by the author. Any quotation from this thesis or use of any of the information contained in it must acknowledge this thesis as the source of the quotation or information.

Abstract

In this thesis we consider stationary states of dissipative many-body quantum systems. We do so using matrix product operator representations of the system. One can find the stationary state by simulating the time evolution of the system [1, 2], or by using a more recently proposed variational search technique [3, 4]. An implementation of the variational search technique was written for MATLAB [5, 6]. Documentation is included in appendix A.

Using these techniques we first considered a geometrically frustrated lattice system, in which particles cannot move coherently [7]. We found that local Markovian dissipation can induce mobility and long range first order coherence in the system. This was true in both the non-interacting and interacting regime, though strong interactions suppress the effect.

We then investigated an array of nonlinear cavities, with a coherent parametric drive to the doubly excited state [8]. The dissipation rate on each site increases with the excitation number. We found that when the hopping rate between sites is low the system forms an incompressible state with commensurate filling, analogous to the Mott insulator. When the hopping rate increases there is a crossover to a delocalized state. In contrast to the equilibrium case, long range correlations do not build up.

We conclude the thesis by considering some initial results from a new investigation, and by commenting on possible future directions for the variational stationary state search code.

Acknowledgements

First of all, I must thank my supervisor Michael Hartmann. He has been incredibly supportive, and allowed me to develop my interests in scientific software development. At times his patience has seemingly tended to infinity, particularly while reviewing this thesis! I would also like to thank my undergraduate supervisor, Sabrina Maniscalco, without whom I would never have begun my PhD. Her enthusiasm inspired me to stick with physics a little longer.

Thank you to the staff of the Condensed Matter CDT, who work extremely hard to give myself and others like me this opportunity. I am especially grateful for the generous travel funding! As anyone who has met me since I spent six weeks in California knows, I once got to spend six weeks doing research in California. I often think fondly of my time there, as I look at the wind and rain outside my window in Edinburgh. Special thanks to the present and former administrative staff of both the CDT and Heriot-Watt: Julie, Christine, Wendy, Loraine, and Sheila. It is clear that without them, nothing would ever get done.

Thank you to all my long-suffering friends, colleagues, and flatmates, present and former. All of them have helped me to enjoy Edinburgh so much that I intend to stick around for some time. Especially the lunch crew, Ash, Adam, Stuart, and James, and Darren, who introduced me to climbing. Special thank you to my friend from ‘back home’ James Puddephatt, as he agreed to proof-read my thesis in exchange for a bag of haribo. Any mistakes that still remain are certainly my fault, but I will blame him anyway.

Thank you to my grandparents, John “Jock” Thomson Brown, Marguerite “Peggy” Brown (Scotland Nan), and Brenda Sneade (Telford Nan). Without their generous support, I would never have completed even my undergraduate degree. It seems unlikely I can return the favour, so I must pass it on instead.

Thank you to my father, Robert Andrew Brown, who first spurred my interest in computers. He is the only person I’ve ever met who could ramble about nothing for as long as I can. If he could, I’m sure he would read this thesis cover to cover. Finally, to my mother Rosemary Helen Brown, who is strong in ways I cannot imagine: thank you for *everything*.

ACADEMIC REGISTRY

Research Thesis Submission

Name:	Oliver Thomson Brown		
School:	Engineering & Physical Sciences		
Version: (i.e. First, Resubmission, Final)		Degree Sought:	PhD

Declaration

In accordance with the appropriate regulations I hereby submit my thesis and I declare that:

- 1) the thesis embodies the results of my own work and has been composed by myself
- 2) where appropriate, I have made acknowledgement of the work of others and have made reference to work carried out in collaboration with other persons
- 3) the thesis is the correct version of the thesis for submission and is the same version as any electronic versions submitted*.
- 4) my thesis for the award referred to, deposited in the Heriot-Watt University Library, should be made available for loan or photocopying and be available via the Institutional Repository, subject to such conditions as the Librarian may require
- 5) I understand that as a student of the University I am required to abide by the Regulations of the University and to conform to its discipline.
- 6) I confirm that the thesis has been verified against plagiarism via an approved plagiarism detection application e.g. Turnitin.

* Please note that it is the responsibility of the candidate to ensure that the correct version of the thesis is submitted.

Signature of Candidate:		Date:	
-------------------------	--	-------	--

Submission

Submitted By (name in capitals):	
Signature of Individual Submitting:	
Date Submitted:	

For Completion in the Student Service Centre (SSC)

Received in the SSC by (name in capitals):		
Method of Submission (Handed in to SSC; posted through internal/external mail):		
E-thesis Submitted (mandatory for final theses)		
Signature:		Date:

Contents

1	Introduction	1
2	MBQT & OQS	4
2.1	Many-body quantum physics	4
2.1.1	How many?	4
2.1.2	Driven-dissipative Bose-Hubbard model	7
2.2	Open quantum systems	14
2.2.1	Density matrix	15
2.2.2	Lindblad master equation	16
2.2.3	The Liouvillian	18
3	Numerical methods	20
3.1	Matrix product states	20
3.2	Matrix product representation of operators	22
3.3	Variational search	26
3.4	Time evolution	35
4	Frustrated lattices	37
4.1	Introduction	37
4.1.1	The model	38
4.1.2	Wannier basis	40
4.2	Non-interacting regime	43
4.2.1	Dissipation-induced mobility	44
4.2.2	Long range first order coherences	45

CONTENTS

4.2.3	Modeling the decay length of the dissipation-induced mobility	47
4.3	Strongly interacting regime	51
4.3.1	MPO design	53
4.3.2	Density and coherence	54
4.4	Conclusions	57
5	Driven nonlinear cavity array	59
5.1	Introduction	60
5.2	The model	62
5.3	Small anharmonic system	64
5.4	Large anharmonic system	67
5.5	Large harmonic system	69
5.6	Conclusions	73
6	Further work	74
6.1	Biased chain	74
6.1.1	The model	75
6.1.2	Initial results	77
6.1.3	Next steps	78
7	Conclusion	80
A	Stationary state search implementation	83
A.1	Standard format	84
A.1.1	Density matrix product operator	84
A.1.2	Matrix product operator	85
A.2	DDMPO	85
A.3	PhasedSearch	87
A.4	ProdDMPO	89
A.5	Stationary	91
A.6	ZDMPO	93
A.7	Can	94
A.8	DMPOHerm	95

CONTENTS

A.9	DMPOResize	96
A.10	EffL	97
A.11	EigenSolver	98
A.12	GrowBlock	101
A.13	TrNorm	102
A.14	ConvTest	102
A.15	DMPOCompress	104
A.16	DMPOConj	105
A.17	DMPOEnlarge	105
A.18	DMPOExp	106
A.19	DMPOScalarDiv	107
A.20	DMPOSum	108
A.21	DMPOTrace	109
A.22	EffLSparse	110
A.23	FWBase	111
A.24	GrowLeft	112
A.25	GrowRight	113
A.26	LCan	115
A.27	MPOHermProd	116
A.28	RCan	117
A.29	SVDNorm	118
B	Wannier basis MPO	119
C	Rotating frame transformation	123
C.1	Single cavity	123
C.2	Coupled cavities	127
D	Two-level effective master equation	131
D.1	Definitions	132
D.2	First order	133
D.3	Second order	136
D.4	Effective master equation	140

Chapter 1

Introduction

This thesis is structured in the following way. We will begin in chapter 2 by discussing many-body quantum physics, in particular the scaling problem, which makes it such a challenging field. We will then introduce the driven-dissipative Bose-Hubbard model, which we are particularly interested in investigating. We will give two examples of physical systems in which such a model can be implemented, paying special attention to the introduction of nonlinearity and dissipation to the system. We will then introduce the basics of open quantum systems, remarking on the Lindblad-form master equation. We limit ourselves to solving for the steady state of a system under the action of Lindblad dynamics, though the relaxation of the approximations inherent to the Lindblad master equation is itself an open and very interesting field of research. Finally in this chapter, we will briefly consider the practicalities of numerically solving for the steady state. We do so as a primer for the following chapter.

In chapter 3 we will begin by introducing matrix product states – one answer to the scaling problem. MPS are a way of representing quantum states which allow for the compression of states with low levels of entanglement. They were first introduced in the form in which we use them by Guifré Vidal [9, 1], though they are essentially an evolution of the DMRG method due to Steven White [10, 11], and the analytical matrix product states previously used to study finitely correlated states [12]. We then introduce the matrix product operator, a way of representing a Hamiltonian or, more importantly as far as we are concerned, a Liouvillian, in a similar format to the matrix product state.

CHAPTER 1. INTRODUCTION

The MPO is critical to the variational search technique, and our work owes most to the recent efforts of Cui [3] and Mascarenhas [4], who extended the variational search approach from finding the ground state of a closed system, to finding the stationary state of an open one. One of, if not *the*, key outputs of my PhD is a variational stationary state search code [5] which was written for MATLAB [6]. The documentation for that code is included in this thesis as appendix A. We also, more briefly, mention time evolution methods using matrix product states. Although powerful, the variational search technique does not work for every system. Time evolution therefore still plays an important role in research presented later in the thesis.

Next in chapter 4 we consider the first published research of this thesis, “Dissipation-induced mobility and coherence in frustrated lattices” [7]. Here we considered a model of a geometrically frustrated lattice system, which was coupled to a dissipative environment in such a way that dissipative transport was possible. The first half of the paper considers the non-interacting regime, which could be solved using the Ehrenfest equations, while the second half considers a strongly interacting regime. This was the first attempt we made to use the variational search code on a ‘real’ problem, and it was successful. We determined that dissipation enabled transport through the lattice in both the non-interacting, and interacting case, although strong interaction suppressed mobility. Designing an MPO which includes so many non-local terms is a little tricky, so the full MPO is included in appendix B along with some explanatory notes, in the hope it may prove useful to others pursuing similar investigations.

Then in chapter 5 we expand on the article “Localization to delocalization crossover in a driven nonlinear cavity array” [8]. This was the principle scientific investigation of my PhD, however, this system was not amenable to solution using the variational search technique as we had hoped it might be. Instead we made use of TEBD, a matrix product state time evolution method. This was effective, though computationally costly. We were able to determine that a parametrically driven nonlinear cavity array, with dissipation that was larger for higher numbers of excitations on a site, exhibits a localized steady state analogous to the Mott insulator when the hopping rate between sites is low. At high hopping rates, we did not observe a superfluid-like state as in

CHAPTER 1. INTRODUCTION

the equilibrium case, as long range coherences did not build up. Appendices C and D are technical appendices containing derivations related to this project, which were too lengthy for inclusion in the article.

In chapter 6 we look at a new project which I have done some preliminary work on, which again features non-local dissipation. It is a biased spin chain, where the splitting of the two levels decreases from one end to the other. It has already shown some interesting results regarding dissipative transport. Such a system has previously been studied as a model of a biological photocell [13], however that investigation was limited to the subspace of only one excitation. We consider a similar system in the many-body context.

Finally, in chapter 7 we indulge in some conjecture as to the future direction of both that project, and of the variational search code, in order to conclude the thesis by casting our eyes forward.

Chapter 2

Many-body quantum theory & open quantum systems

In this chapter we will consider some of the theoretical background of many-body and open quantum systems. These are rather broad fields, so we shall focus in particular on aspects that are relevant to the research presented later in this thesis. We will begin by considering what is meant by the word ‘many’ in many-body quantum systems, and why this presents such a challenge to physicists. We will introduce the driven-dissipative Bose-Hubbard model, and physically motivate its terms in two relevant settings, in order to make later chapters more transparent. Then we will discuss what is meant by ‘open’ quantum systems, and how the dynamics of such a system are calculated. Finally we shall discuss how to reformulate these dynamics as a system of coupled linear equations.

2.1 Many-body quantum physics

2.1.1 How many?

Quantum physics has a problem. More than one actually, but the reader may safely assume that the author considers musing on the interpretation of quantum mechanics to be far above his pay-grade, and that he belongs to the “Shut up and calculate!” school of thought [14]. What hardship then,

does quantum mechanics present to those of us interested only in crunching numbers and getting results?

To answer that, let us first step back and consider a classical system. Consider some system of N components, each of which can be in one of two possible states. In total there are 2^N possible configurations of the system, each of which can be *completely* described by an N -bit string. Furthermore, if we increase N to $N + m$, we only need to add m bits. Even if we change to a system where there are three possible states of each component, although the total state space increases in size to 3^N , since the system must exist in *one and only one* of those configurations, we can still efficiently represent the system with just N digits. Mathematical representations of many-body classical systems scale linearly with the size of the system (the number of ‘bodies’). This does not mean that classical many-body problems are *easy*, just that they get harder only in proportion to the size of the system.

Enter quantum mechanics. We may again consider a system of N components, each of which can be in one of two possible states, meaning there are 2^N possible configurations – so far, so good. However, there is a fundamental principle of quantum mechanics – the superposition principle – that says that if a system may be in one of two states, which we shall label $|0\rangle$ and $|1\rangle$, then it may also be in the state,

$$|\psi\rangle = \alpha|0\rangle + \beta|1\rangle, \quad (2.1)$$

where α and β are complex coefficients. This means that we must replace each of our bits with a complex vector,

$$|\psi\rangle = \begin{pmatrix} \alpha \\ \beta \end{pmatrix}, \quad (2.2)$$

where we have arbitrarily chosen a convention that the first element corresponds to $|0\rangle$, and the second to $|1\rangle$. Nevertheless, if all that is required to transition to the quantum regime is to replace N integers to $2N$ complex floats, this is not so bad. Unfortunately, the superposition principle applies equally to the composite system. Taking $N = 3$, if $|\Psi\rangle = |000\rangle$ and $|\Psi\rangle = |111\rangle$ are

valid configurations, so is

$$|\Psi\rangle = c_{000}|000\rangle + c_{111}|111\rangle, \quad (2.3)$$

where c_{000} and c_{111} are again complex coefficients. In fact, any arbitrary combination of the $2^3 = 8$ possible states of the system,

$$|\Psi\rangle = \sum_{i,j,k=0}^1 c_{ijk}|ijk\rangle, \quad (2.4)$$

is a valid state, so we must use a vector of 8 complex values to describe the state. More generally, if we have some system of N quantum components, each of which may be in any combination of d local states, we require a state vector of d^N complex elements. The representation of the system grows *exponentially* with its size. This scaling problem is the crux of many-body quantum physics [15, 16]. To compound the issue, it is also clear that the properties of a many-body system are unlikely to be well predicted by single- or even few-body systems – it has long been understood that in nature “more is different” [17].

Table 2.1 provides some examples of how different objects scale in a system with d local states, and N sites. The Hamiltonian is an operator which provides an energy description of a quantum system, and generates unitary (non-dissipative) dynamics, but in fact any operator which acts on the many-body quantum state vector will have the same size. The Liouvillian describes the non-unitary dynamics of a quantum system, and is typically written as a super-operator acting on the density matrix, ρ . In order to solve it numerically we re-write it as a system of linear equations acting on the vectorised density matrix, $|\rho\rangle\rangle$. Since we are primarily interested in stationary states of dissipative systems – given by solving $\hat{L}|\rho_{ss}\rangle\rangle = 0$ – it is this d^{4N} element matrix which concerns us the most. It is precisely this very poor exponential scaling that the matrix product state technique, described in detail in the next chapter, was designed to defeat.

Object	Symbol	Size
State Vector	$ \Psi\rangle$	$d^N \times 1$
Hamiltonian	\hat{H}	$d^N \times d^N$
Density Matrix	ρ	$d^N \times d^N$
Vectorised Density Matrix	$ \rho\rangle\rangle$	$d^{2N} \times 1$
Liouvillian Matrix	\hat{L}	$d^{2N} \times d^{2N}$

Table 2.1

2.1.2 Driven-dissipative Bose-Hubbard model

The theme that connects the research presented in this thesis is, of course, the use of matrix product state methods, however it is also true that each of the models is essentially a variant of a driven-dissipative Bose-Hubbard model. As such we will introduce that model here, and then explore two example systems where it *could* be physically implemented. We will pay particular attention to the introduction of an anharmonic energy spectrum, and a carefully engineered dissipative regime, which are of particular importance to the work presented in reference [8]. The work we present is intended to be independent of implementation, but it can nevertheless be instructive to consider physical systems. Note that the above emphasis on ‘could’ is intentional, we expect actual implementation to be highly challenging.

The Bose-Hubbard model is a bosonic variant of the electronic Hubbard model first described by John Hubbard in 1963 [18], and it was first considered by Fisher et al. [19]. In the generic case of a one-dimensional lattice of coupled anharmonic oscillators the Bose-Hubbard Hamiltonian is,

$$\mathcal{H}_{\text{B-H}} = \sum_j \left[\omega \hat{a}_j^\dagger \hat{a}_j + \frac{U}{2} \hat{a}_j^\dagger \hat{a}_j^\dagger \hat{a}_j \hat{a}_j - t \left(\hat{a}_j^\dagger \hat{a}_{j+1} + \hat{a}_j \hat{a}_{j+1}^\dagger \right) \right], \quad (2.5)$$

where ω is the harmonic oscillator energy, U is an interaction energy which introduces anharmonicity to the energy spectrum, t is a hopping rate between sites, the operator $\hat{a}_j(\hat{a}_j^\dagger)$ annihilates (creates) an excitation on the lattice site

j , and where we have set $\hbar = 1$ so that energy is described in units of frequency. We then add a generic coherent drive term,

$$\mathcal{H}_\Omega = \sum_j \left[\left(\Omega e^{-i\omega_D t} + \tilde{\Omega} e^{i\omega_D t} \right) \hat{a}_j^\dagger + \left(\Omega^* e^{i\omega_D t} + \tilde{\Omega}^* e^{-i\omega_D t} \right) \hat{a}_j \right], \quad (2.6)$$

where Ω and $\tilde{\Omega}$ are drive amplitudes, and ω_D is the drive frequency. To eliminate the explicit time-dependence of the drive Hamiltonian we would then transform the whole Hamiltonian in to a rotating frame, and make use of the rotating wave approximation which yields,

$$\mathcal{H} = \sum_j \left[\Delta \hat{a}_j^\dagger \hat{a}_j + \frac{U}{2} \hat{a}_j^\dagger \hat{a}_j^\dagger \hat{a}_j \hat{a}_j - t \left(\hat{a}_j^\dagger \hat{a}_{j+1} + \hat{a}_j \hat{a}_{j+1}^\dagger \right) + \Omega \hat{a}_j^\dagger + \Omega^* \hat{a}_j \right], \quad (2.7)$$

where $\Delta = \omega - \omega_D$ is the detuning of the drive frequency from the harmonic oscillator frequency. Note that in appendix C the rotating frame transformation is shown in detail for the specific parametric driving scheme used in reference [8], and the procedure here would be the same. Dissipation is introduced to the model through a standard Lindblad form dissipator, which is discussed in the following section 2.2.

Having expressed the model of interest in the most general way possible, we now discuss two possible physical systems.

Nonlinear optical cavity array

A photonic implementation of the Hamiltonian given in eq. (2.7) necessitates the trapping of light, a feat achieved with an optical cavity. The simplest such system is the Fabry-Pérot etalon, a planar cavity consisting of two mirrors with some medium of refractive index n between [20, 21]. Such a system is shown diagrammatically in fig. 2.1. In the limit where the mirrors are perfectly reflective on the sides facing in to the cavity, and there are no absorption or scattering losses in the cavity medium, the light will travel an infinite number of round trips through the cavity. It will be totally annihilated unless it is

precisely resonant with the cavity length. That is,

$$\lambda = \frac{2nL_{\text{cav}}}{m}, \quad (2.8)$$

where m is some integer. Under these conditions, the light will be trapped indefinitely in the cavity. This is the canonical ‘particle in a box’ problem, and of course can be treated as a quantum harmonic oscillator. The requirement that there is no absorption or scattering, and perfect reflectivity is physically unrealistic, so it is quite natural to consider such systems in the dissipative regime.

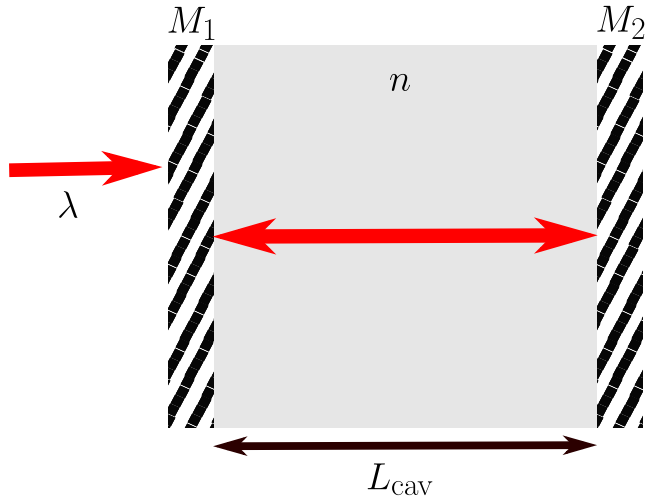


Figure 2.1: Diagram of a simple planar cavity. Light enters through the mirror M_1 and is then reflected between the two mirrors through some medium with a refractive index n . Here we have assumed that M_1 transmits perfectly into the cavity and then light is perfectly reflected by both M_1 and M_2 . Under this approximation the light is confined indefinitely and travels an infinite distance within the cavity. Only light whose wavelength is resonant with the cavity length, $\lambda = 2nL_{\text{cav}}/m$ where m is some integer, will survive under these conditions. Over an infinite number of round trips through the cavity even a small amount of destructive interference will result in total elimination of that wavelength of light. Obviously, real systems have losses in the form of absorption, transmission, and scattering, and will therefore neither perfectly isolate a single wavelength (and its harmonics), nor trap light indefinitely.

In fact whether the physical origin of the photon loss is absorption or scattering by a mirror or the cavity medium, or by transmission from the

cavity is essentially irrelevant to our dynamical equations. All three processes result in a photon leaving the system. In optics the ability of a cavity to retain light is usually referred to as its ‘quality factor’, defined as

$$\mathcal{Q} = \frac{4\pi L_{\text{cav}}}{\lambda} \frac{1}{-\ln(p)}, \quad (2.9)$$

where p is the fraction of initial power remaining in the cavity after one round trip [22]. This measure includes loss from all possible sources, and can be exceedingly high in optical microcavities (> 200 million [23]). This is important, as it allows us to reasonably neglect these losses *which we cannot control*. Dissipation which we *can* control is introduced through the Purcell effect.

First presented to the American Physical Society by Edward Purcell in 1946 [24], the Purcell effect is the phenomenon in which spontaneous emission is enhanced (or suppressed) by the presence of a resonant cavity [25]. The *Purcell factor* is the ratio of spontaneous emission rate in the presence of a cavity to the original rate, so a Purcell factor greater than one implies an enhancement to the spontaneous emission rate. The Purcell factor is proportional to the Q factor of the cavity, and inversely proportional to its modal volume, so smaller cavities with higher Q factors generate larger Purcell factors. In sum, this means that we can *in principle* envision systems in which we are able to tune the dissipation rate on specific transitions – a key feature of the system we investigate in reference [8]. Naturally fabrication of such a device, while possible [26], is undoubtedly challenging.

Having discussed how light can be trapped in an optical cavity, and how loss rates can be controlled, we are left with four parameters still to be accounted for – the drive strength Ω , detuning Δ , hopping rate J , and interaction strength U .

The physical origin of the drive strength is trivial to consider – it parameterises the field strength of whatever pump source is used to introduce photons into the system, and is proportional to the amplitude of the incident electromagnetic wave [27]. As noted above $\Delta = \omega - \omega_D$, and in this system ω is simply the frequency of the fundamental cavity mode, while ω_D is the frequency of the pump source. Hopping between cavities (or sites in our lattice) is again

easily understood. Confinement perpendicular to the cavity mode is limited and the wavefunction of the trapped light will extend somewhat beyond the cavity boundaries. Placing the cavities in close enough proximity to one another will result in an overlap between the wavefunctions and consequently tunnelling between sites [28, 29].

Finally, we must consider how to introduce and control nonlinearity in our cavity array system, and thus define the interaction strength, U . In principle a term of the form $\hat{a}^{\dagger 2}\hat{a}^2$ appears as a result of the optical Kerr effect in certain materials [30], however this effect is third order in the electric susceptibility and therefore requires a high intensity electromagnetic field to become a relevant phenomenon [31]. Another way to introduce nonlinearity is by considering cavities which contain atoms with a four-level structure. Such systems can produce large Kerr-like nonlinearities, as first shown by Schmidt and Imamoğlu [32]. In fact if we move to considering polaritons (which are photon-atom quasiparticles) then we can construct a full Bose-Hubbard Hamiltonian with even stronger nonlinearity, as detailed in reference [29].

Superconducting circuits

Having described how our model of interest may be realised in an optical cavity array, we next consider an alternative superconducting circuit implementation. The fundamental building block of this implementation is an LC circuit which is sufficiently small that both the charge in the capacitor and magnetic flux in the inductor become quantised. Resistance in the circuit would mask quantum effects, so it must be cooled to superconducting temperatures – on the order of tens of millikelvin. In this regime charge is quantised to units of $2e$ (where e is the elementary charge) as the electrons form Cooper pairs [33, 34]. However, a quantum LC circuit is still just a quantum harmonic oscillator. To introduce anharmonicity, a Josephson junction must be added. Named for Brian David Josephson, who first predicted in 1962 that Cooper pairs could tunnel just as single electrons can, a Josephson junction consists of two superconductors separated by a thin insulating barrier [35, 36]. They were first demonstrated by Anderson and Rowell in 1963 [37].

The Hamiltonian of the LCJ circuit shown in fig. 2.2 is,

$$\mathcal{H} = 4E_C(\hat{n} - n_g)^2 - E_J \cos(\varphi) + \frac{E_L}{2}(\varphi - \varphi_{\text{ext}})^2, \quad (2.10)$$

where \hat{n} is the number of Cooper pairs on the Josephson junction, n_g is an offset charge which can be controlled by an externally applied voltage, φ is the phase difference in the superconducting order parameter across the Josephson junction, and φ_{ext} is proportional to the external flux Φ_{ext} which threads the superconducting loops [33]. The charging energy E_C , Josephson energy E_J , and inductive energy E_L are given by,

$$E_C = \frac{e^2}{2C}, \quad (2.11)$$

$$E_J = \frac{\hbar}{2e} I_0, \quad (2.12)$$

$$E_L = \frac{\phi_0^2}{L}, \quad (2.13)$$

where e is the elementary charge, C is the total shunt capacitance, I_0 is the critical current of the Josephson junction, $\phi_0 = \hbar/2e$ is the reduced flux quantum, and L is the total shunt inductance [33, 38].

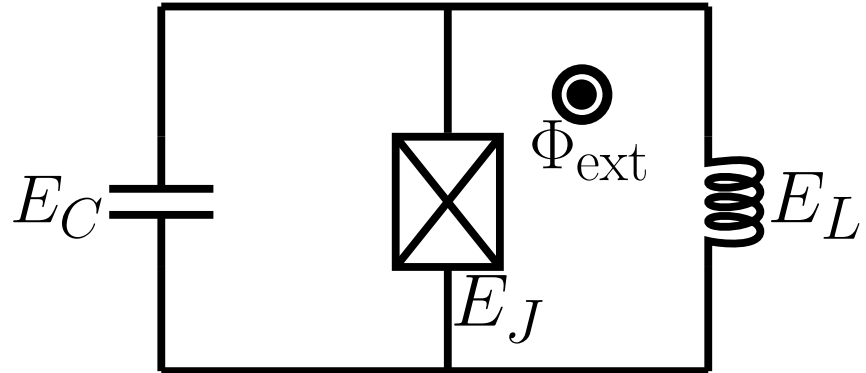


Figure 2.2: Equivalent circuit for all forms of superconducting circuit qubit. The circuit consists of a Josephson junction (depicted by a box with a cross through it), connected to some shunt capacitor C , and some shunt inductor L . An external flux, Φ_{ext} threads the superconducting loops. E_C , E_J , and E_L are given by eqs. (2.11) to (2.13).

The particular quanta of interest in fact depends on the energy parameters

in eq. (2.10), at one extreme when the charging energy is much larger than the Josephson energy, and there is no inductor ($E_J/E_C \ll 1$, $E_L = 0$) the system forms a ‘Cooper pair box’ or charge qubit, where the relevant degree of freedom is the number of Cooper pairs on one side of the Josephson junction. On the other hand, when the charging energy is small, and the Josephson energy and inductive energy are both large ($E_J/E_C \gg 1$, $E_L/(E_J - E_L) \gg 1$) the system forms a ‘flux qubit’, where the relevant degree of freedom is the number of flux quanta in the superconducting ring. We will consider one of the possibilities that lies in between these two, the *transmon*.

The transmon is a modification of the Cooper pair box, formed in the regime where there is no inductor, but unlike the CPB, the Josephson energy is much larger than the charging energy ($E_J/E_C \gg 1$, $E_L = 0$). The Hamiltonian is then given by,

$$\mathcal{H} = 4E_C(\hat{n} - n_g)^2 - E_J \cos(\varphi), \quad (2.14)$$

where we recall that the value of n_g can be controlled through the application of a bias voltage. In the limit where $E_J/E_C \gg 1$ this results in an anharmonic ladder of transmon states with the Hamiltonian,

$$\mathcal{H}_{\text{transmon}} = \sqrt{8E_C E_J} \hat{a}^\dagger \hat{a} - \frac{E_C}{12} (\hat{a} + \hat{a}^\dagger)^4, \quad (2.15)$$

where we have neglected constant terms [39]. The principle advantage of the transmon is its relative insensitivity to charge noise compared to the Cooper pair box.

Hopping between sites can be achieved by directly coupling transmon sites together with a capacitor [40], or indirectly via a transmission line cavity [41], or Josephson junction [42]. The drive term is trivial to consider, as in the optical system, the only difference being that the superconducting circuit is driven at microwave frequencies. Specific dissipative environments can again be engineered through exploitation of the Purcell effect [24, 25].

Having considered the type of model we are interested in, and shown how it could possibly be implemented in two different systems, we will next consider some of the key elements of open quantum systems.

2.2 Open quantum systems

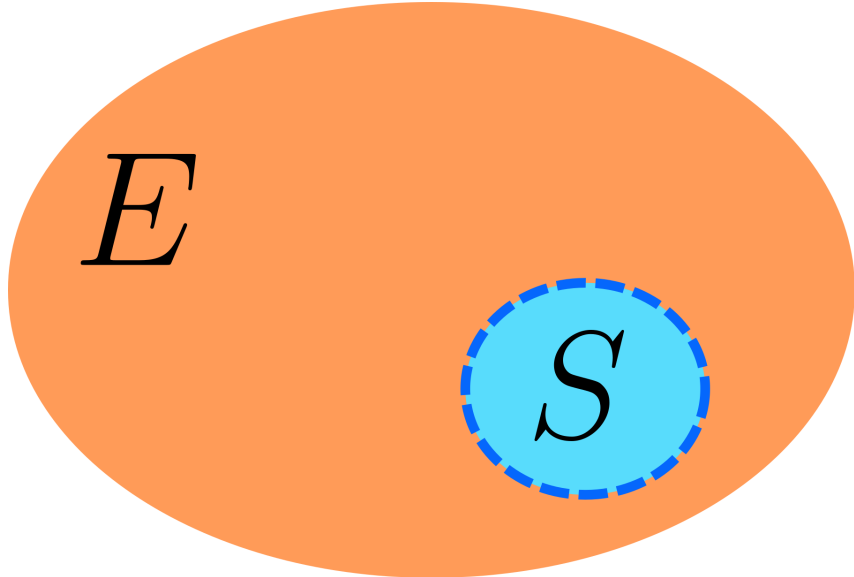


Figure 2.3: The canonical visual representation of an open quantum system. In open quantum systems one considers a composite system, consisting of S , the *system of interest*, here depicted by the blue circle, and E some well-understood environment – here depicted by the orange ellipse. The dark blue dashed line marks the interface between the two systems. That the environment is well understood is rather crucial, and often leads to the environment itself being tightly constrained. One does not need to know the state of the environment, but it is necessary to know what states are available, and to be able to precisely define its interaction with the system of interest.

The study of open quantum systems involves taking a well-behaved closed quantum system, evicting it from the frictionless vacuum every theorist carries in their heart, and embedding it in a noisy environment. The reasons for wanting to do this are obvious – while the study of energy and number conserving closed quantum systems has led to many insights, such systems rarely exist. Even a simple pendulum requires consideration of dissipation through friction to describe its real world behaviour.

In this section we will begin by reminding ourselves of the properties of density matrices, followed by discussion of the Lindblad form master equation, and the approximations inherent to it. Finally, we will discuss some practical

details of solving the dynamics of open quantum systems, which will aid in understanding the next chapter on numerical methods.

2.2.1 Density matrix

The state vector suffices for describing a quantum system which is known to be in one particular state (a *pure* state), but cannot adequately describe a quantum system which may be in one of a number of states. This *ensemble* or *mixed* state must be expressed using the density matrix, commonly denoted by ρ . The density matrix for an ensemble state is defined as,

$$\rho = \sum_j p_j |\psi_j\rangle\langle\psi_j|, \quad (2.16)$$

where $p_j = |c_j|^2$ is the probability of finding the system in the state $|\psi_j\rangle$ [43]. A valid density matrix has three important properties,

$$\text{Tr}[\rho] = 1, \quad (2.17)$$

$$\rho = \rho^\dagger, \quad (2.18)$$

$$\langle\psi_j|\rho|\psi_j\rangle \geq 0 \forall j, \quad (2.19)$$

its trace is equal to one, it is Hermitian, and its diagonal values are all greater-than-or-equal to zero (formally it is *positive semidefinite*). All three can be viewed as consequences of the interpretation of the diagonal values of the density matrix as probabilities for each state. The trace condition is simply the requirement that the probability of the system being in *any* state is one, and the other two ensure that the eigenvalues are real and not negative, making them valid probabilities.

Observables of the system are calculated by taking the trace of the operator product,

$$\langle\hat{O}\rangle = \text{Tr}[\hat{O}\rho], \quad (2.20)$$

while the system is time-evolved by applying the operator to both sides of the

density matrix,

$$\begin{aligned}\rho(t) &= \hat{U}(t)\rho(0)\hat{U}^\dagger(t), \\ &= \hat{U}(t)|\Psi(0)\rangle\langle\Psi(0)|\hat{U}^\dagger(t),\end{aligned}\quad (2.21)$$

where the time-evolution operator $\hat{U}(t) = \exp(-i\mathcal{H}t)$, and \mathcal{H} is the system Hamiltonian. Finally, we can calculate the density matrix of a subsystem of a composite system by calculating the *reduced density matrix*,

$$\begin{aligned}\rho^A &= \text{Tr}_B[\rho^{AB}], \\ &= \text{Tr}_B[c_j|a_j\rangle\langle a_k|c_k^*\otimes d_l|b_l\rangle\langle b_m|d_m^*], \\ &= \sum_{n,j,k,l,m} [\langle b_n| (c_j c_k^* d_l d_m^*) |a_j\rangle\langle a_k| \otimes |b_l\rangle\langle b_m|) |b_n\rangle], \\ &= \sum_{n,j,k} [c_j c_k^* |d_n|^2 |a_j\rangle\langle a_k| \otimes \langle b_n|b_n\rangle], \\ &= \sum_{n,j,k} c_j c_k^* |d_n|^2 |a_j\rangle\langle a_k|,\end{aligned}\quad (2.22)$$

where $|a_j\rangle$ and $|b_l\rangle$ are the basis vectors of the A and B subsystems respectively, with corresponding complex amplitudes c_j and d_l . The replacement of l, m, n with the single index n , and removal of the tensor product, follows from the orthogonality condition $\langle b_l|b_m\rangle = \delta_{lm}$. This ability to separate out subsystems is invaluable to the study of open quantum systems. The system of interest is considered to be part of a composite system with its environment, so the state of the system of interest can be found by tracing over the environment degrees of freedom.

2.2.2 Lindblad master equation

Throughout our research we will limit ourselves to consideration of master equations of a particular form – the Lindblad master equation. We will not derive it here, as this can be found in any good text on open quantum systems, such as Breuer and Petruccione’s ‘The Theory of Open Quantum Systems’, or Carmichael’s ‘An Open Systems Approach to Quantum Optics’ [44, 45]. We

shall, however, discuss why the Lindblad form is important, and the approximations that are encoded within it.

The Lindblad master equation, named for Göran Lindblad but based on both his work and that of Gorini, Kossakowski, and Sudarshan [46, 47], is as follows,

$$\frac{d\rho}{dt} = -i[\mathcal{H}, \rho] + \sum_j \frac{\gamma_j}{2} \left[2\hat{A}_j \rho \hat{A}_j^\dagger - \left\{ \hat{A}_j^\dagger \hat{A}_j, \rho \right\} \right], \quad (2.23)$$

where \mathcal{H} is the Hamiltonian for the system, the operator \hat{A}_j is the jump operator on the site j , which characterises the interaction between the system and its environment, and the anti-commutator is $\{a, b\} = ab + ba$. The first term is in fact just the Liouville-von Neumann equation, which describes the dynamics of the closed (non-dissipative) system [48]. The second term, often referred to as the dissipator,

$$\mathcal{D}[\rho] = \sum_j \frac{\gamma_j}{2} \left[2\hat{A}_j \rho \hat{A}_j^\dagger - \left\{ \hat{A}_j^\dagger \hat{A}_j, \rho \right\} \right], \quad (2.24)$$

encodes the dissipative dynamics. Importantly, a dissipator of this form preserves both the positivity and trace of the density matrix upon which it operates, ensuring physical results. It is quite general, but does implicitly make the following three approximations.

First, the Born approximation. This approximation assumes that the system-environment interaction is weak. This is reasonable, as we would typically consider anything which interacted strongly as part of the system, rather than the environment. We may therefore neglect terms which are greater than second-order in the interaction Hamiltonian during a power series expansion of the time evolution operator, which is considered in deriving the master equation. Specifically we require that,

$$g \ll \frac{1}{\tau}, \quad (2.25)$$

where g is the interaction energy in units of frequency (when $\hbar = 1$), and τ is

the decay time of correlations in the environment such that,

$$\langle \hat{a}_E(t \geq \tau) \hat{a}_E^\dagger(0) \rangle \ll \langle \hat{a}_E(0) \hat{a}_E^\dagger(0) \rangle, \quad (2.26)$$

where $\hat{a}_E(t)$ annihilates an excitation in the environment at time t .

Second, the Markov approximation. This approximation assumes that the environment is very large, and therefore that any excitations from the system move quickly away from the system-environment interaction centre. Equivalently, one can say that the timescale of significant changes in the state of the system should be much longer than the decay of correlations in the environment (τ in eq. (2.26)). This means that excitations cannot return from the environment to the system, and the system's future state is dependent only on its current state, not its history. This approximation also clearly relies on interaction between the system and environment being weak, and is therefore wholly consistent with the Born approximation. For this reason the two are often grouped together as the *Born-Markov approximation* [49, 50].

Finally, the *rotating wave* or *secular* approximation. In this approximation rapidly oscillating terms in the dissipator are averaged out. It is valid when the timescale of evolution of the system is small compared to the relaxation time, which is typical for quantum optical systems [50].

2.2.3 The Liouvillian

The above section explains how we generate the dynamics of the density matrix, but not how we find the stationary state,

$$\frac{d}{dt} \rho_{SS} = 0, \quad (2.27)$$

for this we convert the Lindbladian into a system of linear equations, which is named the Liouvillian after its classical counterpart. The Lindbladian is a *superoperator*, acting on the density matrix from both the left and the right. In order to rephrase the dynamics as a system of coupled linear equations, we

shall make use of the following property of matrix products,

$$\mathbf{AXB} = (\mathbf{B}^T \otimes \mathbf{A}) \bar{\mathbf{X}}, \quad (2.28)$$

where \mathbf{A} , \mathbf{B} and \mathbf{X} are matrices, and $\bar{\mathbf{X}}$ is \mathbf{X} reshaped into a vector [51, 52].

In this way the master equation eq. (2.23) is reformulated as the Liouvillian matrix,

$$\begin{aligned} \hat{L}|\rho\rangle\rangle = \\ \left(\mathbb{I} \otimes -i\mathcal{H} + i\mathcal{H}^T \otimes \mathbb{I} + \sum_j \frac{\gamma_j}{2} \left[\hat{A}_j^* \otimes 2\hat{A}_j - \mathbb{I} \otimes \hat{A}_j^\dagger \hat{A}_j - \hat{A}_j^\dagger \hat{A}_j \otimes \mathbb{I} \right] \right) |\rho\rangle\rangle, \end{aligned} \quad (2.29)$$

where $|\rho\rangle\rangle$ is the vectorised density matrix, and \mathbb{I} is the identity. Our stationary state is then trivially the solution to the system of equations,

$$\hat{L}|\rho_{SS}\rangle\rangle = 0, \quad (2.30)$$

which for a small enough system we can solve directly using linear algebra methods. For larger systems, we make use of matrix product states, which will be the main topic of discussion in our next chapter on numerical methods.

Chapter 3

Numerical methods

In this chapter we consider the numerical methods I have used to study the dynamics of dissipative many-body quantum systems. In particular, we consider the use of matrix product states to approximate the state of the system. We will first discuss the theoretical underpinnings of MPS, and then consider in detail the variational search technique. I implemented a variant of the variational search which seeks stationary states in MATLAB [6], which can be found in a repository hosted at reference [5]. The code, named `mpostat`, is documented in appendix A. We will then briefly discuss time evolution methods, which we have made use of in some of the published work included in this thesis.

3.1 Matrix product states

Matrix product states as we describe them here were first presented by Vidal [1], but in effect grew from the understanding that Steven White's density matrix renormalisation group method [10, 11] could be reformulated to use a matrix product state representation which had previously been used as an analytical tool for finitely correlated states – in particular the AKLT state [12]. Given some generic one dimensional many-body state $|\Psi\rangle$, we may decompose

CHAPTER 3. NUMERICAL METHODS

the state vector as a sum of basis vectors with individual coefficients,

$$|\Psi\rangle = \sum_{\sigma_1 \dots \sigma_N} c_{\sigma_1 \dots \sigma_N} |\sigma_1 \dots \sigma_N\rangle, \quad (3.1)$$

where σ_j is the local state on site j . The matrix product state further decomposes these coefficients in the following way,

$$c_{\sigma_1 \dots \sigma_N} = A_{\sigma_1}^{[1]} A_{\sigma_2}^{[2]} \dots A_{\sigma_N}^{[N]}, \quad (3.2)$$

where each $A_{\sigma}^{[n]}$ is a so-called matrix product state ‘site tensor’. The first site tensor $A^{[1]}$ has a row vector for each physical state on the first site, the last site tensor $A^{[N]}$ has a column vector for each physical state on the last site, and each other tensor $A^{[n]}$ has a matrix for each physical state on the n^{th} site. The product of matrices for a particular set of local states recovers the coefficient for that many-body basis vector. On the face of it, this is nothing more than a convoluted way to write state vectors. While every state vector is unique, MPS representations are degenerate as we have introduced additional degrees of freedom in the form of the virtual dimensions (rows and columns) in each site tensor. There are two things that make this technique fundamentally useful.

Firstly, we can limit the size of the virtual dimensions. Typically in an exact representation the virtual dimensions will grow as we move through the system, reaching a maximum on the middle site(s) and then decrease again, keeping in mind the constraint that the second virtual dimension on the site n must match the size of the first virtual dimension on the site $n+1$, and the first and last sites must be vectors. We can construct the MPS such that the virtual dimension never exceeds some value χ_{\max} to create an approximation to the state, and we can further use the singular value decomposition to programatically ensure that these compressed tensors are optimal. Importantly, thanks to Vidal’s observation that using the SVD in this manner is equivalent to performing a Schmidt decomposition on a bipartite splitting of the state, it is clear what exactly we lose when we compress the state this way [9]. Since the number of non-zero coefficients is a measure of entanglement in the system, if we truncate

our virtual dimensions by removing components with the smallest singular values, we lose access to more highly entangled states. To put it another way, MPS is a useful and efficient representation for states with low levels of entanglement. At the extreme end, a product state could be represented with a virtual dimension of one on every site.

Secondly, we can perform useful operations on individual site tensors. A tensor network can be constructed which when contracted yields the result of some operator acting on the matrix product state. Furthermore, expectation values can be calculated by introducing the conjugate matrix product state [2, 53]. This allows us to efficiently investigate the system represented by the MPS, as long as we do not require representation of a state with more entanglement than compression allows. One example of this which we shall discuss in great detail is the variational search, in which individual site tensors are optimised with respect to some operator such as a Hamiltonian or Liouvillian [54, 3]. One can also efficiently perform time evolution of the state, and indeed this was the first method developed explicitly using MPS, being familiar from DMRG [1].

Key to some of these techniques is the ability to represent operators in a similar way. We shall discuss matrix product operators (MPOs) next.

3.2 Matrix product representation of operators

In order to make effective use of matrix product states it is helpful to write operators in a compatible format. This is achieved through the matrix product operator formalism, however, MPOs must in general be constructed by hand [55–58, 2]. Note that when I refer to MPOs throughout this thesis I mean matrix product representations of operators such as the Hamiltonian, Liouvillian, or observables. The distinction is necessary as the matrix product representation of a density matrix is also a matrix product operator by dint of having both input and output states. I will refer to an MPO representation of a density matrix as a density matrix product operator (DMPO), in order to

CHAPTER 3. NUMERICAL METHODS

distinguish it.

We will now discuss the process of constructing an MPO, beginning with the following simple one-dimensional Heisenberg XXX model with open boundary conditions,

$$\mathcal{H} = -J \sum_{j=1}^{N-1} [\sigma_j^x \sigma_{j+1}^x + \sigma_j^y \sigma_{j+1}^y + \sigma_j^z \sigma_{j+1}^z] - h \sum_{j=1}^N \hat{\sigma}_j^z, \quad (3.3)$$

where $\sigma^{x,y,z}$ are the spin Pauli matrices, J is a coupling constant, and h is an external field. We recall the fact that the notation σ_j^x is shorthand which in fact refers to the tensor product,

$$\dots \mathbb{I} \otimes \mathbb{I} \otimes \sigma^x \otimes \mathbb{I} \otimes \mathbb{I} \dots$$

where the σ^x is the j^{th} operator in the chain. Keeping that in mind, our MPO matrices should deliver chains of operators of the form,

$$\dots \mathbb{I} \otimes -h\sigma^z \otimes \mathbb{I} \dots$$

and

$$\dots \mathbb{I} \otimes -J\sigma^{x,y,z} \otimes \sigma^{x,y,z} \otimes \mathbb{I} \dots$$

for each site. Additionally, as with the MPS, the first site MPO tensor should be a row vector, and the last site MPO tensor should be a column vector. Since the Hamiltonian is homogeneous across all sites in the bulk, the same

CHAPTER 3. NUMERICAL METHODS

MPO tensor can be used for each. One valid formulation then is,

$$H^{[1]} = \begin{bmatrix} -h\sigma^z & -J\sigma^x & -J\sigma^y & -J\sigma^z & \mathbb{I} \end{bmatrix}, \quad (3.4)$$

$$H^{[\text{bulk}]} = \begin{bmatrix} \mathbb{I} & 0 & 0 & 0 & 0 \\ \sigma^x & 0 & 0 & 0 & 0 \\ \sigma^y & 0 & 0 & 0 & 0 \\ \sigma^z & 0 & 0 & 0 & 0 \\ -h\sigma^z & -J\sigma^x & -J\sigma^y & -J\sigma^z & \mathbb{I} \end{bmatrix}, \quad (3.5)$$

$$H^{[N]} = \begin{bmatrix} \mathbb{I} \\ \sigma^x \\ \sigma^y \\ \sigma^z \\ -h\sigma^z \end{bmatrix}, \quad (3.6)$$

which in the simplest, three-site case yields,

$$\begin{aligned} & H^{[1]} H^{[2]} H^{[3]} \\ &= \begin{bmatrix} -h\sigma^z, & -J\sigma^x, & -J\sigma^y, & -J\sigma^z, & \mathbb{I} \end{bmatrix} \\ &\quad \times \begin{bmatrix} \mathbb{I} & 0 & 0 & 0 & 0 \\ \sigma^x & 0 & 0 & 0 & 0 \\ \sigma^y & 0 & 0 & 0 & 0 \\ \sigma^z & 0 & 0 & 0 & 0 \\ -h\sigma^z & -J\sigma^x & -J\sigma^y & -J\sigma^z & \mathbb{I} \end{bmatrix} \begin{bmatrix} \mathbb{I} \\ \sigma^x \\ \sigma^y \\ \sigma^z \\ -h\sigma^z \end{bmatrix}, \\ &= \left[(-h\sigma^z \mathbb{I} - J\sigma^x \sigma^x - J\sigma^y \sigma^y - J\sigma^z \sigma^z - h\mathbb{I}\sigma^z), \quad -J\mathbb{I}\sigma^x, \quad -J\mathbb{I}\sigma^y, \quad -J\mathbb{I}\sigma^z, \quad \mathbb{III} \right] \\ &\quad \times \begin{bmatrix} \mathbb{I} \\ \sigma^x \\ \sigma^y \\ \sigma^z \\ -h\sigma^z \end{bmatrix}, \\ &= -h\sigma^z \mathbb{III} - J\sigma^x \sigma^x \mathbb{I} - J\sigma^y \sigma^y \mathbb{I} - J\sigma^z \sigma^z \mathbb{I} - h\mathbb{I}\sigma^z \mathbb{I} - J\mathbb{I}\sigma^x \sigma^x - J\mathbb{I}\sigma^y \sigma^y \\ &\quad - J\mathbb{I}\sigma^z \sigma^z - h\mathbb{III}\sigma^z, \end{aligned} \quad (3.7)$$

which is indeed correct. How exactly the physical and virtual dimensions are arranged after this point is an implementation detail, which we need not concern ourselves with at the design stage. It should be noted that this formulation is not unique, but we have chosen certain conventions, such as scalar coefficients being included in the ‘leading’ terms, and making use of the bottom row and first column in the bulk MPO. Obviously, more complex Hamiltonians require more complex MPOs – in particular moving beyond nearest neighbour coupling requires making use of the inner space in the bulk MPO, and the creation of ‘passing lanes’ in the main row and column. We defer further discussion of that until later when we discuss reference [7], which relied heavily on such techniques.

We will now briefly discuss the additional complexity involved in creating an MPO for a Liouvillian, as this is directly useful for the variational stationary state code presented later. Firstly, we note that $|\rho(\mathbf{x})\rangle\rangle$ denotes the density matrix vectorised according to the isomorphism,

$$\begin{aligned}\rho &= \sum_{ij} c_{ij} |i\rangle\langle j| \\ \rightarrow |\rho\rangle\rangle &= \sum_{ij} c_{ij} |j\rangle \otimes |i\rangle,\end{aligned}\tag{3.8}$$

where $|i\rangle$ is some complete set of basis states. Secondly, we note that formation of the Liouvillian matrix, $\hat{\mathcal{L}}$ which acts on the vectorised density matrix, $|\rho\rangle\rangle$ relies on the following property. Given the matrix equation,

$$AXB = C,\tag{3.9}$$

one can write,

$$(B^T \otimes A) \vec{X} = \vec{C}.\tag{3.10}$$

Given then that the system dynamics are given by $\dot{\rho} = -i[\mathcal{H}, \rho]$, we must write an MPO form of the equation,

$$\hat{\mathcal{L}}|\rho\rangle\rangle = (\mathbb{I} \otimes -i\mathcal{H} + i\mathcal{H}^T \otimes \mathbb{I}) |\rho\rangle\rangle.\tag{3.11}$$

The additional complexity in the MPO structure is clear – we must account separately for terms on the ‘left’ and ‘right’ side of the tensor product. As an example we consider the bulk MPO for the dynamics of our one-dimensional Heisenberg XXX system eq. (3.3). It is as follows,

$$\hat{\mathcal{L}}^{\text{bulk}} = \begin{bmatrix} \mathbb{I} \otimes \mathbb{I} & 0 & 0 & 0 & 0 & 0 & 0 & 0 \\ \mathbb{I} \otimes \sigma^x & 0 & 0 & 0 & 0 & 0 & 0 & 0 \\ \sigma^x \otimes \mathbb{I} & 0 & 0 & 0 & 0 & 0 & 0 & 0 \\ \mathbb{I} \otimes \sigma^y & 0 & 0 & 0 & 0 & 0 & 0 & 0 \\ \sigma^{yT} \otimes \mathbb{I} & 0 & 0 & 0 & 0 & 0 & 0 & 0 \\ \mathbb{I} \otimes \sigma^z & 0 & 0 & 0 & 0 & 0 & 0 & 0 \\ \sigma^z \otimes \mathbb{I} & 0 & 0 & 0 & 0 & 0 & 0 & 0 \\ \mathbb{I} \otimes i\hbar\sigma^z - i\hbar\sigma^z \otimes \mathbb{I} & \mathbb{I} \otimes iJ\sigma^x & -iJ\sigma^x \otimes \mathbb{I} & \mathbb{I} \otimes iJ\sigma^y & -iJ\sigma^{yT} \otimes \mathbb{I} & \mathbb{I} \otimes iJ\sigma^z & -iJ\sigma^z \otimes \mathbb{I} & \mathbb{I} \otimes \mathbb{I} \end{bmatrix}, \quad (3.12)$$

an essentially trivial extension of the Hamiltonian MPO, however care must be taken over minus signs, and note that $\sigma^{xT} = \sigma^x$, $\sigma^{zT} = \sigma^z$, but $\sigma^{yT} \neq \sigma^y$. The precise arrangement of the virtual and physical dimensions is again an implementation dependent detail, but note that we here have again two virtual dimensions (rows and columns), but four physical dimensions.

Having described matrix product states and operators in a general sense, we will now discuss one particular technique which makes use of them – the variational search procedure.

3.3 Variational search

It is well known that one can use the Rayleigh-Ritz variational technique to find an approximation to the lowest eigenvalue and corresponding eigenfunction of a Hermitian operator. Given a set of variational parameters upon which the eigenfunctions depend, one can move always to a lower eigenvalue, by minimising over one parameter at a time [59, 60]. Consequently, we can find

an approximation to the ground state of a system by minimising the expression,

$$E = \frac{\langle\psi(\mathbf{x}^*)|\hat{H}|\psi(\mathbf{x})\rangle}{\langle\psi(\mathbf{x}^*)|\psi(\mathbf{x})\rangle}, \quad (3.13)$$

with respect to some x , where E is the energy of the system, \hat{H} is a Hamiltonian, ψ is an approximation to the ground state, and \mathbf{x} is a set of *variational parameters*. Equally, we can find an approximation to the stationary state of an open quantum system by minimising the expression,

$$\frac{d}{dt}\langle\langle\rho|\rho\rangle\rangle = \langle\langle\rho(\mathbf{x}^*)|\hat{\mathcal{L}}^\dagger\hat{\mathcal{L}}|\rho(\mathbf{x})\rangle\rangle, \quad (3.14)$$

with respect to some x , where $\hat{\mathcal{L}}$ is a Liouvillian matrix, ρ is an approximation to the stationary state, and \mathbf{x} is again some set of variational parameters. We will discuss here the generic case in which we have some observable O we wish to minimise, which has an operator \hat{O} . As such we seek to use matrix product states to minimise the expression,

$$\langle\psi(\mathbf{x}^*)|\hat{O}|\psi(\mathbf{x})\rangle, \quad (3.15)$$

with respect to some x . A visual representation of the variational search procedure is provided in fig. 3.1.

When using matrix product states the set of variational parameters we employ are the individual site tensors, $A^{[n]}$. We shall discuss the search procedure as prescribed by Ulrich Schollwöck's excellent review article [2]. I begin my explanation by assuming that we have already some initial matrix product state, Ψ_{init} which is normalised according to the vector norm, and has dimensions $N \times \chi_{j-1} \times \chi_j \times d$, where N is the number of sites in the system, d is the local state space dimension, χ_j is the local virtual dimension and meets the condition $\chi_j \leq \chi_{\max}$, which is the maximal allowed virtual dimension. Additionally I assume we may represent the operator \hat{O} as a matrix product operator with site tensors $O^{[n]}$. First, we construct left and right ‘blocks’ for each site in the system. The left block for some site n is a rank-3 tensor which contains the expectation of \hat{O} from the first site up to the site $n - 1$. The right block for

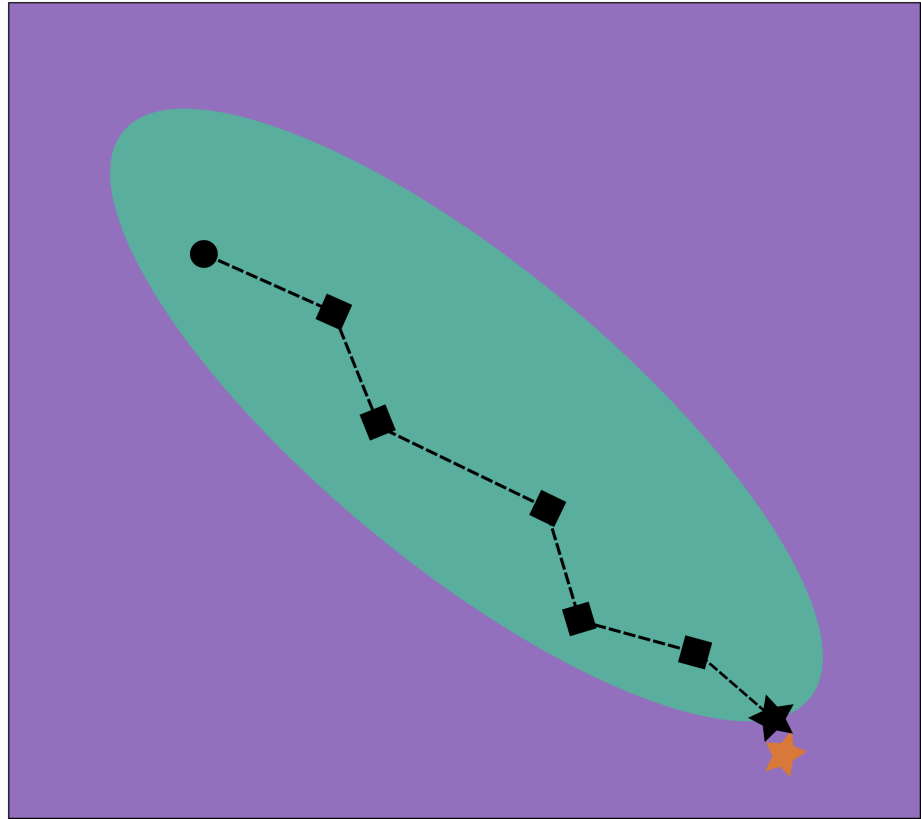


Figure 3.1: A visual representation of a variational search using matrix product states. The purple background represents the total state space of the system, and the green oval is the part of that state space that can be represented by a matrix product state of some finite dimension. The orange star represents our desired solution state, and in this case it is inaccessible to the matrix product state space. The black circle is the initial matrix product state, the black star is the nearest matrix product state approximation to the solution state, and the black squares are states through which the matrix product state transitions on its way to the solution state. The black dashed line represents a variational step – an optimisation over one or more of the variational parameters. The transitional states may or may not have some physical meaning in the context of the variational search depending on the specifics of the system being investigated. In general, however, if one wishes to know *how* a system reaches the solution state a time evolution method should be used, not a variational search.

some site n is a rank-3 tensor which contains the expectation of \hat{O} from the

last site through to the site $n + 1$. This is shown diagrammatically in fig. 3.2.

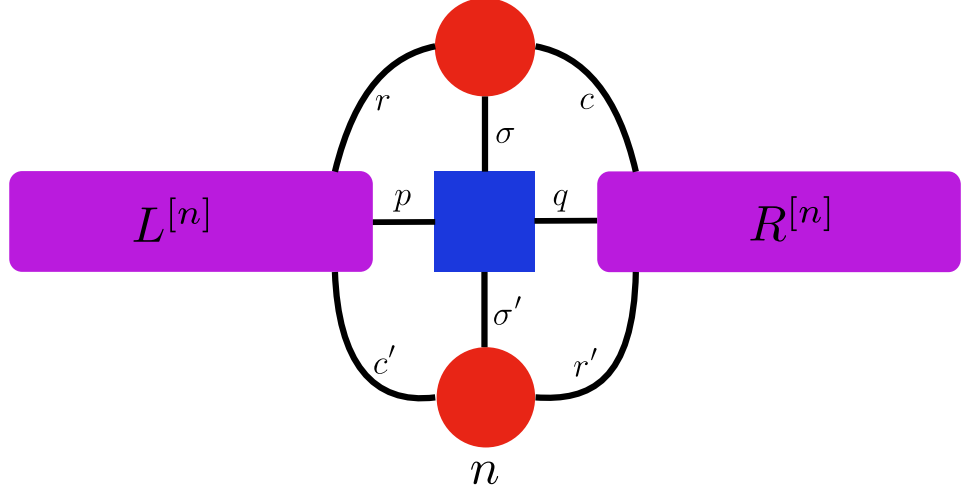


Figure 3.2: A tensor network diagram for a system which has been partially contracted in order to form left and right blocks, $L^{[n]}$ and $R^{[n]}$. The upper red dot here is a tensor for the site n , $A^{[n]}$, and the lower red dot is its conjugate, $A^{\dagger[n]}$. The blue square is the MPO tensor $O^{[n]}$ of some observable with an operator \hat{O} . The black lines represent tensor indices which can be contracted over. If this contraction is completed it will be equivalent to a contraction over the full system, and the result will be the expectation value $\langle \Psi | \hat{O} | \Psi \rangle$.

The first site left block tensor $L^{[1]}$ is just the scalar 1, as there are obviously no sites before the first. The second left block tensor $L^{[2]}$ is then found by performing the contraction procedure,

$$L_{r',c,q}^{[2]} = \sum_{\sigma',c'} A_{r',c'}^{\dagger[1]\sigma'} \left(\sum_{\sigma,p} O_{p,q}^{[1]\sigma,\sigma'} \left(\sum_r A_{r,c}^{[1]\sigma} \right) \right), \quad (3.16)$$

where $A^{[n]}$ is the matrix product state tensor for the site n , σ indexes the local physical state, r and c ('row' and 'column') index the local virtual dimensions, primed indices relate to the conjugate matrix product state tensor $A^{\dagger[n]}$, and p and q index the virtual dimensions of the matrix product operator. The procedure continues from there, much as you might expect, by moving on to the third site and so on until the last site is reached. The general formula for

$L^{[n]}$ is,

$$L_{r',c,q}^{[n]} = \sum_{\sigma',c'} A_{r',c'}^{\dagger[n-1]\sigma'} \left(\sum_{\sigma,p} O_{p,q}^{[n-1]\sigma,\sigma'} \left(\sum_r L_{c',r,p}^{[n-1]} A_{r,c}^{[n-1]\sigma} \right) \right), \quad (3.17)$$

which is shown diagrammatically in fig. 3.3.

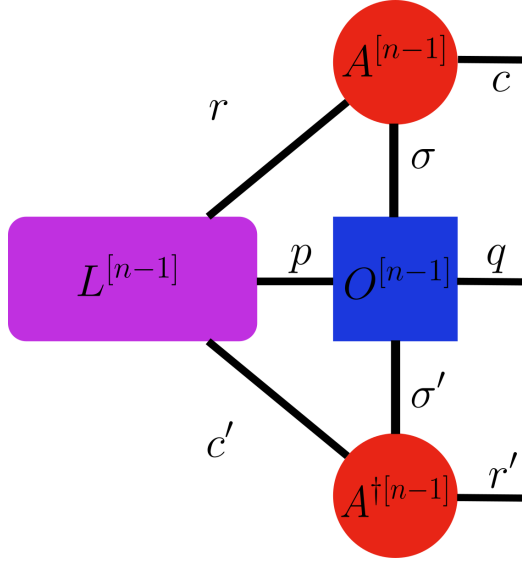


Figure 3.3: A tensor network diagram which, when contracted, yields the ‘left block’ for the site n , $L^{[n]}$. This is the operation described in eq. (3.17). The un-contracted indices c , q , and r' , form the three dimensions of $L^{[n]}$.

The procedure for forming the right block is naturally very similar, starting from the last site with $R^{[N]} = 1$ and,

$$R_{c',r,p}^{[n]} = \sum_{\sigma',r'} A_{r',c'}^{\dagger[n+1]\sigma'} \left(\sum_{\sigma,q} O_{p,q}^{[n+1]\sigma,\sigma'} \left(\sum_c R_{r',c,q}^{[n+1]} A_{r,c}^{[n+1]\sigma} \right) \right). \quad (3.18)$$

Once we have formed these left and right blocks at each site, we move on to the variational procedure proper.

We will sweep backwards and forwards through the system, updating each site tensor to minimise the energy of the overall state. Referring back to eq. (3.13) we can see that it can be minimised by being rephrased as an eigen-

value problem,

$$\begin{aligned}
 \frac{\langle\psi(\mathbf{x}^*)|\hat{H}|\psi(\mathbf{x})\rangle}{\langle\psi(\mathbf{x}^*)|\psi(\mathbf{x})\rangle} &= E, \\
 \Rightarrow \langle\psi(\mathbf{x}^*)|\hat{H}|\psi(\mathbf{x})\rangle &= E\langle\psi(\mathbf{x}^*)|\psi(\mathbf{x})\rangle, \\
 \Rightarrow \frac{d}{d\langle\psi(\mathbf{x}^*)|} (\langle\psi(\mathbf{x}^*)|\hat{H}|\psi(\mathbf{x})\rangle) &= \frac{d}{d\langle\psi(\mathbf{x}^*)|} (E\langle\psi(\mathbf{x}^*)|\psi(\mathbf{x})\rangle), \\
 \Rightarrow \hat{H}|\psi(\mathbf{x})\rangle &= E|\psi(\mathbf{x})\rangle,
 \end{aligned} \tag{3.19}$$

which of course is an expression of the time-independent Schrödinger equation. If we could solve that for the full many-body state $|\psi(\mathbf{x})\rangle$ then we would not need matrix product states at all. Unfortunately, we cannot – the computational effort scales exponentially with the system size as the Hamiltonian has d^{2N} elements for a system with d local states, and N sites. What matrix product states allow us to do is to form an effective Hamiltonian for some particular site $|\psi(n)\rangle$, and instead solve the more limited eigenvalue problem,

$$\hat{H}_{\text{eff}}^{[n]}|\psi(n)\rangle = E_n|\psi(n)\rangle, \tag{3.20}$$

from which we simply select $|\psi(n)\rangle$ which corresponds to the lowest real value of E_n . In our case $|\psi(x)\rangle$ is $A^{[n]}$, and \hat{H}_{eff} is formed by the contraction of the *environment* of $A^{[n]}$ [53]. That is we calculate,

$$\hat{H}_{\text{eff}}^{[n]} = \langle\psi(\tilde{\mathbf{x}})|\hat{H}|\psi(\tilde{\mathbf{x}})\rangle, \tag{3.21}$$

where $|\psi(\tilde{\mathbf{x}})\rangle$ is our matrix product state *excluding the tensor for the site n*. Such a contraction is shown diagrammatically in fig. 3.4. Mathematically, the contraction is performed as,

$$\hat{H}_{r,c,r',c',\sigma,\sigma'}^{[n]\text{ eff}} = \sum_{p,q} L_{r,r',p}^{[n]} O_{p,q}^{[n]\sigma,\sigma'} R_{c,c',q}^{[n]}, \tag{3.22}$$

which seems simple enough, and indeed would be except that we have an eigenvalue problem to solve. As such we require $\hat{H}_{\text{eff}}^{[n]}$ to be a matrix, not a rank-6 tensor. This can be accomplished by joining the indices corresponding

to the matrix product state, and joining those of its conjugate to form a matrix $\hat{H}_{(\sigma,r,c),(\sigma',r',c')}^{[n]\text{eff}}$. Once this is achieved it is a simple matter of finding the eigenvector of $\hat{H}_{(\sigma,r,c),(\sigma',r',c')}^{[n]\text{eff}}$ corresponding to the optimal eigenvalue. Which eigenvalue depends explicitly on the problem you are trying to solve, and the eigenspectrum of the relevant operator – some examples are given in table 3.1.

Problem	Operator	Eigenspectrum	Optimal Eigenvalue
Ground state	Hamiltonian, \hat{H}	$\lambda \in \mathbb{R}$	$\min(\lambda)$
Stationary state	Liouvillian, $\hat{\mathcal{L}}$	$\lambda = a + ib$ $\{a \in \mathbb{R}^-, b \in \mathbb{R}\}$	$\max(\text{Re}(\lambda))$
Stationary state	$\hat{\mathcal{L}}^\dagger \hat{\mathcal{L}}$	$\lambda \in \mathbb{R}^+$	$\min(\lambda)$

Table 3.1: Examples of appropriate optimal eigenvalues for different variational problems.

This eigenvector is the vectorised site tensor $A_{(\sigma,r,c)}^{[n]}$, which we reshape to be $A_{r,c}^{[n]\sigma}$ and use to update our matrix product state. Given that, it should be clear that the size of the effective Hamiltonian is dependent on the local virtual dimensions. If the maximum size of the virtual dimensions is χ_{\max} , then the effective Hamiltonian has at most $\chi_{\max}^4 d^2$ elements, which is certain to be less than d^{2N} provided $\chi_{\max} < d^{\frac{1}{2}(N-1)}$. It should come as no surprise that $\chi_{\max} \geq d^{\frac{1}{2}(N-1)}$ is also the condition for a guaranteed exact MPS representation. Consider that an MPS tensor with square matrices for each physical state, and $\chi = d^{\frac{1}{2}(N-1)}$ has $d^{\frac{1}{2}(N-1)} \times d^{\frac{1}{2}(N-1)} \times d = d^N$ elements.

We update the first site in our system, and must then renormalise the site. Note that computationally, the appropriate norm for a matrix product state is the vector norm,

$$\langle \psi(\mathbf{x}^*) | \psi(\mathbf{x}) \rangle = 1, \quad (3.23)$$

regardless of the physical system being represented. For ground state searches this is no issue since the vector norm is also the appropriate measure for state vectors, however for density matrices the appropriate norm is the trace

norm – the vector norm must nevertheless be maintained to prevent numerical problems. The physically relevant trace norm condition,

$$\text{Tr}[\rho] = 1, \quad (3.24)$$

must be separately enforced (often by simply rescaling at the end of a calculation). In principle, one could recalculate the vector norm after every update and rescale the newly updated site in order to maintain the vector norm, however this is computationally costly, requiring a contraction through the full system. A smarter approach is to begin with an appropriately normalised MPS, and to use the singular value decomposition to maintain this normalisation. The SVD decomposes some matrix M in the following way,

$$M = USV^\dagger, \quad (3.25)$$

where S is a diagonal matrix of singular values, and U and V are unitary matrices. We reshape our updated site tensor $A_{r,c}^{[n]\sigma}$ into a matrix by joining the physical indices to the first virtual index (the *rows*), and performing the SVD procedure on it. The first unitary matrix U is retained and reshaped to (once again) replace the site tensor. The singular value matrix and the second unitary are multiplied together, and then the product SV^\dagger is multiplied into the following site tensor $A_{r,c}^{[n+1]\sigma}$. This procedure ensures that normalisation is maintained throughout the system, and prevents large differences in scale between site tensors, which would cause numerical problems. That said, there is clearly a directionality to this procedure – the reverse procedure is to retain the second unitary V^\dagger , and to multiply US into the site tensor $A_{r,c}^{[n-1]\sigma}$. We therefore refer to site tensors as either left or right ‘canonical’, and we ensure that all sites left of the update site are left-canonical, and all sites right of the update site are right-canonical. Finally we note that in a sense, this procedure ‘pushes’ the normalisation of the MPS through the system. Consequently, if the system is made left-canonical up to the last site (or right-canonical up to the first), then performing the canonisation procedure on the last (first) site yields a single non-zero singular value, which is the vector norm of the state.

Having performed the full update and renormalisation procedure on the first site, we then update the left block tensor for the second site in the system, $L^{[2]}$ using eq. (3.17). We are then ready to find an effective Hamiltonian for the second site and update it. This procedure repeats sweeping ‘right’ through our system until we reach and update the N th site – at this point we have updated every site in the system, but it is unlikely that our observable has converged after only one such sweep. The procedure for sweeping ‘left’ through the system back to the first site is very similar, except when renormalising we make our newly updated site right-canonical and then update the right block, $R^{[n]}$. In this way we are always using the most up-to-date version of the system when we calculate the effective operator for a given site. The whole procedure repeats, sweeping left and right through the system until our chosen observable converges.

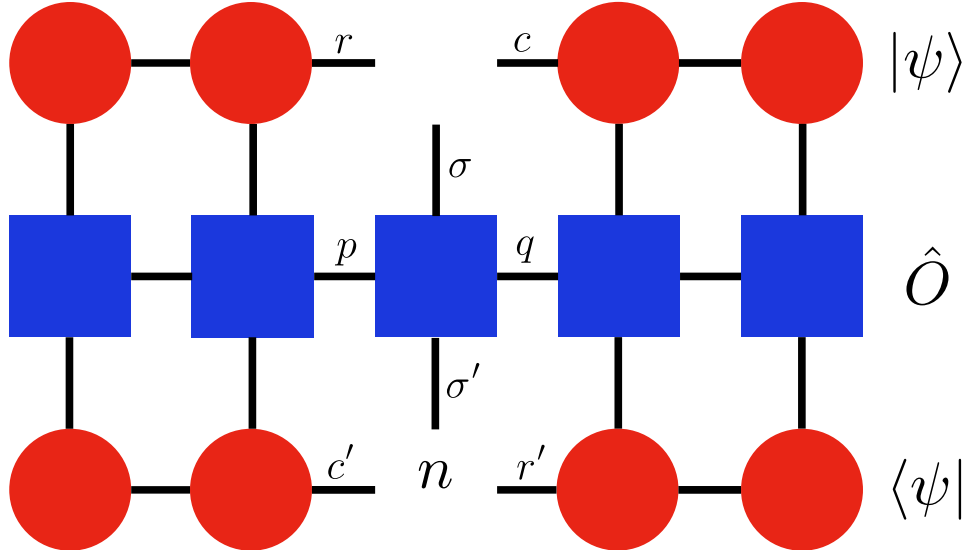


Figure 3.4: A diagrammatic representation of the contraction that must be performed in order to find the effective operator on some site n . As usual the red circles represent matrix product state tensors, the blue squares represent some matrix product operator, and black lines are indices. The lines which reach into the gap left by the missing site n are indices which are left free, and will become the indices of the effective operator. As such, it can be seen that the effective operator will be a rank-6 tensor.

3.4 Time evolution

Although the code written by myself implements the variational stationary state search, results included in this thesis were calculated using time evolution [8]. As such, we will briefly discuss how a matrix product state can be time evolved, specifically using the time evolving block decimation (TEBD) method due to Vidal [9].

First of all note that in TEBD we do not use an MPO, but instead split the Hamiltonian into commuting terms. For the sake of this explanation, we shall assume that the Hamiltonian only has nearest neighbour interactions, and can therefore be written as a sum of terms on odd and even sites,

$$\mathcal{H} = \mathcal{H}_{\text{odd}} + \mathcal{H}_{\text{even}}, \quad (3.26)$$

where importantly, the following commutation relations hold,

$$[\mathcal{H}_{\text{odd}}, \mathcal{H}_{\text{odd}}] = 0, \quad (3.27)$$

$$[\mathcal{H}_{\text{even}}, \mathcal{H}_{\text{even}}] = 0. \quad (3.28)$$

We can then make use of the Suzuki-Trotter expansion [61] which in general is,

$$e^{A+B} = \lim_{n \rightarrow \infty} \left[e^{\frac{A}{n}} e^{\frac{B}{n}} \right]^n, \quad (3.29)$$

and which allows us to expand (to first order) the time evolution over some time-step τ ,

$$\begin{aligned} |\psi(t+\tau)\rangle &= e^{-i\mathcal{H}\tau} |\psi(t)\rangle, \\ &= e^{-i\mathcal{H}_{\text{odd}}\tau} e^{-i\mathcal{H}_{\text{even}}\tau} |\psi(t)\rangle + \mathcal{O}(\tau^2). \end{aligned} \quad (3.30)$$

In fact, it is more conventional to use the second-order expansion,

$$e^{-i\mathcal{H}\tau} = e^{-i\mathcal{H}_{\text{odd}}\tau/2} e^{-i\mathcal{H}_{\text{even}}\tau} e^{-i\mathcal{H}_{\text{odd}}\tau/2} + \mathcal{O}(\tau^3), \quad (3.31)$$

which provides additional precision for little extra computational effort [2]. Note that since we have assumed nearest neighbour interactions here, the time-

evolution operators will take the form of two-site gates, as shown in fig. 3.5. Having determined the format of the operators, we consider the TEBD proce-

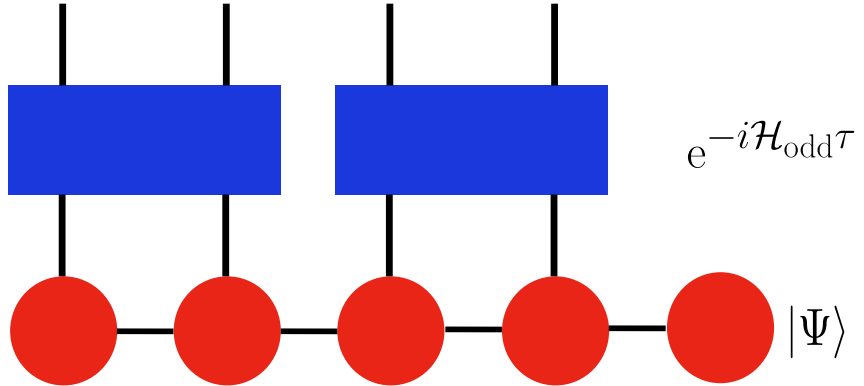


Figure 3.5: A time-evolution operator, $e^{-i\mathcal{H}_{\text{odd}}\tau}$, being applied to a five site matrix product state system. The Hamiltonian contains only terms beginning on odd sites, j , and extending only to $j + 1$. This means that each two site gate commutes with each other gate, and they can all be applied at once.

dure. We begin with some normalised matrix product state $|\psi\rangle$ with N sites, d local states, and a virtual dimension of χ . At each time-step each time-evolution operator is applied in turn by first combining and reshaping pairs of matrix product state site tensors. The two-site gate is then applied to each two-site MPS block, and the new matrix product state separated back into individual site tensors. During this separation step, the virtual dimension is truncated back to χ , by retaining the χ largest singular values. This process is repeated until the desired integration time is reached.

The difference when considering stationary states of a dissipative quantum system is simply that, as before, we use a density matrix product operator describing the vectorised density matrix $|\rho\rangle\rangle$, and we replace the two-site Hamiltonian gates with two-site Liouvillian gates. Naturally, there is a commensurate increase in the dimensions of the problem.

The requirement to be able to separate the operator into self-commuting terms is a clear disadvantage of this method, especially in systems with long range interactions. More modern approaches exist which attempt to overcome this limitation [62, 63], but it is still an open area of research.

Chapter 4

Dissipation-induced mobility and coherence in frustrated lattices

In this chapter we will discuss the article ‘Dissipation-induced mobility and coherence in frustrated lattices’ [7]. We will begin by discussing the motivation and theoretical background to the investigation, and results from the non-interacting regime. Then we will discuss the strongly interacting regime, focusing in some detail on the design of the matrix product operator for variational search calculations, which was complex due to the presence of long range nonlocal terms in this model, and was my primary contribution to the article.

4.1 Introduction

In a perfect crystal the wave functions are described by Bloch states, which are delocalized over the entire crystal, thus allowing transport. On the other hand, an imperfect crystal where disorder or impurities create scattering centres leads to localized wave functions, a phenomenon known as Anderson localization [64–66]. In fact the key to localization is destructive interference of the wave functions and this can also be induced through geometric constraints on the

tunneling rates in the lattice. Such systems allow the construction of flat band states with infinite effective mass (zero kinetic energy) which are insulating. Synthetic flat band crystals have recently been demonstrated in a variety of systems including photonic lattices [67–70], polaritons in etched semiconductor heterostructures [71, 72], ultracold atomic gases in optical lattices [73], surface plasmons [74, 75], and they have been proposed in superconducting resonators [76]. As remarked earlier in this thesis, the photonic systems we tend to consider are inherently lossy, and so a coherent or incoherent drive is required to repopulate the system for a non-vacuum stationary state. The aim of this work then, was to investigate the properties of a geometrically frustrated lattice in the driven-dissipative regime.

4.1.1 The model

The model is a sawtooth lattice – consisting of two one-dimensional sublattices, labelled A and B . Each site in the B sublattice is coupled to its two adjacent sites with some tunneling rate t . Each site in the A sublattice is connected to its two adjacent sites in the B sublattice with some tunneling rate t' , but is *not* connected to other sites in the A sublattice. Both sublattices have an interaction energy U_X and each site has a coherent drive with amplitude $\Omega_{X,i}$, where the label X is A or B denoting the sublattice. The dissipative regime is one where the two sublattices have independent dissipation rates γ_X where again $X = A, B$, and each site is dissipatively coupled to its own independent bath. The model is shown diagrammatically in fig. 4.1.

In the site basis the Hamiltonian for the system is,

$$H = H_0 + H_t + H_U + H_D, \quad (4.1)$$

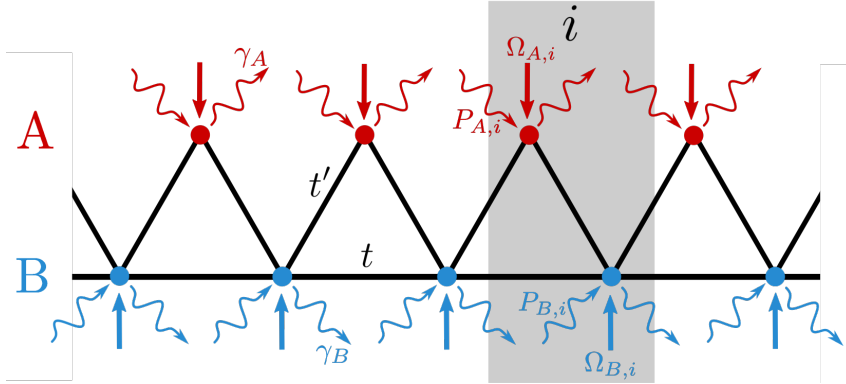


Figure 4.1: The lattice with tunneling rates t and t' along with the labeling of the A and B sublattices and the unit cell i . Excitations dissipate at a rate $\gamma_{A(B)}$ from the individual sites of the $A(B)$ sublattice and coherent or incoherent drives are applied with amplitude $\Omega_{X,i}$ or intensity $P_{X,i}$, where $X = A, B$). Reproduced from reference [7].

where,

$$H_0 = \sum_i \omega_0 (\hat{a}_i^\dagger \hat{a}_i + \hat{b}_i^\dagger \hat{b}_i), \quad (4.2)$$

$$H_t = \sum_i \left[t(\hat{b}_{i-1}^\dagger \hat{b}_i + \hat{b}_{i-1} \hat{b}_i^\dagger) + t'(\hat{b}_i^\dagger \hat{a}_i + \hat{b}_i^\dagger \hat{a}_{i-1} + \hat{b}_i \hat{a}_{i-1}^\dagger + \hat{b}_i \hat{a}_i^\dagger) \right], \quad (4.3)$$

$$H_U = \sum_i \left[U_A \hat{a}_i^\dagger \hat{a}_i^\dagger \hat{a}_i \hat{a}_i + U_B \hat{b}_i^\dagger \hat{b}_i^\dagger \hat{b}_i \hat{b}_i \right], \quad (4.4)$$

where ω_0 is some on-site energy (setting $\hbar = 1$ and working in terms of frequencies), and $\hat{a}_i(\hat{b}_i)$ is the bosonic annihilation operator for the site i on sublattice $A(B)$. We defer specification of the driving Hamiltonian, H_D , until after we have introduced the Wannier basis since we intend to drive a Wannier state directly. The master equation then has the standard Lindblad form,

$$\begin{aligned} \dot{\rho} = -i[H, \rho] &+ \frac{\gamma_A}{2} \sum_i \left[2\hat{a}_i \rho \hat{a}_i^\dagger - \{\hat{a}_i^\dagger \hat{a}_i, \rho\} \right] \\ &+ \frac{\gamma_B}{2} \sum_i \left[2\hat{b}_i \rho \hat{b}_i^\dagger - \{\hat{b}_i^\dagger \hat{b}_i, \rho\} \right]. \end{aligned} \quad (4.5)$$

In the non-interacting regime ($U_A = U_B = 0$), the undriven Hamiltonian given by $H_0 + H_t$ can be written in terms of decoupled Bloch modes with

frequencies given by,

$$E_k = \omega_0 + t \cos k \pm \sqrt{t^2 \cos^2 k + 2t'^2(1 + \cos k)}. \quad (4.6)$$

If we take the limit $t' \rightarrow \sqrt{2}t$ we find,

$$E_k = \omega_0 + t \cos k \pm (t \cos k + 2t), \quad (4.7)$$

which yields a flat lower band at $E_{k,-} = \omega_0 - 2t$ and a $2t$ gap to the dispersive band, $E_{k,+} = \omega_0 + 2t + 2t \cos k$. This is the geometrically frustrated regime, in which the kinetic energy of the flat band is quenched. We can most easily represent (and investigate) the system in this frustrated state using Wannier states. The Wannier bands are pictured in fig. 4.2.

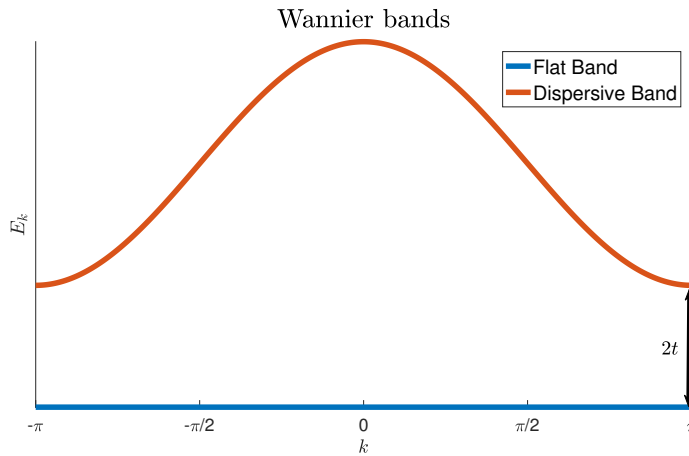


Figure 4.2: A schematic diagram of the Wannier flat and dispersive bands. A gap of $2t$ exists between the flat band, and the lowest energy point of the dispersive band.

4.1.2 Wannier basis

The Wannier basis is an orthogonal set of states defined by the summation of Bloch states for individual bands in a lattice [77]. For a sufficiently large band gap, $2t \gg g_{k,i}^a, g_{k,i}^b, w_A, w_B$, where $g_{k,i}^{a(b)}$ is the coupling strength between the A(B) sublattice and the environment, we can neglect the dispersive band. In

which case the tight-binding bosonic operators can then be expressed as,

$$\hat{a}_i^\dagger = \sum_j w_A(r_i - r_j) W_j^\dagger, \quad (4.8)$$

$$\hat{b}_i^\dagger = \sum_j w_B(r_i - r_j) W_j^\dagger, \quad (4.9)$$

where,

$$w_A(r) = \frac{\sqrt{2}}{2\pi} \int_{-\pi}^{\pi} \frac{\cos\left(\frac{k}{2}\right) e^{-ikr} e^{ik/2}}{\sqrt{\cos(k) + 2}} dk, \quad (4.10)$$

$$w_B(r) = \frac{-1}{2\pi} \int_{-\pi}^{\pi} \frac{e^{-ikr}}{\sqrt{\cos(k) + 2}} dk, \quad (4.11)$$

and W_j annihilates an excitation in the flat-band Wannier basis which is exponentially localized on the unit cell j .

We may then write our master equation, eq. (4.5), as

$$\dot{\rho} = -i[H_W, \rho] + \frac{1}{2} \sum_{j,l} \gamma_l \left[2W_j \rho W_{j+l}^\dagger - \left\{ W_{j+l}^\dagger W_j, \rho \right\} \right], \quad (4.12)$$

where the Hamiltonian is now,

$$H_W = H_{0,W} + H_{\Omega,W} + H_{U,W}, \quad (4.13)$$

and where,

$$H_{0,W} = \sum_i \Delta W_i^\dagger W_i, \quad (4.14)$$

$$H_{\Omega,W} = \sum_i \left[\Omega_{W,i} W_i + \Omega_{W,i}^* W_i^\dagger \right], \quad (4.15)$$

where we have again moved into the rotating frame, such that the detuning of the drive from the flat band is $\Delta = \omega_0 - 2t - \omega_D$, and neglected rapidly rotating terms in H_Ω . We set the coherent drive amplitude such that,

$$\Omega_{W,i} W_i = \sum_j [\Omega_{A,j} w_A(r_i - r_j) + \Omega_{B,j} w_B(r_i - r_j)] W_i. \quad (4.16)$$

CHAPTER 4. FRUSTRATED LATTICES

The interaction term $H_{U,W}$ is given by substituting eqs. (4.8) to (4.11) in to eq. (4.4) yielding,

$$H_{U,W} = \sum_i \sum_{j',l',m'} \left(U_{j',l',m'}^{\text{eff},A} + U_{j',l',m'}^{\text{eff},B} \right) W_i^\dagger W_{i+j'}^\dagger W_{i+l'} W_{i+m'}, \quad (4.17)$$

where,

$$\begin{aligned} U_{j',l',m'}^{\text{eff},A} &= \frac{4U_A}{(2\pi)^3} \int_{-\pi}^{\pi} \int_{-\pi}^{\pi} \int_{-\pi}^{\pi} dk' dq dq' \frac{e^{ik'j'} e^{iql'} e^{iq'm'}}{\mathcal{N}(k', q, q')} \Pi\left(\frac{k' + q + q'}{2\pi}\right) \\ &\times \cos[(k' + q + q')/2] \cos(k'/2) \cos(q/2) \cos(q'/2), \end{aligned} \quad (4.18)$$

$$U_{j',l',m'}^{\text{eff},B} = \frac{U_B}{(2\pi)^3} \int_{-\pi}^{\pi} \int_{-\pi}^{\pi} \int_{-\pi}^{\pi} dk' dq dq' \frac{e^{ik'j'} e^{iql'} e^{iq'm'}}{\mathcal{N}(k', q, q')} \Pi\left(\frac{k' + q + q'}{2\pi}\right) \quad (4.19)$$

and where,

$$\mathcal{N}(k', q, q') = \sqrt{[\cos(k' + q + q') + 2] (\cos k' + 2) (\cos q + 2) (\cos q' + 2)}, \quad (4.20)$$

and $\Pi(x)$ is the rectangle function. It is given by,

$$\Pi(x) = \begin{cases} 0, & |x| > \frac{1}{2}, \\ 1, & |x| < \frac{1}{2}, \\ \frac{1}{2}, & |x| = \frac{1}{2}, \end{cases} \quad (4.21)$$

so in eq. (4.20) it serves to ensure that only values of $k' + q + q'$ between $-\pi$ and π are counted.

The Wannier basis dissipation coefficient is given by,

$$\gamma_l = \sum_i \sum_{x=A,B} \gamma_x w_x(r_i) w_x(r_i - r_l), \quad (4.22)$$

which can be simplified to,

$$\frac{\gamma_l}{\gamma_A} = (2f_0 + f_1) - (1 - \kappa)f_0, \quad \text{for } l = 0, \quad (4.23)$$

$$\frac{\gamma_l}{\gamma_A} = -(1 - \kappa)f_l, \quad \text{for } l \neq 0, \quad (4.24)$$

where $f_l = (\sqrt{3} - 2)^{|l|}/\sqrt{3}$, $f_l = f_{-l}$ and $\kappa = \gamma_B/\gamma_A$, so that the dissipation is entirely local when $\kappa = 1$.

Having defined our model in the Wannier basis, we will first consider results from the non-interacting regime, where $U_A = U_B = 0$.

4.2 Non-interacting regime

In this regime the master equation eq. (4.12) can be solved using Ehrenfest's theorem [78, 79],

$$\begin{aligned} \frac{d}{dt}\langle\hat{O}\rangle &= \langle\hat{O}\dot{\rho}\rangle, \\ &= \text{Tr}\left\{-i\hat{O}[H_W, \rho] + \hat{O}\mathcal{D}(W)\right\}, \end{aligned} \quad (4.25)$$

where \hat{O} is the operator for some observable of the system, and $\mathcal{D}(x) = (\gamma/2)\sum_j 2x_j\rho x_j^\dagger - \{x_j^\dagger x_j, \rho\}$ is the Lindblad-form dissipator. From Ehrenfest's theorem we find the following equations of motion,

$$\frac{d}{dt}\langle W_i \rangle = -\frac{i}{2}\Omega_W^*\delta_{i,0} - \sum_l \gamma_l \langle W_{i+l} \rangle, \quad (4.26)$$

$$\begin{aligned} \frac{d}{dt}\langle W_i^\dagger W_{i+j} \rangle &= \frac{i}{2}\langle \Omega_W \delta_{i,0} W_{i+j} - \Omega_W^* \delta_{i+j,0} W_i^\dagger \rangle \\ &\quad - \frac{1}{2} \sum_l \gamma_l (\langle W_{i+l}^\dagger W_{i+j} \rangle + \langle W_i^\dagger W_{i+j-l} \rangle), \end{aligned} \quad (4.27)$$

where the Kronecker delta, $\delta_{i,0}$, in the drive term indicates that the system is driven only in a single Wannier state which we label zero. Equations (4.26) and (4.27) provide a set of coupled equations which we solve numerically. A cutoff is applied to both the nonlocal dissipation coefficient γ_l , which decays exponentially with l , and to the correlations which we expect to be negligible at very long range. As such we make the approximations that $\gamma_l = 0$ for $l > 10$, and that $\langle W_i^\dagger W_{i+j} \rangle = 0$ for $j > 10$.

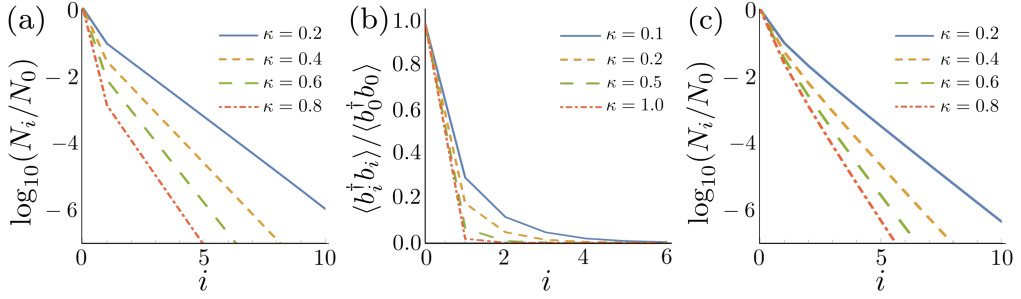


Figure 4.3: Results from finding the stationary state in the non-interacting regime. (a) Normalized excitation density in the Wannier basis for coherent drive with amplitude $\Omega_W = \gamma_A$ at the $i = 0$ Wannier state. (b) Normalized density of the B sublattice. (c) Normalized density with an incoherent pump with intensity $P_{B,i=0} = \gamma_A/100$.

4.2.1 Dissipation-induced mobility

In fig. 4.3 we see results from solving eqs. (4.26) and (4.27). Figure 4.3 (a) shows the density of Wannier state excitations, normalized by the density on the pumped site, $i = 0$. It can be seen that in spite of the lack of coherent transport processes, in the steady state the density is found to be non-zero away from the pumped site. This effect is also shown in fig. 4.3 (b) which shows the B sublattice density $\langle \hat{b}_i^\dagger \hat{b}_i \rangle$. Recall that the Wannier drive amplitude is given by eq. (4.16), so in the lattice site basis the drive amplitudes $\Omega_{A,i}$ and $\Omega_{B,i}$ are non-zero for $i \neq 0$, however the density profile widens noticeably as κ tends to zero, increasing the amount of nonlocal dissipation, indicating that the effect is not simply an artifact of transformation into the Wannier basis.

In the Wannier basis the density decays exponentially from the driven site, and can be approximated by,

$$N_i = e^{-\frac{|r_i|}{\xi}}, \quad (4.28)$$

in turn allowing one to extract a decay length $\xi_i = |\log_{10} N_i - \log_{10} N_{i+1}|^{-1}$. This decay length is shown in fig. 4.4 for $i = 4$. Recalling eqs. (4.23) and (4.24), as κ decreases, the nonlocal dissipation rates γ_l increase, leading to a divergence in the decay length as $\kappa \rightarrow 0$. In this limit, the B sublattice dissipation

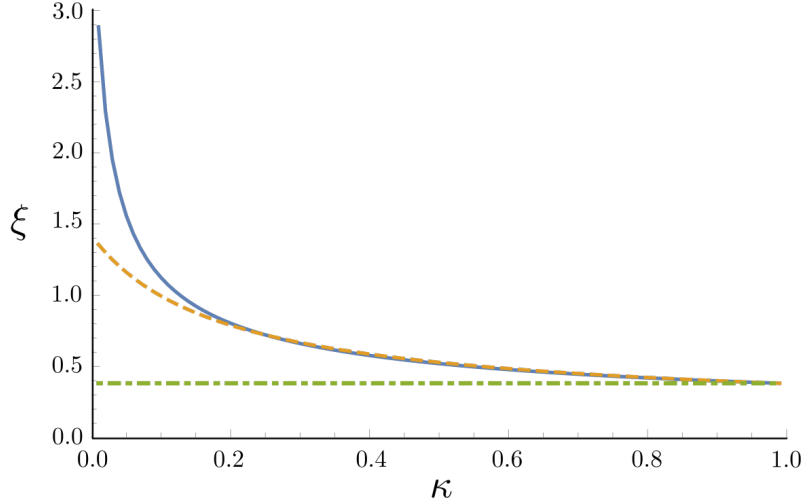


Figure 4.4: Decay length of the density profile $\xi_i = |\log_{10} N_i - \log_{10} N_{i+1}|^{-1}$ for $i = 4$ as a function of $\kappa = \gamma_B/\gamma_A$. The solid line gives the results of the exact model, the dashed line of the effective drive model, and the dot-dashed line of the direct coupling model. In all three models the Wannier state W_0 was driven with amplitude $\Omega_W = \gamma_A$.

rate tends to zero and the dark state $\sum_i (-1)^i W_i^\dagger |0\rangle = \sum_i (-1)^i \hat{b}_i^\dagger |0\rangle$ forms. This dark state extends over the entire lattice, hence the divergence in ξ . The limit $\kappa \rightarrow \infty$, where the A sublattice dissipation rate tends to zero, is inaccessible with the driving mechanism we use, as the corresponding dark state $\sum_i (-1)^i \hat{a}_i^\dagger |0\rangle$ would involve contributions from the dispersive band.

4.2.2 Long range first order coherences

In the coherently driven system the first order coherence,

$$g^{(1)}(j, l) = \frac{\langle W_j^\dagger W_l \rangle}{\sqrt{\langle W_j^\dagger W_j \rangle \langle W_l^\dagger W_l \rangle}}, \quad (4.29)$$

is perfectly correlated with $g^{(1)}(j, l) = (-1)^{|j-l|}$ as the density matrix is a product of coherent states with alternating phases. Long range first order coherence therefore exists in spite of the exponentially decaying density profile. This is indicative of a condensate whose extension is the decay length ξ of the

spatial density profile.

In order to check that the coherence we find is not simply inherited from the coherent drive, we replace the coherent drive in the Wannier basis (setting $\Omega_W = 0$) with an incoherent pump in the site basis of the form,

$$\mathcal{L}_{\text{pump}} = \sum_i \left[\frac{P_{A,i}}{2} \left(2\hat{a}_i^\dagger \rho \hat{a}_i - \{\hat{a}_i \hat{a}_i^\dagger, \rho\} \right) + \frac{P_{B,i}}{2} \left(2\hat{b}_i^\dagger \rho \hat{b}_i - \{\hat{b}_i \hat{b}_i^\dagger, \rho\} \right) \right], \quad (4.30)$$

where $P_{x,i}$ is the intensity of pump on the i^{th} site of the $x = A, B$ sublattice. In fact we pump only the B sublattice and, as with the coherent drive, we pump only one site, $i = 0$. This driving scheme leads to the density profile shown in fig. 4.3 (c), which also shows exponential decay. The resulting first order coherences are shown in fig. 4.5, and we see that the dissipation-induced mobility continues to generate significant coherences, even without coherent input. In the Wannier basis the incoherent drive is still localized around site zero, and so suppresses coherence around $g^{(1)}(0, l)$.

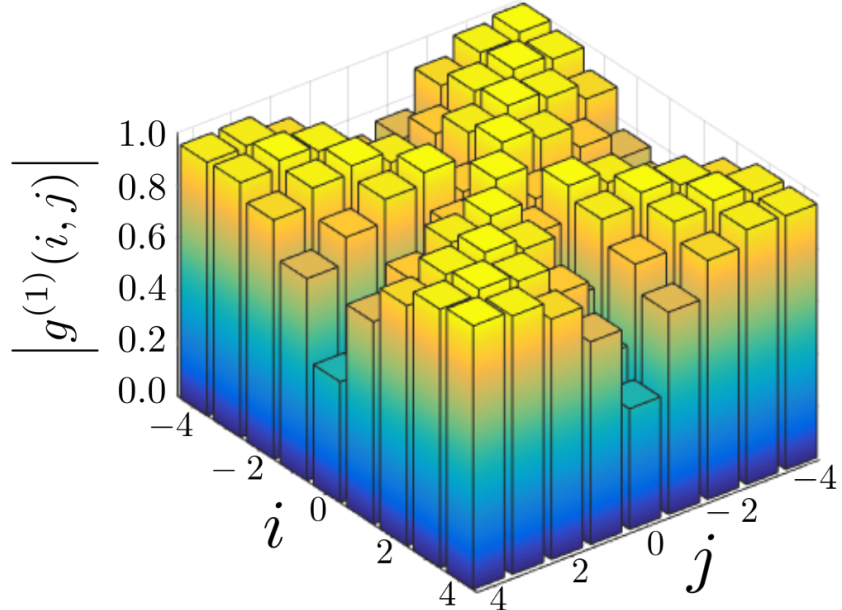


Figure 4.5: Spatial coherences in the steady state $g^{(1)}(i, j)$ for an incoherent pump at $i = 0$ with $P_{B,0} = \gamma_A/100$ and $\kappa = 0.1$. These results were again obtained by numerical solution of the Ehrenfest equations (4.26) and (4.27).

4.2.3 Modeling the decay length of the dissipation-induced mobility

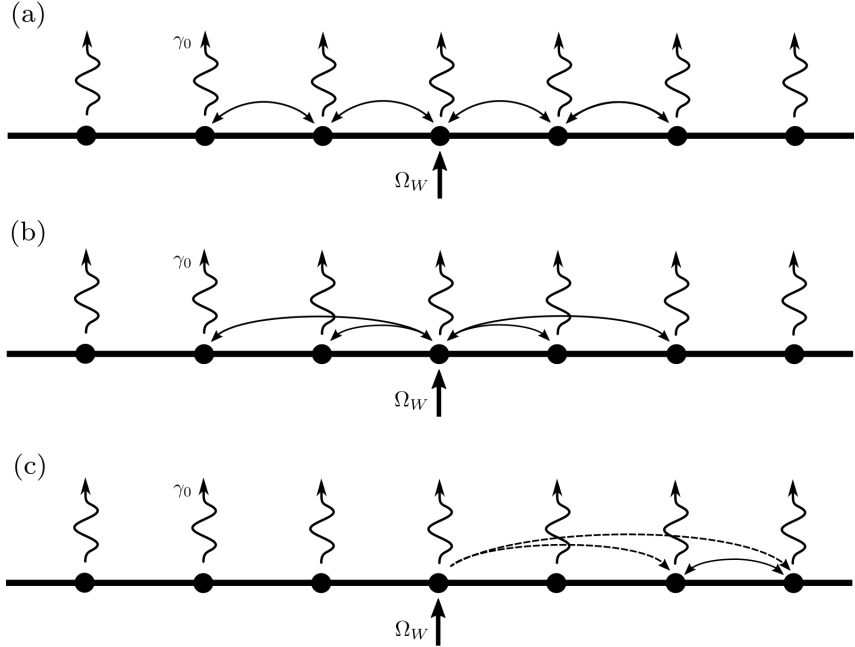


Figure 4.6: Diagrammatic representations of the models we consider to explain dissipation-induced mobility in the non-interacting regime. The central site is pumped with a drive of strength $\Omega_{W,0}$ and there is a dissipation rate γ_0 on each site. (a) The single-site diffusion model assumes that only tunneling between neighbouring sites is important. (b) The direct nonlocal dissipative coupling model, where each site is coupled directly to the pumped site (site 0) by a nonlocal dissipation term. (c) The effective drive model consists of a three-site model where the pumped site is not affected by the two remote, coupled, unpumped sites. Reproduced from reference [7].

In order to clarify that the transport we observe *is* the result of nonlocal dissipation processes, we first attempt to model it as a diffusion process, and compare the decay length of the resulting density profile. This diffusive random walk model, shown diagrammatically in fig. 4.6 (a), has the following continuity equation,

$$\frac{\partial N_i}{\partial t} = - \left. \frac{\partial N_i}{\partial t} \right|_L - \left. \frac{\partial N_i}{\partial t} \right|_R - \Gamma N_i + F(x_i), \quad (4.31)$$

where N_i is the excitation density on the site i , $\partial N_i / \partial t|_{L,R}$ is the number of

excitations on site i moving to the left (L) and right (R), Γ is the dissipation rate, and $F(x_i)$ is a source distribution. The net particle flow to the right, from the site i to the site $i + 1$, in a time interval $\Delta\tau$ is given by,

$$\frac{\partial N_i}{\partial t} \Big|_R = -J \frac{\Delta x}{\Delta\tau} \frac{\partial N_i}{\partial x}, \quad (4.32)$$

where J is the hopping rate between adjacent sites. The same equation holds for $\partial N_i / \partial t|_L$. The diffusion equation is then,

$$\frac{\partial N_i}{\partial t} = J \frac{\Delta x^2}{\Delta\tau} \frac{\partial^2 N_i}{\partial x^2} - \Gamma N_i + F(x_i), \quad (4.33)$$

where $\Delta x^2 / \Delta\tau$ is a scaled diffusion constant D . Without sources, the steady-state solution of eq. (4.33) is,

$$N_i = A e^{-\frac{x_i}{\Xi}} + B e^{\frac{x_i}{\Xi}}, \quad (4.34)$$

where $\Xi = \sqrt{JD/\Gamma}$ is the decay length.

If the dissipative coupling can be modelled as a diffusive process, we should be able to recover the same functional form for the decay length. Assuming $\Gamma \propto \gamma_0$ and $J \propto \gamma_1$ (the $i + 1$ nonlocal dissipation constant) we find,

$$\Xi(\kappa) \propto \sqrt{\frac{\gamma_1}{\gamma_0}} \propto \left(\frac{2f_0 + f_1}{f_0(1 - \kappa)} - 1 \right)^{-\frac{1}{2}}, \quad (4.35)$$

which is plotted in fig. 4.7, and clearly has a different form to the decay length extracted from the exact calculation shown in fig. 4.4. Even if we include the direct nonlocal dissipative coupling of the pump site to remote sites as a source term in eq. (4.33), we find the same functional form for $\Xi(\kappa)$. From this, we conclude that the transport we see cannot be explained by diffusion processes.

We next consider which of the nonlocal dissipative processes contribute most significantly to the mobility by comparing the predicted density distributions for two approximate models, to that which we find by numerically solving the exact model. First we consider an approximation in which we neglect the dissipative coupling between sites which are not pumped. Transport

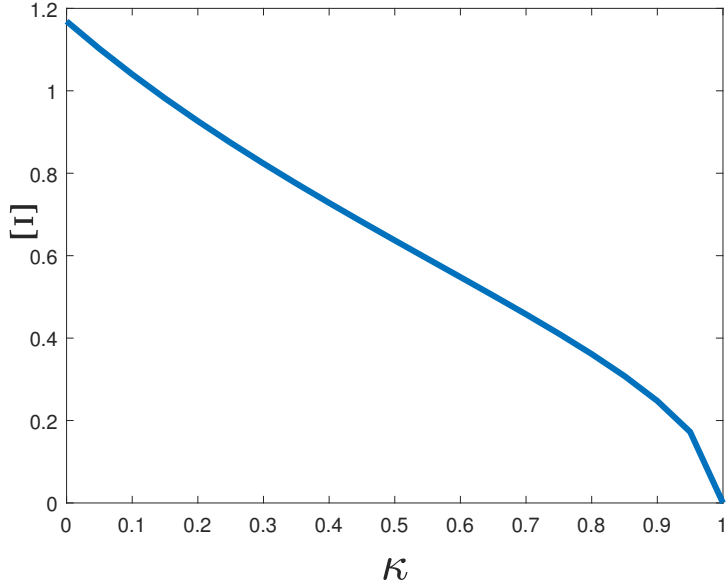


Figure 4.7: Plot of the diffusive decay constant, $\Xi(\kappa) \propto \sqrt{\gamma_1/\gamma_0}$ against κ .

between the pumped site $i = 0$ to any other site, j , is therefore mediated solely by the nonlocal dissipative constant γ_j . This model is shown diagrammatically in fig. 4.6 (b).

The density distribution can be calculated by solving the Ehrenfest equations eqs. (4.26) and (4.27) for a two-site system consisting of site zero and site j , where site zero is pumped with a drive strength Ω_W . Doing so yields,

$$\langle W_j^\dagger W_j \rangle = \frac{\gamma_j^2 |\Omega_W|^2}{4(\gamma_0^2 - \gamma_j^2)^2}, \quad (4.36)$$

$$\approx \frac{\gamma_j^2 |\Omega_W|^2}{4\gamma_0^4}, \quad (4.37)$$

where we justify the approximation $\gamma_0 \gg \gamma_j$ by recalling that the Wannier states are exponentially localized. The decay length in this model is then given by,

$$\xi_\Omega \approx \left[\log_{10} \left(\frac{\gamma_{j+1}^2}{\gamma_j^2} \right) \right]^{-1} \approx 0.38, \quad (4.38)$$

which is plotted as the dot-dashed line in fig. 4.4. It can be seen that in the

limit $\kappa \rightarrow 1$ the nonlocal dissipation rates vanish, and this model predicts the density distribution well.

As an improved approximation we consider a three-site model with nearest neighbour hopping, and sites 0, j , and $j + 1$, where $j > 1$ so that the $j, j + 1$ sites are not directly coupled to the pumped site. This model is shown diagrammatically in fig. 4.6 (c). We are again solving the Ehrenfest equations of motion, and make the assumption that for $i = \{j, j + 1\}$ only the contribution from the pumped site is relevant in eq. (4.26), such that,

$$\sum_{l \neq \{0,1\}} \gamma_l \langle W_{j+l} \rangle \approx \gamma_{-j} \langle W_0 \rangle. \quad (4.39)$$

We also assume that the two unpumped sites $j, j + 1$ do not affect the field amplitude of site zero. This means that it is a constant determined by evaluating the three-site system $i = \{-1, 0, 1\}$. Doing so, we find that

$$\langle W_0 \rangle \approx \frac{-i\gamma_0 \Omega_W^*}{2(\gamma_0^2 - 2\gamma_1^2)}, \quad (4.40)$$

which we can substitute back in to eq. (4.26) in order to solve the $i = \{0, j, j + 1\}$ model. We find that the pumped site acts as an effective drive for the two-site system with coefficients,

$$\Omega_{W,j}^* = \frac{\gamma_0 \gamma_j \Omega_W^*}{\gamma_0^2 - 2\gamma_1^2}, \quad (4.41)$$

$$\Omega_{W,j+1}^* = \frac{\gamma_0 \gamma_{j+1} \Omega_W^*}{\gamma_0^2 - 2\gamma_1^2}, \quad (4.42)$$

which we this time substitute in to eq. (4.27) to determine the approximate density profile of this model. From this we calculate the approximate decay length,

$$\xi \approx \left[2 \log_{10} \left(\frac{\gamma_0 \gamma_j - \gamma_1 \gamma_{j+1}}{\gamma_1 \gamma_j - \gamma_0 \gamma_{j+1}} \right) \right]^{-1}, \quad (4.43)$$

which is plotted as the dashed line in fig. 4.4. This approximation works well for a wide range of nonlocal dissipation strengths, but breaks down as $\kappa \rightarrow 0$. This is due to multiple hopping processes not being included in the model.

We conclude that for $\kappa \approx 1$, where the Wannier states are decoupled, direct dissipative coupling between the pumped site and each other site plays the most significant role. As κ decreases transfer of particles from neighbouring sites plays an increasing role, and as κ decreases further the extent of these significant interactions increases to next-nearest neighbour and beyond.

4.3 Strongly interacting regime

We next consider the interacting regime, which in the Wannier basis results in nonlocal terms, like those in the dissipator. The exact form of the interaction term in the Wannier basis Hamiltonian is given in eqs. (4.17) to (4.20). Such nonlocal terms can also result in transport, a phenomenon which has been explored in detail [80–84]. This is suppressed in the limit of very strong interaction, and so it is this limit we explore in order to explore the effect of dissipation. The very strong interaction limit is also advantageous as it allows us to truncate to the single excitation subspace. To facilitate this truncation we calculated the second-order correlation function for the pumped site $\langle W_0^\dagger W_0^\dagger W_0 W_0 \rangle$ under the assumption that the pumped site is completely decoupled. This gives an upper bound on the probability that the pumped site, which will always have the highest density, has at least two excitations. This correlation function can be calculated exactly using an approach by Drummond and Walls [85, 86], the result of which is plotted in fig. 4.8 as a function of $U_0/\Omega_{W,0}$ and $\gamma_0/\Omega_{W,0}$ where $U_0 = U_{0,0,0}^{\text{eff},A} + U_{0,0,0}^{\text{eff},B}$. This allows us to select a regime where the double-excitation probability on site zero is much lower than the density on the adjacent sites, $\langle W_0^\dagger W_0^\dagger W_0 W_0 \rangle < \langle W_1^\dagger W_1 \rangle$, validating the truncation to the single-excitation subspace.

In principle the nonlocal terms in eq. (4.17) extend infinitely across the lattice, but clearly it is computationally infeasible to include all of them. Therefore we calculated the coefficients $U_{j',l',m'}^{\text{eff},A}$ and $U_{j',l',m'}^{\text{eff},B}$ for all Wannier interaction terms in the single-excitation subspace. After doing so, we find the leading order values given in table 4.1 below. It is clear that interactions on the B sublattice make a much more significant contribution to interactions in the Wannier basis than those on the A sublattice. For this reason, we choose $U_A = 0$.

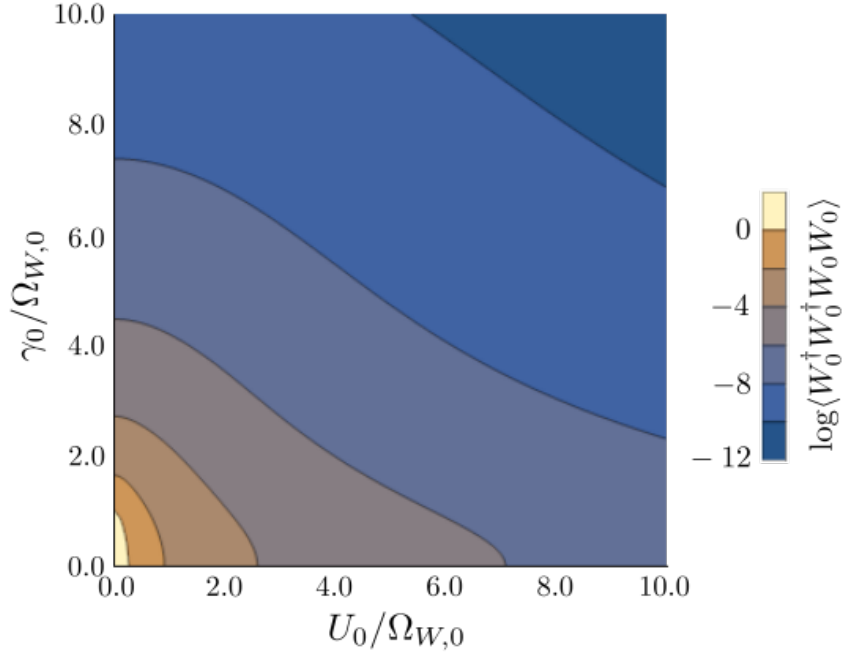


Figure 4.8: Second-order correlation function for the pumped site $\log(\langle W_0^\dagger W_0^\dagger W_0 W_0 \rangle)$ with coherent and incoherent transfer processes set to zero. Excitations cannot leave the pumped site, so we consider that the second order correlation function gives the maximum possible probability of double occupation.

Additionally we have applied a cut-off at $U_{j',l',m'}^{\text{eff},B}/U_B < 0.01$ which allows us to truncate nonlocal interactions to an extent of two lattice sites. Finally, to determine the coefficients for implementation we must take in to account multiplicity due to symmetries in $U_{j',l',m'}^{\text{eff},B}$. There is a fourfold multiplicity in the cross-Kerr interactions with $\{j', l', m'\} = \{1, 1, 0\}, \{2, 2, 0\}$, and a twofold multiplicity in the density-assisted tunneling term with $\{j', l', m'\} = \{-1, 0, 1\}$.

The Wannier basis interaction term we intend to implement is then given by,

$$H_{W,U} \approx \sum_i \left[0.192U_B W_i^\dagger W_i^\dagger W_i W_i + 0.133U_B W_i^\dagger W_i W_{i+1}^\dagger W_{i+1} + 0.054U_B W_i^\dagger W_i W_{i+2}^\dagger W_{i+2} + 0.023U_B (W_{i-1}^\dagger W_i^\dagger W_i W_{i+1} + W_{i-1} W_i^\dagger W_i W_{i+1}^\dagger) \right], \quad (4.44)$$

$\{j', l', m'\}$	$U_{j', l', m'}^{\text{eff}, A}/U_A$	$\{j', l', m'\}$	$U_{j', l', m'}^{\text{eff}, B}/U_B$
{0,0,0}	0.028032	{0,0,0}	0.191937
{1,1,0}	0.007568	{1,1,0}	0.033196
{2,1,0}	0.000748	{2,2,0}	0.013613
{2,2,0}	0.000582	{-1,0,1}	0.011298

Table 4.1: The leading order values of the Wannier lattice interaction coefficients $U_{j', l', m'}^{\text{eff}, A}$ and $U_{j', l', m'}^{\text{eff}, B}$ in terms of the site basis coefficients for the A and B sublattices, U_A and U_B . It is clear that interaction in the B sublattice makes a more significant contribution.

where we note that we require $U_B \gtrsim 10$ to make the single-excitation subspace truncation, as from fig. 4.8 this takes us into the region where $\langle W_0^\dagger W_0^\dagger W_0 W_0 \rangle \lesssim 10^{-3}$, when we have set $\Omega_{W,0} = \gamma_0 = 1$.

4.3.1 MPO design

Now that we have the complete form of the master equation for the strongly interacting regime,

$$\dot{\rho} = -i [H, \rho] + \frac{1}{2} \sum_{j,l=-3}^{l=3} \gamma_l \left[2W_j \rho W_{j+l}^\dagger - \{W_{j+l}^\dagger W_j, \rho\} \right], \quad (4.45)$$

where we note that we have truncated the nonlocal dissipators to $l = 3$, and where,

$$\begin{aligned} H = & \sum_i \left[\Delta W_i^\dagger W_i + \frac{\Omega_{W,i}}{2} W_i + \frac{\Omega_{W,i}^*}{2} W_i^\dagger \right] \\ & + \sum_i \left[U_{0,0,0}^{\text{eff}, B} W_i^\dagger W_i^\dagger W_i W_i + 4U_{1,1,0}^{\text{eff}, B} W_i^\dagger W_i W_{i+1}^\dagger W_{i+1} \right. \\ & + 4U_{2,2,0}^{\text{eff}, B} W_i^\dagger W_i W_{i+2}^\dagger W_{i+2} \\ & \left. + 2U_{-1,0,1}^{\text{eff}, B} (W_{i-1}^\dagger W_i^\dagger W_i W_{i+1} + W_{i-1} W_i^\dagger W_i W_{i+1}^\dagger) \right], \end{aligned} \quad (4.46)$$

which, as a consequence of the nonlocal terms in both the Hamiltonian and the dissipator, is highly non-trivial to represent as an MPO. Designing the MPO for this system, as well as writing the variational stationary state code, was my most significant contribution to this publication.

To begin the process of designing the MPO we recall that we in fact require an MPO representation of the Liouvillian matrix,

$$\begin{aligned} \mathcal{L} = & \mathbb{I} \otimes -iH + iH^T \otimes \mathbb{I} \\ & + \frac{1}{2} \sum_{j,l=-3}^{l=3} \gamma_l \left[W_{j+l}^* \otimes 2W_j - \mathbb{I} \otimes W_{j+l}^\dagger W_j - W_j^T W_{j+l}^* \otimes \mathbb{I} \right], \end{aligned} \quad (4.47)$$

which contains 22 unique operator combinations which must be accounted for. Here we have used the relation $(AB)^T = B^T A^T$, and since the operator W_j is a normal bosonic creation operator we expect it to be real, and therefore $W^T = W^\dagger$ and $W^* = W$.

The bulk-site matrix product operator is stated in full in table B.1 in appendix B. The MPO had a virtual dimension of 27×27 for the representation of \mathcal{L} , and hence 729×729 for $\mathcal{L}^\dagger \mathcal{L}$ which proved more effective in spite of the additional computational effort. In part the large size was due to the inclusion of interaction terms with $\{j', l', m'\} = \{2, 1, 0\}$, which appear in the leading order values for $U_{j',l',m'}^{\text{eff},A}/U_A$ in table 4.1, and were close to appearing in the B sublattice coefficients, with $U_{2,1,0}^{\text{eff},B}/U_B = 0.009605$. It was therefore included in some initial calculations to check that both setting $U_A = 0$, and neglecting $U_{2,1,0}^{\text{eff},B}$ did not have a significant effect on the results. These terms' inclusion created an additional 8 unique operator combinations, which were later excluded simply by setting $U_A = U_{2,1,0}^{\text{eff},B} = 0$ rather than modifying the form of the MPO. The correctness of the MPO was tested by comparing results from exact calculations and variational searches on a small system.

4.3.2 Density and coherence

Having designed and tested the MPO we were able to begin using the `mpostat` code to find the stationary state. It is worth remarking that these calculations

were performed in late 2016, and consequently performed using a much earlier version of the code. Notably the approach, due to Mascarenhas [4], of beginning with some very small matrix dimension χ and steadily increasing it while decreasing the convergence threshold had yet to be implemented. This is now precisely what the top-level function `PhasedSearch` does, but at the time we had to make do with simply setting the matrix dimensions large enough. I do not doubt the veracity of these results – testing has existed in `mpostat` for as long as a working version has, but I suspect that the current version of the code would make lighter work of these calculations.

The steady-state density distribution is shown in fig. 4.9 (a) for a system driven on site $i = 0$ with drive amplitude $\Omega_{W,0} = \gamma_A = 1$, and $\kappa = \gamma_B/\gamma_A = 0.2$, for three different values of the nearest neighbour cross-Kerr interaction strength $U_1 \approx 0.133U_B$. In contrast to results from the non-interacting regime, the density distribution does not decay exponentially away from the pumped site. This means we can no longer consider the density decay length, so to study how interactions affect the dissipation-induced mobility we now instead use the fraction of excitations in the unpumped Wannier states as the figure of merit. This value, $f = (\sum_{i \neq 0} N_i) / (\sum_i N_i)$ is shown in fig. 4.9 (b) as a function of κ , again for a range of U_1 values. We find that for some fixed κ mobility decreases with increasing interaction strength, which we attribute to the cross-Kerr interactions which shift the energy of the neighbouring site, detuning the nonlocal dissipative transition and preventing transport between sites. We find that the density assisted tunneling term is insignificant, as removing it from the calculation leads to a variation in f only of order 10^{-2} . It is also clear from fig. 4.9 (b) that the dependence of mobility on the cross-Kerr interaction strength U_1 is significantly weaker than its dependence on κ . This indicates that nonlocal dissipation is the dominant contributor in the steady state of the system in the strongly interacting limit.

Finally, we considered first order coherence in the strongly interacting regime. Figure 4.10 shows that, similarly to fig. 4.5 which showed coherences with an incoherent pump in the non-interacting regime, interactions counteract the buildup of first order coherence. As the density is highest on the pumped site, it is there that interactions are most significant, and coherences most heav-

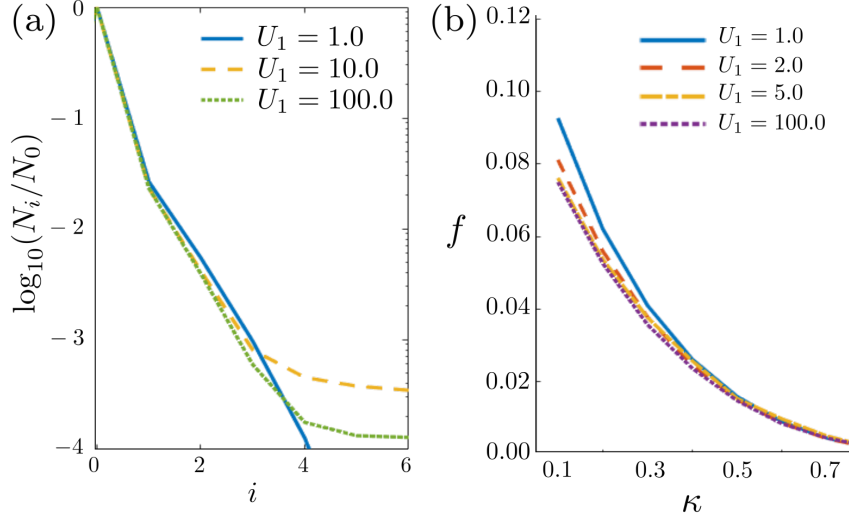


Figure 4.9: (a) Normalized steady-state density of excitations in the Wannier basis for the interacting regime and a single driven Wannier state at $i = 0$, $\Omega_{W,0} = \gamma_A$, and $\kappa = 0.2$ [c.f. fig. 4.3 (a)]. (b) Fraction of excitations not on the pumped site f as a function of the dissipation rate asymmetry ratio κ for an interacting system with a cross-Kerr interaction strength U_1 .

ily suppressed. Nevertheless, the buildup of coherences between other sites in the system indicates that as a phenomenon, the generation of coherences due to dissipation-induced mobility is not limited to non-interacting systems.

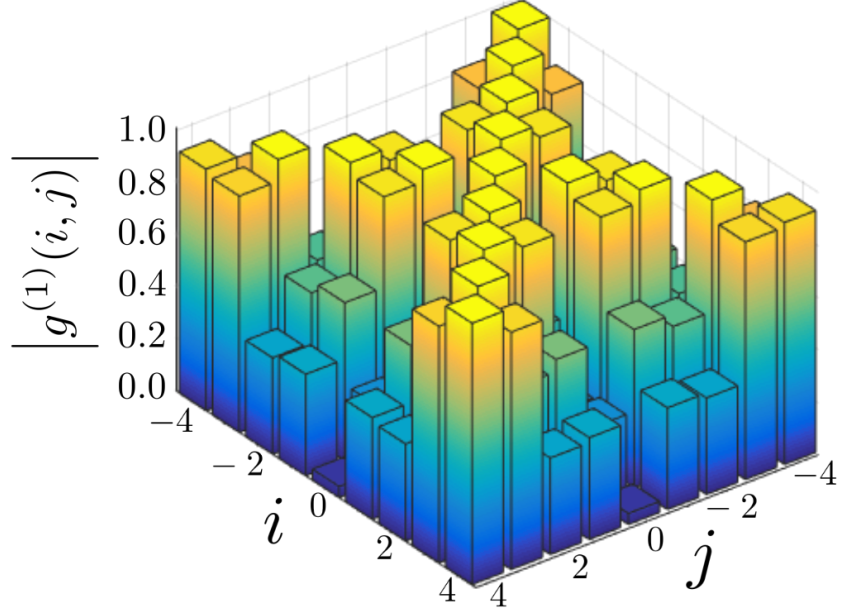


Figure 4.10: Spatial coherences in the steady state, $g^{(1)}(j, l)$ for a coherent drive at $i = 0$ with $\Omega_W = \gamma_A$ and $\kappa = 0.1$, in the strongly interacting regime with $U_1 = 100$.

4.4 Conclusions

Our results show that local Markovian dissipation can induce mobility and long range coherence in frustrated lattice systems in the absence of kinetic energy. This effect could be experimentally realised in any driven-dissipative lattice with a flat band, for example, a photonic waveguide lattice [69]. In such a system, couplings between sites can be engineered to realise a flat-band system where defects and disorder are low enough to not affect lattice excitation dynamics. Neighbouring waveguides can be used to simulate local Markovian baths with a strong degree of control over the environmental dynamics, as has been recently demonstrated [87]. An imbalance in the dissipation rates of A and B sublattices could be engineered via Purcell enhancements. An interesting extension to this work would be to study the effect dynamically, rather than in the steady state. Varying the imbalance in dissipation rates, κ , would change the rate at which a localized excitation would disperse across the lattice. Again, photonic waveguide lattices would be well-suited for such

CHAPTER 4. FRUSTRATED LATTICES

an experiment [69].

This research represented the first real test of the `mpostat` code, and although not as well optimised as it is now, performance was adequate. The nonlocal terms in the model made this system challenging, but also well-suited to the variational search technique. It would have been difficult to use time-evolving block decimation for example, as this relies on multi-site gates covering the extent of the interactions.

Chapter 5

Localization to delocalization crossover in a driven nonlinear cavity array

In this chapter we will discuss the article ‘Localization to delocalization crossover in a driven nonlinear cavity array’ [8]. In this work we studied a nonlinear cavity array where the dissipation rate in each cavity increased with the excitation number. It was shown that with a coherent parametric drive such arrays can be driven into incompressible states with commensurate filling – a non-equilibrium analogue of the Mott insulating state. We explore the boundaries of this Mott insulating phase and the crossover to a delocalized phase with spontaneous first order coherence. This crossover is similar to the equilibrium Mott insulator to superfluid phase transition, but we also find marked differences in the phase-diagrams. In particular, in this system, the off-diagonal order does not become long range.

As ever we will begin by discussing the motivation and theoretical background to the work, followed by a thorough description of the model. We will then go through the results, mostly from TEBD calculations [9], which are presented in the article.

This was the primary research project of my PhD, and it was originally hoped that it could be used to test out the `mpostat` code. Unfortunately, this

was a challenging investigation, and the master equation proved resistant to numerical solution. Ultimately, the matrix dimensions required for solution by variational search were simply too high. Nevertheless, we were able to determine the steady state using time-evolution methods.

5.1 Introduction

Photons are not usually conserved in light-matter interactions. Consequently, there is no chemical potential for photons, and the rich vein of many-body quantum effects in equilibrium systems is seemingly lost to photonics. Some exceptions, where the concept of an effective chemical potential can be meaningfully applied to photons, include photon emission in semiconductors [88], photons in a cavity that couple to excitons and thermalize [89–91], and photons interacting with a nonlinear medium that form a Bose-Einstein condensate [92, 93]. Settings where light-matter interactions can mediate strong photon-photon interactions have garnered significant interest recently, as these allow generation of matter-like phases including photonic fluids [91, 94] and strongly correlated phases [29, 95, 96].

Since photons are bosons, a key question for many-body phenomena in strongly interacting photon or polariton systems is whether a phase transition can be observed from a Mott insulator to a superfluid [97] as it is in Bose-Einstein condensates [19, 98, 99]. Phase diagrams of equilibrium photonic or polaritonic systems have previously been studied by introducing a chemical potential. How such a thing could be physically realised remains an open question [95, 100–102]. In any case, we consider the non-equilibrium setting a more natural one in which to study such systems, given the limited lifetime of photons trapped in a cavity. One approach to that is to use auxiliary systems and specific driving mechanisms to generate an *effective* chemical potential for photons [103–106], allowing one to explore the phase diagram [107].

In this work we show that a Mott insulator phase can be generated in a dissipative nonlinear cavity array using only a coherent parametric drive directly applied to the cavities. We thus explore the crossover from this Mott insulating state to a delocalized phase with incommensurate filling [86, 108–

[113], which exhibits first order coherence between lattice sites. A key feature of the Mott insulator phase is that there is an integer number of excitations on every site, and that number fluctuations are strongly suppressed. However, this cannot be achieved in a nonlinear resonator array which is coherently driven at the frequency of a single excitation. The Mott insulator phase is expected in the limit of very strong nonlinearity, and very weak coupling between sites. In this regime each lattice site may be approximated as a two level system where filling cannot exceed half – a consequence of the depopulation of the upper state under a coherent drive. Additionally, the phase relation between the coherent drive on different lattice sites is fixed. As a result, any phase-coherence between excitations on distant sites could be said to be inherited from the drive [114], and it is unclear whether such coherence forms spontaneously at equilibrium [19, 98, 99].

It is for these reasons that we consider instead a parametric coherent drive, which resonantly drives each cavity from empty to doubly-excited [105, 115], but is detuned from all other transitions. We also include a cascade of decay processes, where the decay from the doubly-excited state to a single excitation state, γ_1 , is much faster than the decay of a single excitation state to the empty state, γ_0 . This arrangement results in a very high probability for the single excitation state on each lattice site to be stationary – the probability approaches unity as $\gamma_0/\gamma_1 \rightarrow 1$. The drive and decay process combine to form an effective incoherent drive from the empty state to the single excitation state. As any excitations in level $|1\rangle$ are generated via the fast decay rate γ_1 , they are insensitive to the coherent nature of the drive, thus allowing us to attribute any first order correlations we find to the formation of a superfluid component. This could be experimentally achieved through Purcell enhancement [24, 25] of the relaxation on a specific transition, through coupling to a lossy resonator [116]. Figure 5.1 shows a sketch of a two site model.

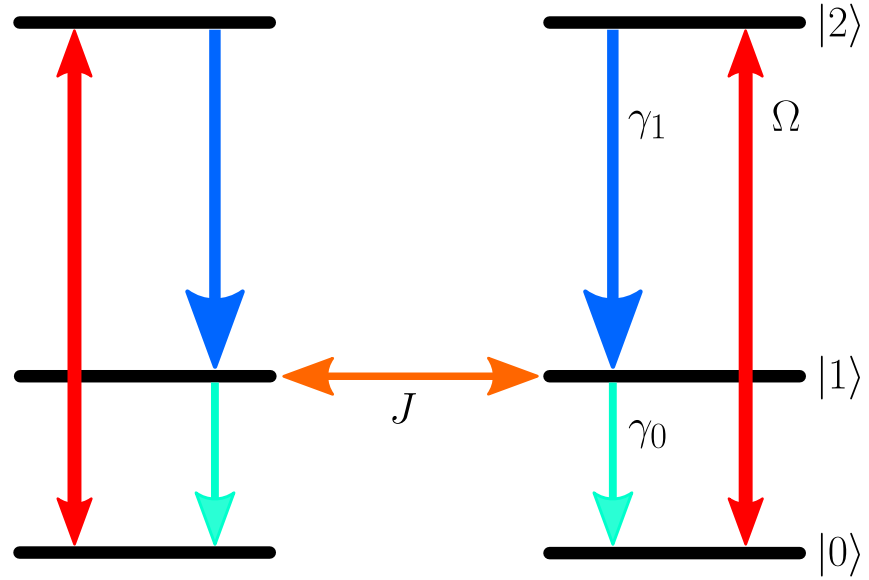


Figure 5.1: A diagram of the two site model, showing states with zero ($|0\rangle$), one ($|1\rangle$), and two ($|2\rangle$) excitations in each cavity, as well as the key parameters. The two sites are coupled by a hopping rate J , there is a coherent parametric drive on each site with amplitude Ω , and there are two dissipative transition rates, $\gamma_1 \gg \gamma_0$.

5.2 The model

We consider a system of N coupled nonlinear cavities in a one-dimensional array, governed by a Bose-Hubbard Hamiltonian, with an additional term for the parametric coherent driving scheme described above. We move into a rotating frame and apply the rotating wave approximation, which is shown in detail in appendix C, and set $\hbar = 1$ to work in units of frequency. Our Hamiltonian then is,

$$\mathcal{H} = \mathcal{H}_0 + \mathcal{H}_J + \mathcal{H}_\Omega, \quad (5.1)$$

where,

$$\mathcal{H}_0 = \sum_j \left[\Delta \hat{a}_j^\dagger \hat{a}_j + \frac{U}{2} \hat{a}_j^\dagger \hat{a}_j^\dagger \hat{a}_j \hat{a}_j \right], \quad (5.2)$$

$$\mathcal{H}_J = -J \sum_j \left[\hat{a}_j \hat{a}_{j+1}^\dagger + \hat{a}_j^\dagger \hat{a}_{j+1} \right], \quad (5.3)$$

$$\mathcal{H}_\Omega = \sum_j \left[\frac{\Omega}{\sqrt{2}} \hat{a}_j^\dagger \hat{a}_j^\dagger + \frac{\Omega^*}{\sqrt{2}} \hat{a}_j \hat{a}_j \right], \quad (5.4)$$

where $\Delta = \omega - \omega_L/2$ is the detuning between the drive laser frequency ω_L , and the cavity frequency ω , U is the interaction strength, J is the hopping rate between sites, and Ω is the amplitude of the drive laser. The drive laser is tuned to the two excitation frequency $\omega_L = 2\omega + U$, so the detuning $\Delta = -U/2$.

The dissipative environment we consider is characterized by a cascade of dissipation rates, so the dissipation rate γ_m from $|m+1\rangle \rightarrow |m\rangle$ is greater than the dissipation rate γ_n from $|n+1\rangle \rightarrow |n\rangle$ where $m > n$. We describe this dissipation with a Lindblad-form master equation,

$$\dot{\rho} = -i [\mathcal{H}, \rho] + \sum_{m \geq 0} \mathcal{D}_m[\rho], \quad (5.5)$$

where,

$$\mathcal{D}_m[\rho] = \frac{\gamma_m}{2} \sum_j^N \left[2\kappa_{m,j} \rho \kappa_{m,j}^\dagger - \left\{ \kappa_{m,j}^\dagger \kappa_{m,j}, \rho \right\} \right], \quad (5.6)$$

where the jump operators $\kappa_{m,j} = |m_j\rangle \langle m+1_j|$. Note that this model assumes that the dissipation is dominated by single particle losses and would reduce to the standard dissipator $\frac{\gamma}{2} \sum_j [2\hat{a}_j \rho \hat{a}_j^\dagger - \{\hat{a}_j^\dagger \hat{a}_j, \rho\}]$ in the limit where all relaxation rates become equal, $\gamma_m = \gamma$. Furthermore, we assume that $U \gg \Omega$ so that the occupation of levels $|m\rangle$ with $m > 2$ is negligible, allowing us to truncate our description to the subspace of at most two excitations on each site.

5.3 Small anharmonic system

We first considered a small exactly solvable model with just three sites and periodic boundary conditions, so that there is a hopping term of the form $-J(\hat{a}_3\hat{a}_1^\dagger + \hat{a}_3^\dagger\hat{a}_1)$ included in the model. This model should tell us something about the behaviour of larger systems in the limit of a small hopping rate between sites $J/\gamma_1 \ll 1$, where we expect long range correlations to be absent. Additionally, we extended the local state space to include up to three excitations per site, in order to test the validity of our truncation to three levels. The stationary state was determined by forming the Liouvillian matrix,

$$\begin{aligned} \hat{L} = & \mathbb{I} \otimes -i\mathcal{H} + i\mathcal{H}^T \otimes \mathbb{I} \\ & + \sum_{m=0,j=1}^{m=2,j=3} \frac{\gamma_m}{2} \left[\kappa_{m,j}^* \otimes 2\kappa_{m,j} - \mathbb{I} \otimes \kappa_{m,j}^\dagger \kappa_{m,j} - \kappa_{m,j}^\dagger \kappa_{m,j} \otimes \mathbb{I} \right], \end{aligned} \quad (5.7)$$

and then replacing the bottom row of the Liouvillian with one which enforces the trace norm condition, $\sum_j \rho_{j,j} = 1$. We can then find the stationary state numerically by solving the system of coupled linear equations,

$$\begin{aligned} \hat{L}|\rho\rangle\rangle &= \bar{S}, \\ \implies |\rho\rangle\rangle &= \hat{L}^{-1}\bar{S}, \end{aligned} \quad (5.8)$$

where $|\rho\rangle\rangle$ is the vectorised density matrix, and \bar{S} is a solution vector which is all-zero except for the last element which corresponds to the trace norm condition.

The equilibrium phase diagram for the Bose-Hubbard model is typically parameterized by the chemical potential and the hopping rate between sites. In our non-equilibrium case, the drive strength and dissipation rates balance out to create an effective chemical potential, so we explore a phase diagram parameterized by the drive strength and hopping rate.

Figure 5.2 shows the density $\langle \hat{n}_2 \rangle$, and its variance $\langle \hat{n}_2^2 \rangle - \langle \hat{n}_2 \rangle^2$ for the second site in this translation invariant system. Both are plotted against the drive strength Ω , and the hopping rate J , for the reasons given above. In fig. 5.2 (a) there is a region bounded by a black line, in which the density

is unity (within 10%), and the density variance is much less than one. This means there is a stationary phase of our model with very similar properties to the Mott insulator phase, though the shape differs somewhat from that found in equilibrium systems [117]. We note that even at the strongest driving we consider here, the density barely exceeds unity, validating our decision to truncate to the subspace of at most two excitations per site in calculations on larger systems.

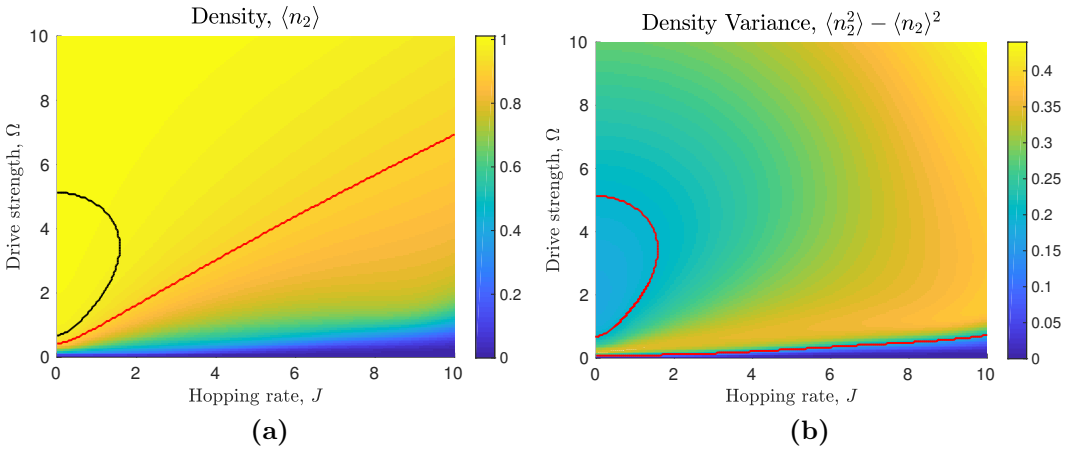


Figure 5.2: (a) The density of one site in a translationally invariant three site system, plotted against drive strength Ω , and coupling strength J . The area above the red line has a density of 1 ± 0.1 . (b) The variance, $\langle \hat{n}_2^2 \rangle - \langle \hat{n}_2 \rangle^2$ over the same parameter range. For this calculation, $\gamma_2 = 10$, $\gamma_1 = 1$, $\gamma_0 = 0.1$, $U = 100$, and so $\Delta = -50$. The area bounded by the red line has a variance of ≤ 0.2 . The area bounded by the black line in panel (a) has both unit density and a density variance $\ll 1$, which we identify with the Mott insulator phase.

For comparison, in fig. 5.3 we consider a schematic phase diagram of the lattice model for interacting bosons in the absence of disorder. It is parameterized by the chemical potential μ , and the hopping rate between sites J . Two phases are pictured on the diagram – Mott insulator, and superfluid. The Mott insulator phase was first predicted in 1937 by Nevill Mott and Rudolf Peierls as an explanation for why certain metal oxides predicted by band theory to be conducting were in fact insulators [118, 119]. In 1989 Fisher et al. showed theoretically that it could also be found in interacting bosonic systems, and this was observed experimentally by Greiner et al. in 2002 [19, 99]. The funda-

mental properties of the MI phase are that it has a density commensurate with the lattice size, and that it is incompressible ($dn/d\mu = 0$), it is this property that we are looking for when considering the variance in fig. 5.2 (b) [120].

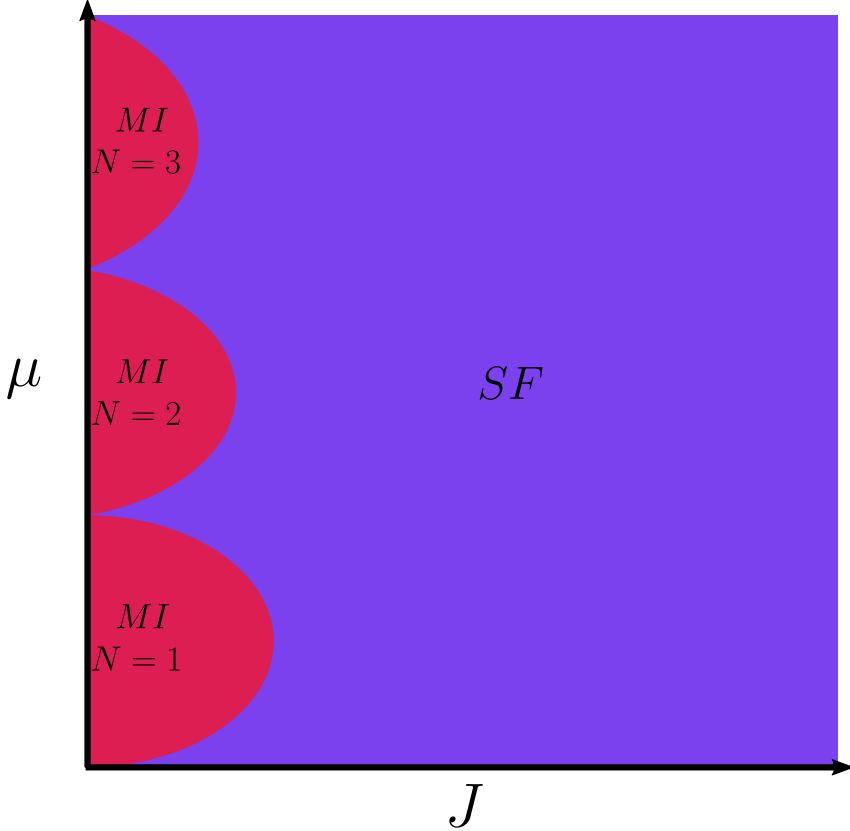


Figure 5.3: A schematic zero-temperature phase diagram for the lattice model of interacting bosons, in the absence of disorder. Based on figure 1 of Fisher et al. [19]. The phase diagram is parameterized by the chemical potential μ , and the hopping rate between sites J . The two phases pictured are the superfluid phase (SF), and three Mott insulator ‘lobes’ (MI).

To further explore the boundaries of the Mott insulator phase in our system, and its predicted crossover to a highly-correlated delocalized phase, we next considered a much larger lattice.

5.4 Large anharmonic system

Here we consider a fifteen site lattice with open boundaries, and up to two excitations per site. We find the stationary state by representing the system with a density matrix product operator, then time-evolving it using the TEBD method [1] until convergence. Figure 5.4 shows the density of the middle site and its variance plotted against drive strength and hopping rate. It can be seen that for strong enough drive the density is near unity, and as with the small system, the variance is much less than one at low hopping rates. The non-equilibrium Mott insulator-like phase survives the increase in system size.

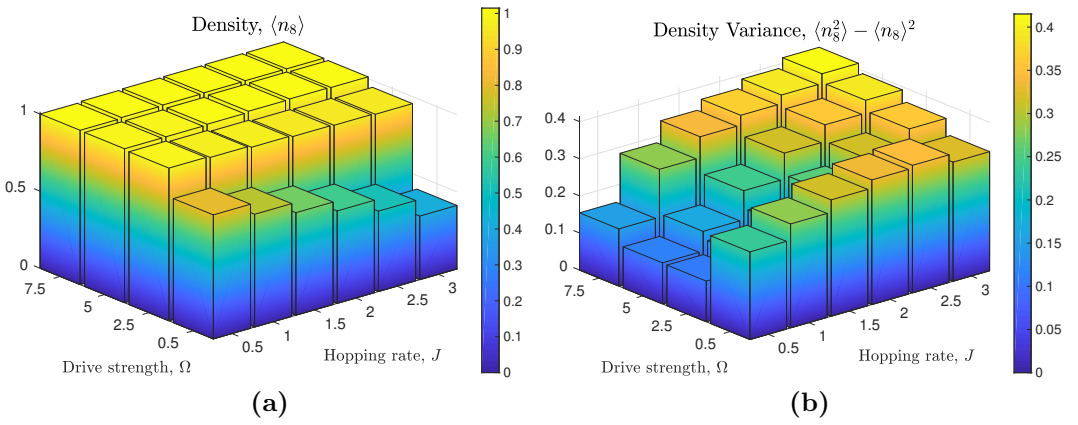


Figure 5.4: (a) The density of the middle site in a fifteen site system, plotted against drive strength Ω , and coupling strength J . (b) The variance in the density over the same parameter range. For this calculation $\gamma_1 = 1$, $\gamma_0 = 0.1$, $U = 20$, and so $\Delta = -10$.

In the region where the local density fluctuations are larger we are interested in determining if a transition to a superfluid state occurs, as is the case in equilibrium systems. Such a transition would be signified by an increase in long range first order coherence. Since the single excitation state in our system is populated by incoherent decay from the upper state, this state is insensitive to the coherence of the drive. The combination of the coherent drive to the upper state and incoherent decay creates an effective incoherent pump process to the middle state. This interpretation is borne out by an adiabatic elimination of the upper state, which is shown in detail in appendix D. We

can therefore attribute any first order correlations we observe to the formation of a superfluid component. Such correlations are quantified by the normalised $g^{(1)}$ -function,

$$g^{(1)}(i, j) = \frac{\langle \hat{a}_i^\dagger \hat{a}_j \rangle}{\sqrt{\langle \hat{n}_i \rangle \langle \hat{n}_j \rangle}}. \quad (5.9)$$

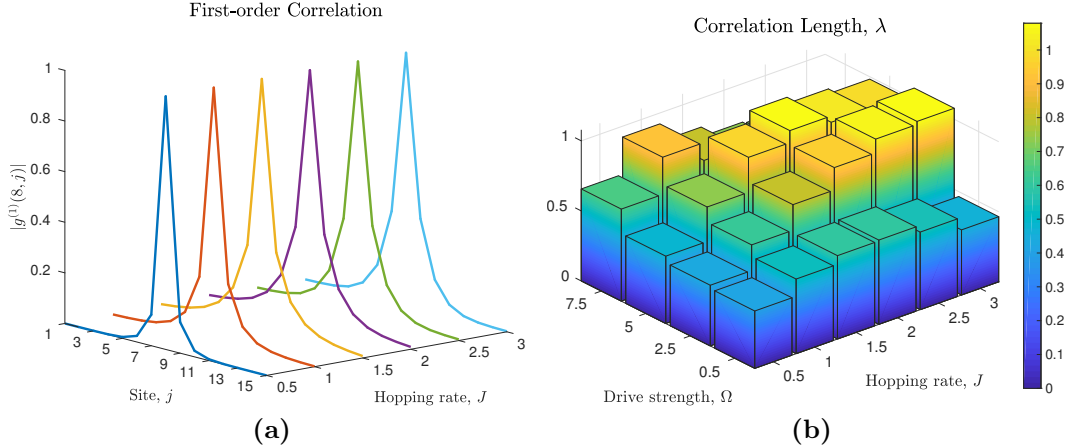


Figure 5.5: The first order correlation $g^{(1)}(i, j)$ and the correlation length λ . For this calculation, $\gamma_1 = 1$, and $\gamma_0 = 0.1$. The interaction strength, $U = 20$, and so $\Delta = -10$. The first order correlation is plotted for a range of coupling strengths at a fixed drive strength, $\Omega = 5$. The correlation length was determined by an $\exp(-|j - j_0|/\lambda)$ fit to the $g^{(1)}$ data.

It can be seen in fig. 5.5 (a) that the build up of first order correlations occurs as the hopping rate increases. On the other hand, the range of these correlations does not increase monotonically with J , but instead reaches a peak, and then decreases. We performed an exponential fit to the $g^{(1)}$ data of the form,

$$g^{(1)}(j) = e^{-\frac{|j-j_0|}{\lambda}}, \quad (5.10)$$

where j labels each lattice site, j_0 is the site on which correlations with other sites are measured (chosen to be the middle site of the system), and λ is the correlation length. The result of this fit is shown in fig. 5.5 (b). We attribute the non-monotonic behaviour of the correlation length to competition between tunneling processes and dephasing processes. An increase in the hopping rate J enhances the long range coherence, but also enhances the local density fluc-

tuations, resulting in more occupation of the doubly excited state. As double occupation increases, so does the contribution of the fast dissipation mechanism governed by the fast decay rate γ_1 , thus the enhanced dephasing.

Another characteristic of the equilibrium Mott insulator state is incompressibility – the suppression of two-excitation coincidences. This effect can be quantified by the normalised $g^{(2)}$ -function,

$$g^{(2)}(i, j) = \frac{\langle \hat{a}_i^\dagger \hat{a}_j^\dagger \hat{a}_j \hat{a}_i \rangle}{\sqrt{\langle \hat{n}_i \rangle \langle \hat{n}_j \rangle}}. \quad (5.11)$$

Figure 5.6 shows that the on-site density correlations are fully suppressed in the low hopping rate regime, and increase monotonically across the region.

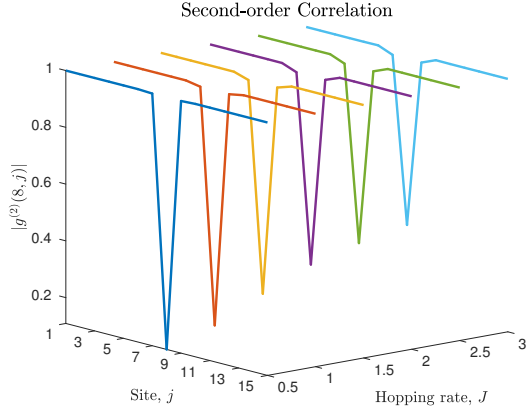


Figure 5.6: Second order correlation between sites, $g^{(2)}(i, j)$ plotted against coupling strength. For this calculation, drive strength $\Omega = 5$, $\gamma_1 = 1$, and $\gamma_0 = 0.1$. The interaction strength, $U = 20$, and so $\Delta = -10$.

5.5 Large harmonic system

To further explore this class of systems we considered a lattice with $\Delta = -U/2 = 0$, the harmonic regime. Though the case for truncation to the subspace of at most two excitations per site is weaker in this regime, we may rely on dissipation to ensure that no significant population will gather in energy levels above the doubly excited state in the steady state. As such, we again

make this truncation, and use a TEBD code to find the steady state of an 11-site system with open boundary conditions.

In fig. 5.7 we show the density and density variance of the middle site plotted, as with the anharmonic calculations, against drive strength Ω and hopping rate J . It can be seen that we again find a region where the excitation density is commensurate with the lattice size, and the variance is much less than one, indicative of the Mott insulator state. In contrast to the anharmonic results, this region is shifted in parameter space to a higher drive strength.

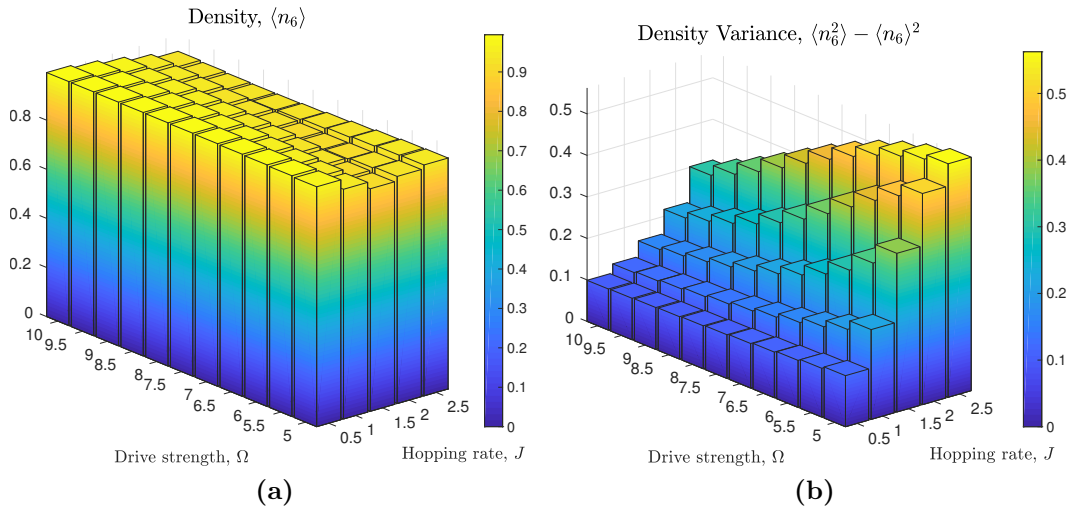


Figure 5.7: Plots of the density on the middle site of an eleven site system, and its variance, plotted against drive strength Ω , and coupling strength J . For this calculation, $\gamma_1 = 1$, and $\gamma_0 = 0.1$.

In figs. 5.8 and 5.9 we show the correlation length, and first and second order correlations for a fixed drive strength. The principal difference between the correlations in the harmonic and anharmonic case is the presence of peaks and troughs on alternating sites in the first order correlations in the harmonic case. This can be understood from the momentum basis representation of the

master equation,

$$\begin{aligned}\dot{\rho} = & -i[\mathcal{H}_b, \rho] + \frac{\gamma_0}{2} \sum_{k=0}^{N-1} [2\hat{b}_k \rho \hat{b}_k^\dagger - \{\hat{b}_k^\dagger \hat{b}_k, \rho\}] \\ & + \frac{\gamma_1}{4N^2} \sum_{[k,l,m,p,q,r]} \left[2\hat{b}_p^\dagger \hat{b}_q \hat{b}_r \rho \hat{b}_k^\dagger \hat{b}_l^\dagger \hat{b}_m - \{\hat{b}_k^\dagger \hat{b}_l^\dagger \hat{b}_m \hat{b}_p^\dagger \hat{b}_q \hat{b}_r, \rho\} \right],\end{aligned}\quad (5.12)$$

where the momentum basis Hamiltonian,

$$\begin{aligned}\mathcal{H}_b = & \sum_{k=0}^{N-1} \left[\frac{\Omega}{\sqrt{2}} \hat{b}_k^\dagger \hat{b}_{N-k}^\dagger + \frac{\Omega^*}{\sqrt{2}} \hat{b}_k \hat{b}_{N-k} \right] + \sum_{k=0}^{N-1} \left[\Delta - 2J \cos\left(\frac{2\pi k}{N}\right) \right] \hat{b}_k^\dagger \hat{b}_k \\ & + \sum_{(j,k,l,m)} \left[\frac{U}{N} \hat{b}_j^\dagger \hat{b}_k^\dagger \hat{b}_l \hat{b}_m \right],\end{aligned}\quad (5.13)$$

and where,

$$\hat{a}_n = \frac{1}{\sqrt{N}} \sum_{k=0}^{N-1} e^{i\frac{2\pi n}{N}k} \hat{b}_k,\quad (5.14)$$

and we have assumed periodic boundary conditions. The notation $[k, l, m, p, q, r]$ indicates that the indices range from 0 to $N - 1$ and follow the condition $m + q + r - k - l - p = nN$ where n is some integer. The notation (j, k, l, m) indicates that the indices range from 0 to $N - 1$ and follow the condition $l + m - j - k = nN$, where n is again some integer. When $\Delta = 0$, as it does here, the detuning $\Delta - 2J \cos(2\pi k/N)$ is zero for modes with $k = nN/4$. The drive is therefore resonant to these modes, and these momenta determine the correlation profile. In the anharmonic case the detuning Δ is large compared to $2J$ and the mode with $k = 0$ is closest to resonance with the drive.

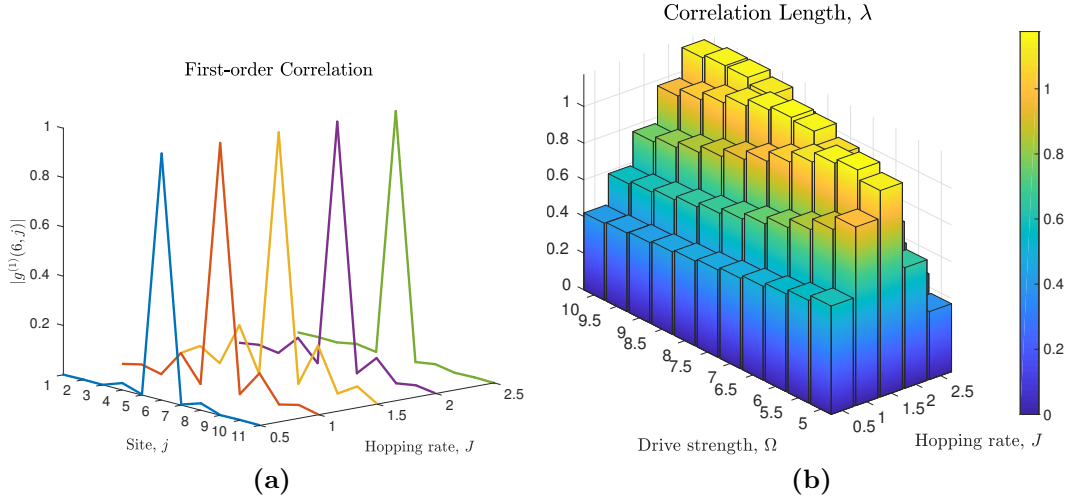


Figure 5.8: The first order correlation $g^{(1)}(i,j)$ and the correlation length λ . For this calculation, $\gamma_1 = 1$, and $\gamma_0 = 0.1$. The first order correlation is plotted for a range of coupling strengths at a fixed drive strength, $\Omega = 5.5$. The correlation length was determined by an $\exp(-|j - j_0|/\lambda)$ fit to the $g^{(1)}$ data.

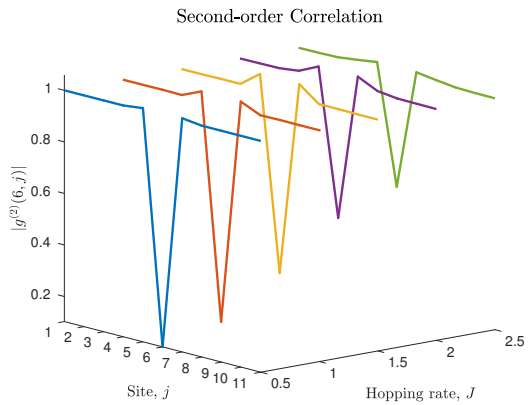


Figure 5.9: Second order correlation between sites, $g^{(2)}(i,j)$, plotted against coupling strength. For this calculation, drive strength $\Omega = 5.5$, $\gamma_1 = 1$, and $\gamma_0 = 0.1$.

5.6 Conclusions

In conclusion, we have shown that in this driven-dissipative nonlinear cavity array, a stationary state exists with similar properties to the Mott insulator. Moreover we have shown that a crossover to a delocalized phase with spontaneous first order coherence can be found by increasing the hopping rate between sites. Unlike the equilibrium case, where we would find a superfluid phase, the first order coherence does not become long range, and indeed decreases with increasing hopping rate after reaching a peak. We attribute this behaviour to dephasing processes becoming more prevalent as the number fluctuations increase as a result of the larger hopping rate.

Chapter 6

Further work

In this chapter we present some initial work on a promising project begun right at the very end of my PhD, which it is hoped the group will eventually bring to fruition.

6.1 Biased chain

In recent work a biased spin chain, where the excited state on each site has a lower energy level than the excited state on all preceding sites, was used as a model to describe the quantum dynamics of a chain of photocells [13]. This investigation however only considered the subspace in which there is a single excitation in the system. We are interested in considering a similar system in which many excitations exist. In particular, we are interested in the transport properties of such a system – in the previous work the system was considered as a quantum heat engine where work is extracted through the drain on the last site [121]. Consequently the question of how to maximise the current from pump to drain is an interesting one. We are also interested in it more generally as a system which may exhibit incoherent transport, as we were in reference [7]. The system (excluding the dissipator) is sketched in fig. 6.1.

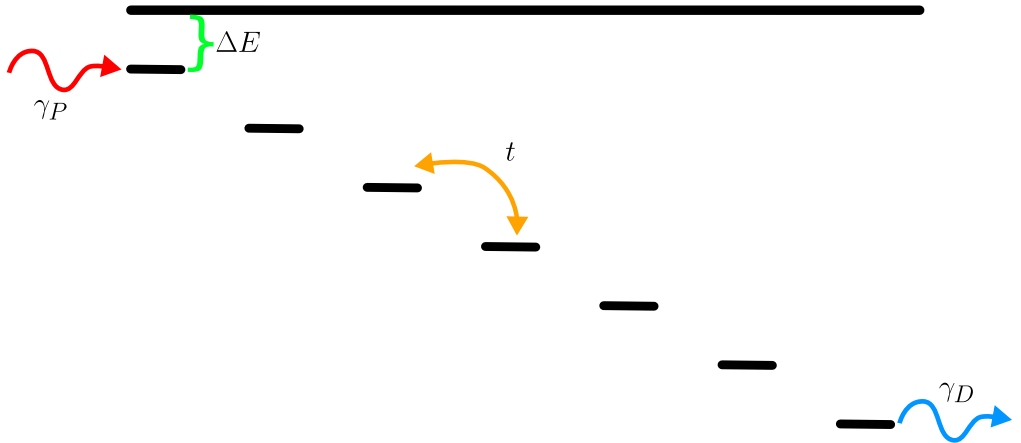


Figure 6.1: A sketch of a seven site system. The Hamiltonian for the system is given in eq. (6.2), and the sketch shows the bias energy ΔE , the hopping interaction with rate t , and the incoherent pump and drain terms with rates γ_P and γ_D . For simplicity, the dissipative interactions are not shown.

6.1.1 The model

We consider an N -site spin chain governed by the full system-environment Hamiltonian,

$$\mathcal{H} = \mathcal{H}_S + \mathcal{H}_{S-E} + \mathcal{H}_E, \quad (6.1)$$

where the system Hamiltonian

$$\mathcal{H}_S = \sum_j^N \left[-j\Delta E \hat{a}_j^\dagger \hat{a}_j + t \left(\hat{a}_j^\dagger \hat{a}_{j+1} + \hat{a}_j \hat{a}_{j+1}^\dagger \right) \right], \quad (6.2)$$

and where ΔE is the bias energy, and t is the hopping rate between sites. Each of the sites in this system is coupled to an independent environment. Each environment is approximated as a set of harmonic oscillators,

$$\mathcal{H}_E = \sum_{j,k} \omega \hat{b}_{j,k}^\dagger \hat{b}_{j,k}, \quad (6.3)$$

where the operator $\hat{b}_{j,k}$ ($\hat{b}_{j,k}^\dagger$) annihilates (creates) an excitation in mode k of the reservoir connected to site j of the system, and ω is the harmonic energy in units of frequency ($\hbar = 1$). The system-environment coupling is a dephasing

interaction of the form,

$$\mathcal{H}_{S-E} = \sum_{j,k} \left[g_{j,k} \hat{a}_j^\dagger \hat{a}_j \left(\hat{b}_{j,k} + \hat{b}_{j,k}^\dagger \right) \right], \quad (6.4)$$

where $g_{j,k}$ is the coupling frequency. Following the usual procedure for deriving a Lindblad-form master equation, including application of the Born-Markov approximation, such an environment leads to relaxation of energy eigenstates of the system Hamiltonian where the energy difference matches the harmonic energy of the environment $\varepsilon - \varepsilon' = \omega$ [122]. In the site basis the Lindblad operators are of the form,

$$\kappa_j = \sum_{m,n} \alpha_{m,n}^j \hat{a}_m^\dagger \hat{a}_n, \quad (6.5)$$

where the action of the dissipator is to transfer an excitation from site n to site m at a rate determined both by the dissipation rate γ_d , and the coefficient $\alpha_{m,n}^j$. The coefficients are given by the projection of energy eigenstates of the system on to the site basis,

$$\alpha_{m,n}^j = \sum_{\varepsilon - \varepsilon' = \omega} \left[\langle \varepsilon | \hat{a}_j^\dagger \hat{a}_j | \varepsilon' \rangle \langle m | \varepsilon \rangle \langle \varepsilon' | n \rangle \right], \quad (6.6)$$

where $|\varepsilon\rangle$ is some state from the energy eigenbasis,

$$\mathcal{H}|\varepsilon\rangle = \varepsilon|\varepsilon\rangle, \quad (6.7)$$

and the state $|n\rangle$ is not a number state, but here represents the single-excitation state $|n\rangle = |0\rangle_1 \otimes \dots \otimes |1\rangle_n \otimes \dots \otimes |0\rangle_N$.

The Lindblad form master equation for the system is,

$$\begin{aligned} \dot{\rho} = & -i[\mathcal{H}, \rho] + \frac{\gamma_d}{2} \sum_j \left[2\kappa_j \rho \kappa_j^\dagger - \{\kappa_j^\dagger \kappa_j, \rho\} \right] \\ & + \frac{\gamma_P}{2} \left[2\hat{a}_1^\dagger \rho \hat{a}_1 - \{\hat{a}_1^\dagger \hat{a}_1, \rho\} \right] \\ & + \frac{\gamma_D}{2} \left[2\hat{a}_N^\dagger \rho \hat{a}_N - \{\hat{a}_N^\dagger \hat{a}_N, \rho\} \right], \end{aligned} \quad (6.8)$$

where γ_d is the dissipation rate, γ_P is the pump rate of an incoherent pump on the first site, and γ_D is the drain rate on the last site.

6.1.2 Initial results

The dissipator given in eqs. (6.5) and (6.6) extends across the whole lattice, however this is computationally impractical. As such, in order to solve the system, we apply a cutoff to the $\alpha_{m,n}$ coefficients, so that $\alpha_{m,n} < 0.01$ is set to zero. Note that since these coefficients are calculated in part using the eigenvectors of the system Hamiltonian \mathcal{H} , they also rely on the system parameters, ΔE and t . In particular, the larger the hopping rate t , the longer the range of non-zero alpha coefficients. Figure 6.2 shows the coefficients for the middle site of an eleven site system, $\alpha_{6,n}^6$ against the extent, $|6 - n|$, for a range of values of $t/\Delta E$. In order to limit the extent of interactions to two sites for initial calculations, we consider only values of the hopping rate and bias energy $t/\Delta E \leq 0.1$.

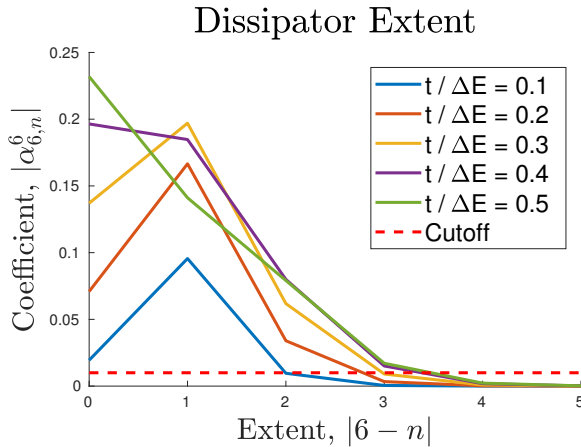


Figure 6.2: Plot of the non-local dissipation coefficients, given by eq. (6.6), for the middle site of an eleven site system. The coefficients are plotted against the extent $|6 - n|$. The red dashed line marks the cutoff at $\alpha_{m,n} = 0.01$.

With these parameter restrictions we calculated the steady state of an eleven site system, using the variational stationary state search code. Design of the MPO followed a similar process to that followed for the MPO in reference [7], which is discussed in appendix B. For these calculations the energy

bias $\Delta E = 1$, the pump rate $\gamma_P = 0.05$, the drain rate $\gamma_D = 0.05$, the dissipation rate $\gamma_d = 0.05$, and the hopping rate t is scanned between 0.01 and 0.1. Naturally the results of these calculations are still under investigation, but the plots in figs. 6.3 and 6.4 show some features of interest. In particular, the density profile in fig. 6.3 remains the same despite the change in the hopping rate. In fig. 6.4 it can be seen that coherent transport, given by

$$i\langle[\mathcal{H}_S, \hat{a}_j^\dagger \hat{a}_j]\rangle = \langle it (\hat{a}_j^\dagger \hat{a}_{j+1} - \hat{a}_j \hat{a}_{j+1}^\dagger)\rangle, \quad (6.9)$$

undergoes an apparent phase change as the hopping rate increases. The dashed line in fig. 6.4 (a) demonstrates this for coherent transport through the bond between the fifth and sixth sites in the system – the same line is plotted separately in fig. 6.4 (b).

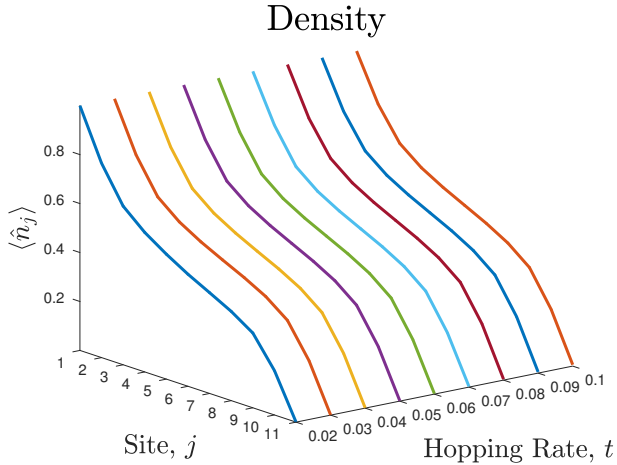


Figure 6.3: The density of an eleven site system $\langle \hat{n}_j \rangle$, against the site j , and hopping rate t . In this calculation the bias energy $\Delta E = 1$, and the pump, drain, and dissipation rates $\gamma_P = \gamma_D = \gamma_d = 0.05$.

6.1.3 Next steps

Most immediately we would like to carry out other calculations to verify that the results we have are accurate. The variational search method cannot guarantee physical results, but confidence can be improved by running calculations with lower convergence thresholds (and higher matrix dimensions).

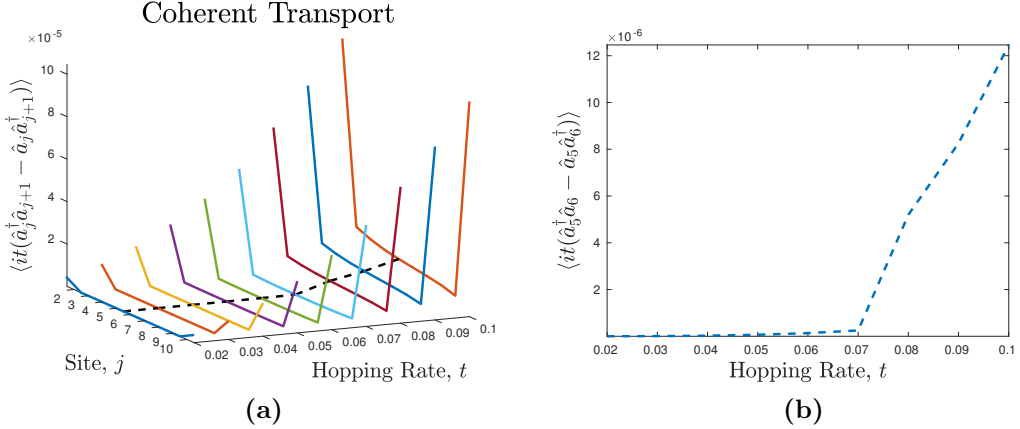


Figure 6.4: (a) Coherent transport between sites in the lattice, against site j , and hopping rate t . (b) Coherent transport between sites five and six in the lattice, against hopping rate t . In this calculation the bias energy $\Delta E = 1$, and the pump, drain, and dissipation rates $\gamma_P = \gamma_D = \gamma_d = 0.05$.

From the initial results we anticipate that the apparent phase transition from incoherent to coherent transport evidenced in fig. 6.4 (b) may become the focus of our investigation, rather than how transport might be maximised as we initially expected. For both lines of investigation we would like to calculate the full derivative of the density on some site j , rather than just the contribution from the coherent dynamics. This would particularly help us understand what is happening in the region where coherent transport is lower.

We would also like to extend the range of the MPO, which would allow us to either reduce the alpha cutoff, or increase the hopping rate, and to consider different configurations of the system.

Chapter 7

Conclusion

In this thesis we began by introducing the scaling problem, the fundamental difficulty of many-body quantum physics, and then went on to describe in some detail the driven Bose-Hubbard model which the research presented focuses on. In addition we provided some physical motivation for such a model. Next we introduced some standard tools of open quantum systems – the Lindblad-form master equation, and the Liouvillian matrix. Ultimately the problem of finding the stationary state of a driven-dissipative system is the same as finding the ground state of a closed system, except that the matrix is much larger and not Hermitian! In the next chapter we considered one method for overcoming the challenge this presents computationally – matrix product states (and operators). We went in to a lot of detail on one particular technique, the variational search, and for good reason. The `mpostat` code found in the online repository hosted at [5], and available under an open source license, implements this technique. It is one of the principle outputs of my PhD, and the documentation is included in this thesis in appendix A. Like any technique, the variational search has both advantages and disadvantages. It is generally quicker than time-evolution methods, and it is easy to encode long range interactions in the matrix product operator format used to specify the system to be solved. On the other hand, it is memory hungry, and the result is not guaranteed to be physical, so it must be used with care. Nevertheless, as is shown in reference [7], in the work presented in this chapter, and in work done by others [3, 4], the technique is powerful enough to push at and expand

CHAPTER 7. CONCLUSION

the boundaries of what is possible in this challenging field.

We then considered the two research papers produced during my PhD, reference [7] and reference [8], and expanded on what is available in their original format. In the first, we considered a geometrically frustrated lattice system where each site in one of the two sublattices was dissipatively coupled to an independent bath. We found that doing so enabled transport through the lattice in both the non-interacting, and interacting regimes, although strong interaction did suppress mobility. In the second we considered an array of nonlinear cavities with a parametric coherent drive to the doubly excited state, and dissipation which increased with number of excitations in the cavity. We showed that in this system there is a crossover in the steady state from a localized state, analogous to the Mott insulator, to a delocalized state. We found that in contrast to the equilibrium case, first order coherence does not become long ranged in this system, and we do not see a superfluid state form. Finally, in the previous chapter we have discussed one of the new projects that we have begun working on, and which will make use of the variational search code. This has shown some promising initial results, with a possible transition from a phase in which incoherent processes dominate transport, to one in which coherent processes dominate.

As for the code itself, future directions for improvement would include making it more flexible, while not compromising its focus. Other libraries such as the TNT Library [123, 124] implement matrix product state methods more generally, and do it well, and it would be unwise to attempt to replicate that effort by allowing `mpostat` to bloat. One specific recommendation would be to simplify the data structures by reimplementing matrix product states and operators as classes rather than cell arrays, which could make it easier for users to write the MPO for any given system, and would make it easier to make the code more flexible. If I were to have another four years to work on the code, that is one of the first things I would do! Other than that, I would continue to make improvements to the top-level control logic and reporting, so as to make the code more user-friendly, and I would introduce some automatic testing of the results.

Improvements to the code would in turn contribute to investigating the

CHAPTER 7. CONCLUSION

physics of more computationally challenging systems. We could, for example, consider higher dimensional systems. This would be an interesting way to extend the investigation of the localization to delocalization transition in a driven nonlinear cavity array, as it would allow us to consider a more complex driving scheme. A four-level scheme for instance would make it easier to reach the Mott insulator state and we could investigate integer filling of greater than one particle per site. It would also allow us to investigate the same system at a higher hopping rate, where we might find the long range coherence we had originally hoped to find. We could also, in general, consider larger systems which would serve to ensure that we eliminate boundary effects, and could help us uncover emergent many-body behaviour. Improving the code and extending the size of the lattice would mean that we could consider longer range dissipative interactions in the frustrated lattice system – though that would certainly be a challenging set of calculations.

It is my hope that `mpostat` will continue to be used to investigate challenging systems in the field of driven dissipative many-body quantum systems, and will continue to be improved, and I am pleased that it has already proven useful. That is all, thank you for reading.

Appendix A

Stationary state search implementation

We will discuss the `mpostat` variational stationary state search code. The implementation is written for MATLAB [6], and at the time of writing is held in a git repository hosted at reference [5]. In this section we will use the conventions that N is the number of sites in our system, and d is the dimension of the local state space, so the total state space of our system would be d^N , and the full density matrix has d^{2N} elements. Figure A.1 shows the structure of the code diagrammatically. To clearly distinguish between this and a ground state search, we refer to the matrix product state as a ‘density matrix product operator’. In order to write this code I referred to the ever useful reference [2], and also to two more recent papers which dealt specifically with variational stationary state searches [3, 4]. Finally, we note that this code makes use of an external library, the PRIMME eigensolver [125, 126].

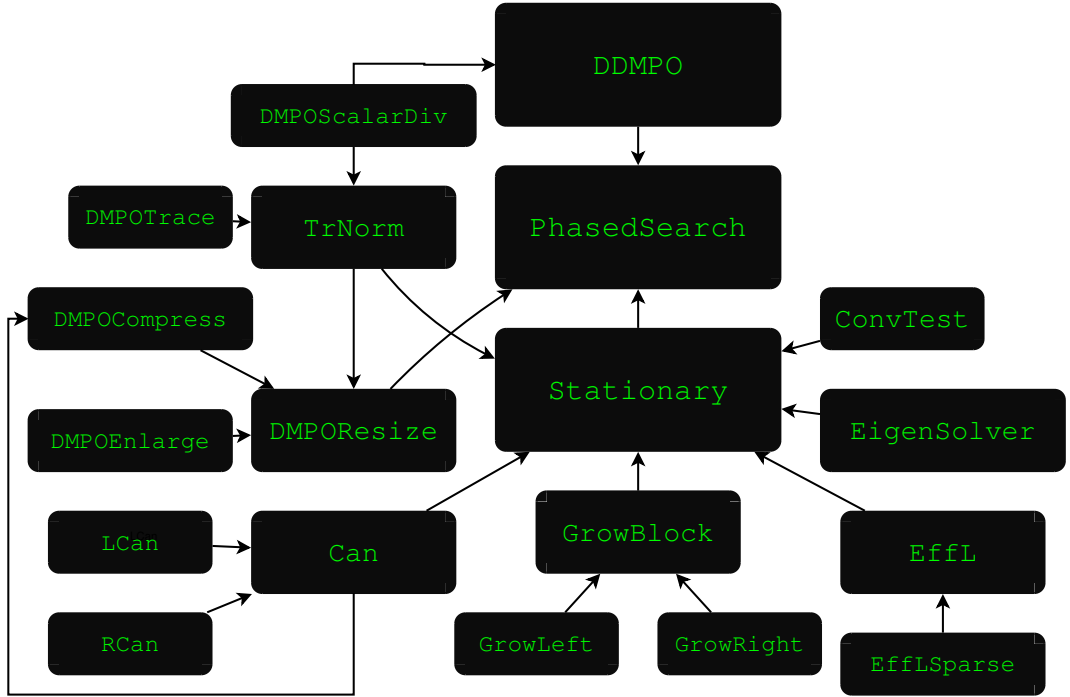


Figure A.1: A diagram showing the structure of the variational stationary state search code. Each rectangle is a function, with its size indicating position in the program hierarchy. The largest are *top level* functions which are intended to be called by the user, the medium sized are *core* functions which are interface functions to the smallest squares, the *utility* functions. The arrows represent calls and returns, with the return direction indicated by the arrow head i.e. `Stationary` calls `GrowBlock` and `GrowBlock` returns values to `Stationary`.

A.1 Standard format

Throughout this implementation I assume a standard format for both the density matrix product operator, and matrix product operator. Note that this format is specific to this implementation, and does not conform to any standard which may or may not exist within the wider community.

A.1.1 Density matrix product operator

The density matrix product operator is, at the highest level, an $N \times 1$ cell array. Each cell, n , contains the site tensor $A_{r,c,i,j}^{[n]}$. The cell array is used rather than a standard array structure, as it allows each site tensor to have

different dimensions. Each site tensor is a 4-dimensional complex double array, with the first two indices corresponding to the virtual dimensions ('row' and 'column'), and the second two corresponding to the physical indices of the density matrix, $\rho = |i\rangle\langle j|$. The size of the virtual dimensions will always be $1 \times d^2$ on the first site, and $d^2 \times 1$ on the last site, and will grow by a factor of d^2 up to the middle site, after which they will shrink by a factor of d^2 . The virtual dimensions will not be allowed to exceed the limit imposed by χ_{\max} . If the limit is reached the size of each virtual dimension will be χ_{\max} until it naturally drops back below this limit, nearer the end of the system.

$$A_{r,c,i,j}^{[n]} \quad | \quad \text{dmpo}\{n\}(r, c, i, j)$$

A.1.2 Matrix product operator

The matrix product operator is also an $N \times 1$ cell array. Each cell contains the MPO tensor $O_{i,j,k,l,p,q}^{[n]}$. Each tensor is a 6-dimensional complex double array, with the first four indices corresponding to the physical dimensions of the Liouvillian (an input and output density matrix), and the last two indices corresponding to the MPO virtual dimensions. The size of the first virtual dimension on the first site, and the second virtual dimension on the last site is always 1, as the MPO also follows the convention of beginning with a row vector, and ending with a column vector. Unlike the DMPO, the MPO has the same virtual dimensions on every site between the first and last.

$$O_{i,j,k,l,p,q}^{[n]} \quad | \quad \text{mpo}\{n\}(i, j, k, l, p, q)$$

A.2 DDMPO

Docstring This is a constructor function for a density matrix product operator. It creates a DMPO which represents a normalised density matrix with the same real value in every element. For example, for a two qubit system DDMPO would create a density matrix product operator corresponding to the

density matrix,

$$\rho = \begin{pmatrix} 0.25 & 0.25 & 0.25 & 0.25 \\ 0.25 & 0.25 & 0.25 & 0.25 \\ 0.25 & 0.25 & 0.25 & 0.25 \\ 0.25 & 0.25 & 0.25 & 0.25 \end{pmatrix}. \quad (\text{A.1})$$

This function depends on `DMPOScalarDiv`.

```
function [dmpo] = DDMPO(HILBY, LENGTH, COMPRESS)
```

Return

<code>dmpo</code>	$N \times 1$ <i>cell array</i> . A density matrix product operator in the standard format. Created by making the first element in every matrix $A_{i,j}^{[n]}$ one, with the rest all zeros. The DMPO is then trace normalised.
-------------------	---

Input

<code>HILBY</code>	<i>Double</i> . The size of the local state space, d . Should be a positive integer, greater than 1.
<code>LENGTH</code>	<i>Double</i> . The number of sites in the system, N . Should be a positive integer, greater than 1.
<code>COMPRESS</code>	<i>Double</i> . The maximum size, χ_{\max} of the virtual dimensions of the density matrix product state site tensors, $A^{[n]}$. If <code>COMPRESS == 0</code> on input, it will be set to <code>Inf</code> , leaving the DMPO uncompressed. Should be a positive integer either equal to zero, or greater than or equal to d^2 . If $0 < \text{COMPRESS} < d^2$ an error will be thrown.

Testing `DDMPOTest`. Checks the type, size, and shape of the density matrix product operator. It checks that compression is properly applied, and that the error `DDMPO:BadCOMPRESS` is thrown if a bad value of `COMPRESS` is supplied. It checks that the trace is one, and that a sample of the density matrix elements are all equal to one another.

A.3 PhasedSearch

Docstring This is a top-level function for the variational stationary state search. It takes information about the system which is to be solved, and some calculation parameters. The function has two return values – a DMPO which approximates the stationary state of the system, and a vector containing the eigenvalue recorded at the end of each *phase* of the calculation. This terminology is borrowed from sports (a phase of play). Here it describes the process of finding the stationary state of the system using a DMPO of some particular dimension, at the end of the calculation the eigenvalue is evaluated against the desired accuracy threshold, and if it is not close enough to zero the current state is copied to a DMPO representation with a larger matrix dimension (as long as this can be done without breaching a limit set by the user). The available calculation variants are `direct` which solves the Liouvillian, $\hat{\mathcal{L}}$, `hermitian` which solves the Hermitian product of the Liouvillian, $\hat{\mathcal{L}}^\dagger \hat{\mathcal{L}}$, and `primme` which solves the Hermitian problem using the PRIMME eigensolver [125, 126]. The user is expected to provide the appropriate MPO for the variant they specify, but an error will be thrown if you try to run a Hermitian calculation with the MPO for $\hat{\mathcal{L}}$. The reverse is not checked on the basis that finding the MPO of the Hermitian product of the Liouvillian involves an additional computational step which the end user is unlikely to invoke accidentally. This function is dependent on `DDMPO`, `Stationary`, and `DMPOResize`.

```
function [dmipoStat, phaseTrack] = PhasedSearch(HILBY
    , LENGTH, mpo, ULTIMATE_THRESHOLD, MAX_COMPRESS,
    VARIANT)
```

Return

<code>dmipoStat</code>	$N \times 1$ cell array. Contains a density matrix product operator representing the approximate stationary state of the system. DMPO is in the standard format used in this implementation.
------------------------	--

APPENDIX A. STATIONARY STATE SEARCH IMPLEMENTATION

<code>phaseTrack</code>	<i>1 dimensional complex double array.</i> Contains the eigenvalue recorded at the end of each phase of the calculation. If the last entry is less than the threshold set by the user then the calculation is regarded as having been successful.
<hr/>	
<code>Input</code>	
<code>HILBY</code>	<i>Double.</i> The size of the local state space, d . Should be a positive integer, greater than one.
<code>LENGTH</code>	<i>Double.</i> The number of sites in the system, N . Should be a positive integer greater than one.
<code>mpo</code>	$N \times 1$ <i>cell array.</i> Liouvillian for the system in matrix product operator form. It is important that the supplied Liouvillian matches the requested calculation variant. If the Hermitian calculation variant is requested, then the MPO should represent the Hermitian product Liouvillian $\mathcal{L}^\dagger \mathcal{L}$, or the <code>EigenSolver</code> function will throw an error.
<code>ULTIMATE_THRESHOLD</code>	<i>Double.</i> The desired final accuracy, as determined by the residual $ \mathcal{L}\rho $, or $ \mathcal{L}^\dagger \mathcal{L}\rho $ in the Hermitian case. The calculation will end and return the results once it crosses this threshold (if it crosses this threshold).
<code>MAX_COMPRESS</code>	<i>Double.</i> The maximum allowed DMPO matrix dimension, χ . Should be a positive integer greater than or equal to d^2 .

VARIANT	<i>String</i> . Specifies the form and method of the calculation. There are three options: ‘direct’, ‘hermitian’, and ‘primme’. If ‘direct’ is supplied, the non-Hermitian Liouvillian \mathcal{L} is solved using MATLAB’s sparse eigensolver, <code>eigs</code> . If ‘hermitian’ or ‘primme’ is supplied, the Hermitian product of the Liouvillian $\mathcal{L}^\dagger \mathcal{L}$ is solved using the <code>eigs</code> and PRIMME eigensolvers respectively. Additionally, if ‘hermitian’ is supplied, but <code>eigs</code> fails to find a solution on some site, a second attempt will be made using the PRIMME eigensolver.
---------	---

Testing `PhasedSearchTest`. Checks that an error is thrown if the Hermiticity error in the effective Liouvillian is large – this is a symptom of having supplied an MPO for the Liouvillian operator \mathcal{L} , but requested the Hermitian problem be solved. Checks that the two return values are the right size, shape and class. Checks that for all three calculation variants, the trace of the solution density matrix is one, and that the eigenvalue is as close to zero as it ought to be (i.e. that it is less than `ULTIMATE_THRESHOLD`). A test problem is run which has the trivial stationary state of no occupation in any site (the ‘all-zero’ state), it is checked that the solution density matrix has a 1 in this state, and other elements are sampled and checked for erroneous non-zero values.

A.4 ProdDMPO

Docstring This is a constructor function for a density matrix product operator. It creates a DMPO which represents a specified simple product state. That is it forms the density matrix,

$$\rho = |i_1 i_2 \dots i_N\rangle \langle i_1 i_2 \dots i_N|, \quad (\text{A.2})$$

for some product state $|i_1 i_2 \dots i_N\rangle$. This function depends on `FWBase`.

APPENDIX A. STATIONARY STATE SEARCH IMPLEMENTATION

```
function [prodDMPO] = ProdDMPO(HILBY, LENGTH,
    COMPRESS, STATE)
```

Return

prodDMPO	<i>N × 1 cell array.</i> A density matrix product operator in the standard format which corresponds to a simple product state, specified by STATE . Created by initialising all tensors $A^{[n]}$ as zero arrays, and then replacing the appropriate $A_{i,j}^{[n]}$ matrices with identities.
-----------------	---

Input

HILBY	<i>Double.</i> The size of the local state space, d . Should be a positive integer, greater than 1.
LENGTH	<i>Double.</i> The number of sites in the system, N . Should be a positive integer, greater than 1.
COMPRESS	<i>Double.</i> The maximum size, χ_{\max} of the virtual dimensions of the density matrix product state site tensors, $A^{[n]}$. If COMPRESS == 0, it will be set to Inf , leaving the DMPO uncompressed. Should be a positive integer either equal to zero, or greater than or equal to d^2 . If $0 < \text{COMPRESS} < d^2$ an error will be thrown.
STATE	<i>Double.</i> The decimal value given by treating the desired state as a big-endian, N -bit, base d string. For example for any size system, STATE = 0 gives the state $ 0_1 0_2 \dots 0_N\rangle$. For a 3 site, 3-level system, STATE = 12 would correspond to the state $ 1_1 1_2 0_3\rangle$.

Testing `ProdDMPOTest`. Checks the type, size, and shape of the density matrix product operator. It checks that compression is properly applied, and that the error `ProdDMPO:BadCOMPRESS` is thrown if a bad value of **COMPRESS** is supplied. It checks that the trace is one, and that the specific density matrix element corresponding to the specified state is one.

A.5 Stationary

Docstring This is a top-level function for the variational stationary state search. It takes information about the system to be solved, and returns an approximation to the stationary state. The difference between this and the `PhasedSearch` top-level function is that `Stationary` will try to solve the problem using the supplied matrix dimension and will either succeed, or fail – it will *not* attempt any resizing of the DMPO. In fact during each phase `PhasedSearch` calls `Stationary` with either a lower accuracy threshold, or a larger matrix dimension. In the event that `Stationary` fails to reach the specified threshold it will print a message to stdout, and return the current state. This function is dependent on `Can`, `GrowBlock`, `EffL`, `EigenSolver`, `ConvTest`, and `TrNorm`.

```
function [dmpoStat, eigTrack] = Stationary(dmpoInit,
                                             mpo, THRESHOLD, variant)
```

Return

<code>dmpoStat</code>	$N \times 1$ <i>cell array</i> . A density matrix product operator representing the approximate stationary state of the system. DMPO is in the standard format used in this implementation.
<code>eigTrack</code>	<i>1 dimensional complex double array</i> . The eigenvalues from the last $2(N - 1)$ site updates. These eigenvalues are tested for convergence after each update, and if the last element is lower than the threshold set by the user, then the calculation is regarded as having been successful.

Input

<code>dmpoInit</code>	$N \times 1$ <i>cell array</i> . Contains some initial density matrix product operator. The closer this is to the stationary state, the faster the calculation will converge. The matrix dimensions of this input DMPO determine the matrix dimensions of the output DMPO, <code>dmpoStat</code> .
<code>mpo</code>	$N \times 1$ <i>cell array</i> . Liouvillian for the system in matrix product operator form. It is important that the supplied Liouvillian matches the requested calculation variant. If the Hermitian calculation variant is requested, then the MPO should represent the Hermitian product Liouvillian $\mathcal{L}^\dagger \mathcal{L}$, or the <code>EigenSolver</code> function will throw an error.
<code>THRESHOLD</code>	<i>Double</i> . The desired final accuracy, as determined by the residual $ \mathcal{L}\rho $, or $ \mathcal{L}^\dagger \mathcal{L}\rho $ in the Hermitian case. The calculation will end and return the results once it crosses this threshold (if it crosses this threshold).
<code>variant</code>	<i>String</i> . Specifies the form and method of the calculation. There are three options: ‘ <code>direct</code> ’, ‘ <code>hermitian</code> ’, and ‘ <code>primme</code> ’. If ‘ <code>direct</code> ’ is supplied, the non-Hermitian Liouvillian \mathcal{L} is solved using MATLAB’s sparse eigensolver, <code>eigs</code> . If ‘ <code>hermitian</code> ’ or ‘ <code>primme</code> ’ is supplied, the Hermitian product of the Liouvillian $\mathcal{L}^\dagger \mathcal{L}$ is solved using the <code>eigs</code> and PRIMME eigensolvers respectively. Additionally, if ‘ <code>hermitian</code> ’ is supplied, but <code>eigs</code> fails to find a solution on some site, a second attempt will be made using the PRIMME eigensolver.

Testing `StationaryTest`. Checks that the two return values are the right size, shape, and class. Checks that errors are thrown in the event that a bad `variant` is supplied, or if a non-Hermitian MPO is supplied with a Hermitian variant. Checks that for all three calculation variants the returned stationary state has a trace of one, and is in the correct state, and that the final eigenvalue is less than `THRESHOLD`.

A.6 ZDMPO

Docstring This is a constructor function for a density matrix product operator. This function creates a DMPO which represents a density matrix with the same real value as every element, precisely the same as `DDMPO`. The difference is in the construction – `ZDMPO` fills every element in every tensor $A^{[n]}$ with a complex number. This is useful for testing and debugging, as the very sparse and completely real tensors created by `DDMPO` can sometimes help conceal bugs. This function depends on `TrNorm`.

```
function [dmpo] = ZDMPO(HILBY, LENGTH, COMPRESS)
```

Return

<code>dmpo</code>	$N \times 1$ cell array. A density matrix product operator in the standard format. Created by filling every site tensor with the complex number $Z = \frac{1}{\sqrt{2}}(1 + 1i)$. The density matrix product operator is then trace normalised.
-------------------	--

Input

<code>HILBY</code>	<i>Double</i> . The size of the local state space, d . Should be a positive integer, greater than one.
<code>LENGTH</code>	<i>Double</i> . The number of sites in the system, N . Should be a positive integer, greater than one.

COMPRESS

Double. The maximum size, χ_{\max} of the virtual dimensions of the density matrix product state site tensors, $A^{[n]}$. As in the ground state code, if **COMPRESS == 0**, it will be set to **Inf**, leaving the density matrix product operator uncompressed. Should be a positive integer either equal to zero, or greater than or equal to d^2 . If $0 < \text{COMPRESS} < d^2$ an error will be thrown.

Testing **ZDMPOTest**. Checks that the density matrix product operator is the right type, size, and shape, including that compression is properly applied. Additionally, the test checks that the error **ZDMPO:BadCOMPRESS** is thrown in the event of a bad value of **COMPRESS** being supplied, and that the state is trace normalised.

A.7 Can

Docstring This is an interface function for the two DMPO normalisation functions, **LCan** and **RCan**. Normalisation of a matrix product state is performed by taking the singular value decomposition of a (reshaped) site tensor, $A^{[n]} = USV^\dagger$. The new renormalised site tensor $\tilde{A}^{[n]}$ is formed from the product US , while V^\dagger is multiplied into the following site – this is referred to as ‘left-canonical’ normalisation. Alternatively, the new site tensor is formed from V^\dagger and US is multiplied into the following site – this is referred to as ‘right-canonical’ normalisation. The two procedures are sufficiently different to warrant entirely separate implementations, and the correct one must be called depending on which direction the code is presently ‘sweeping’ through the system. This function’s purpose is to simplify the call syntax, and control logic in the top-level functions. This function is dependent on **LCan**, and **RCan**.

```
function [cdmpon] = Can(dmpo, route, direction)
```

Return

<code>cdmpo</code>	$N \times 1$ <i>cell array</i> . A density matrix product operator which represents the same state as the input DMPO, <code>dmpo</code> , but with the site(s) specified by <code>route</code> left or right canonically normalised.
<hr/>	
<code>Input</code>	
<code>dmpo</code>	$N \times 1$ <i>cell array</i> . A density matrix product operator in the standard format.
<code>route</code>	<i>1 dimensional double array</i> . Specifies the site or site which should be normalised. An error will be thrown if the last site in the system (site N for left-canonical, site 1 for right-canonical) is included in the route. An error will also be thrown if the supplied route does not match the supplied direction – meaning the indices must be increasing for left-canonical normalisation, and decreasing for right-canonical normalisation.
<code>direction</code>	<i>Character</i> . This should be ‘L’ for left-canonical normalisation, or ‘R’ for right-canonical normalisation.

Testing `CanTest`. Checks that the trace of the DMPO is preserved, and that the appropriate error messages are thrown.

A.8 DMPOHerm

Docstring This mid-level function returns the Hermitian part of a supplied density matrix product operator. It does this by performing the following operation,

$$\tilde{\rho} = \frac{\rho + \rho^\dagger}{2}. \quad (\text{A.3})$$

It should be noted that the operation to add two matrix product operators involves doubling the size of the virtual dimensions on each site. Consequently, this function will do the same regardless of what compression limits

may have been previously set. The state should therefore be compressed after the use of this function. This function depends on `DMPOConj`, `DMPOSum`, and `DMPOScalarDiv`.

```
function [hermDMPO] = DMPOHerm(dmpo)
```

Return

<code>hermDMPO</code>	<i>N × 1 cell array.</i> The Hermitian part of the supplied density matrix product operator, in the standard format. Will have double the virtual dimensions on each site.
-----------------------	--

Input

<code>dmpo</code>	<i>N × 1 cell array.</i> A density matrix product operator, in the standard format.
-------------------	---

Testing `DMPOHermTest`. Checks the `hermDMPO` has the right type, size, and shape. Additionally checks that the trace has been preserved from the input, that the trace is real, and that `hermDMPO` is Hermitian. It does the test for Hermiticity by sampling elements from the density matrix, and checking the transpose element.

A.9 DMPOResize

Docstring This is an interface function for the two DMPO resizing functions, `DMPOCompress`, and `DMPOEnlarge`. It greatly simplifies call syntax in the top-level functions. This function depends on `DMPOCompress`, `DMPOEnlarge`, and `TrNorm`.

```
function [rsDMPO] = DMPOResize(dmpo, COMPRESS)
```

Return

<code>rsDMPO</code>	<i>N × 1 cell array.</i> The appropriately resized density matrix operator, in the standard format.
---------------------	---

Input

<code>dmpo</code>	$N \times 1$ <i>cell array</i> . A density matrix product operator, in the standard format.
<code>COMPRESS</code>	<i>Double</i> . Should be a positive integer, greater than or equal to d^2 . The new maximum matrix dimension for the DMPO, χ . The first thing the function does is check the current maximum dimension of the supplied DMPO, by measuring the middle site tensor. If <code>COMPRESS</code> is smaller, but larger than d^2 then the function hands over to <code>DMPOCompress</code> . If <code>COMPRESS</code> is larger, and then the current dimension is less than that required for an exact representation, the function hands over to <code>DMPOEnlarge</code> . Finally, if the current dimension is the same as <code>COMPRESS</code> , the function quietly returns <code>dmpo</code> .

Testing `DMPOResizeTest`. Checks that the returned DMPO is the right size (across all variants of the ‘right’ size), and that a too small value of `COMPRESS` is rejected, and an error thrown.

A.10 EffL

Docstring This is an interface function for the low-level function which forms the effective Liouvillian matrix using the contraction procedure given in eq. (3.22) and fig. 3.4. It does not perform the contraction itself, but provides a simplified call syntax for top-level functions, and allows for easier replacement of the low-level function. This function is dependent on `EffLSparse`.

```
function [effectiveLiouv] = EffL(TARGET, dmpo, mpo,  
left, right)
```

Return

effectiveLiouv *2 dimensional sparse complex double array.* This very large sparse matrix is an effective Liouvillian for that particular site in the system. It is eigensolved, and the eigenvector reshaped to replace the site tensor. The exact dimensions are dependent on the particular matrix dimensions, but it will be largest in the middle of the system where the matrix dimensions approach the maximum allowed, χ . There the dimensions will be $\chi^2 d^2 \times \chi^2 d^2$. For that reason it is this point in the calculation that places the greatest burden on the available memory. This function is dependent on **EffLSparse**.

Input	
TARGET	<i>Double.</i> The site on which the effective Liouvillian is to be formed, should be a positive integer.
dmpo	$N \times 1$ <i>cell array.</i> A density matrix product operator in the standard format.
mpo	$N \times 1$ <i>cell array.</i> The Liouvillian for the system in matrix product operator form.
left	$N \times 1$ <i>cell array.</i> Contractions from site 1 up to each site in the system.
right	$N \times 1$ <i>cell array.</i> Contractions from site N up to each site in the system.

Testing **EffLTest.** Checks that **effectiveLiouv** is a double array, is sparse, and is the right size.

A.11 EigenSolver

Docstring This is an interface function for the eigensolving routines. Depending on the calculation variant chosen by the user MATLAB's built-in **eigs**

APPENDIX A. STATIONARY STATE SEARCH IMPLEMENTATION

function, or `primme_eigs` from the PRIMME library may be used. This function simplifies the call syntax and control logic in the top-level function, and makes it easier to experiment with different eigensolvers.

```
function [eigVector, eigValue] = EigenSolver(effL,
    HERMITIAN, PRIMME, initVec, HERMITICITY_THRESHOLD)
```

Return	
<code>eigVector</code>	<i>1 dimensional complex double array.</i> The eigenvector of the effective Liouvillian with the eigenvalue closest to zero. This will be reshaped to replace the site tensor, $A^{[n]}$.
<code>eigValue</code>	<i>Complex double.</i> The eigenvalue corresponding to <code>eigVector</code> . This is the closest to zero of all the eigenvalues of the supplied effective Liouvillian. How close it actually is to zero is used as a measure of success for the whole calculation.
Input	
<code>effL</code>	<i>2 dimensional complex double array.</i> The effective Liouvillian $\hat{L}_{\text{eff}}^{[n]}$ for some site, may be formed from the Liouvillian \mathcal{L} , or the Hermitian product of the Liouvillian, $\mathcal{L}^\dagger \mathcal{L}$.
<code>HERMITIAN</code>	<i>Bool.</i> Should be true if the Hermitian product of the Liouvillian is being used.
<code>PRIMME</code>	<i>Bool.</i> Should be true if use of PRIMME is desired. Note that this will only have an impact if <code>HERMITIAN = true</code> , as PRIMME's eigensolver only operates on Hermitian matrices. If <code>HERMITIAN</code> is false, then <code>PRIMME</code> should be too, but its value will be ignored.

<code>initVec</code>	<i>1 dimensional complex double array.</i> An initial guess for the eigenvector – supplying this improves the stability and speed of the eigensolvers. In general this will be the current site tensor reshaped into a vector.
<code>HERMITICITY_THRESHOLD</code>	<i>Double, optional.</i> This is an optional argument. If the Hermitian product Liouvillian is being used then the effective Liouvillian should also be Hermitian. That said, due to numerical error, it almost certainly is not. This problem is solved by taking the average of the effective Liouvillian and its Hermitian conjugate, and supplying that to the eigensolving routines. If <code>HERMITICITY_THRESHOLD</code> is supplied, the difference $ \hat{L} - \hat{L}^\dagger $ is calculated and tested against it. If this test is failed it indicates that the MPO supplied to the top-level function is for \mathcal{L} , not $\mathcal{L}^\dagger\mathcal{L}$. If <code>HERMITIAN = false</code> , this argument will be ignored.

Testing EigenSolverTest. Checks that an error is thrown if `HERMITICITY_THRESHOLD` is supplied and an MPO for \mathcal{L} is used, and that the eigenvalue and eigenvectors found by each variant of the problem are self-consistent. That is if the non-Hermitian eigensolver is used, it consistently finds the same eigenvector and eigenvalue for some fixed input – each of the three return a slightly different eigenvalue and vector, which is to be expected.

A.12 GrowBlock

Docstring This is an interface function for the two tensor network contraction functions, `GrowLeft`, and `GrowRight`. After each site update in a sweep the contraction of the network up to and including that site must be updated. Obviously this is dependent on the direction through the system the sweep is moving, so this function exists to simplify the call syntax, and control logic of the top-level functions. This function is dependent on `GrowLeft`, and `GrowRight`.

```
function [updateBlock] = GrowBlock(dmpo, mpo, left,
right, site, direction)
```

Return

<code>updateBlock</code>	<i>3 dimensional complex double array.</i> Contains the contraction through the network, which comprises the DMPO, its vector conjugate, and the MPO, up to and including the site specified by <code>site</code> . If <code>direction</code> is ‘L’ the contraction is from site 1, if it is ‘R’ the contraction is from site N .
--------------------------	--

Input

<code>dmpo</code>	$N \times 1$ <i>cell array.</i> A density matrix product operator in the standard format.
<code>mpo</code>	$N \times 1$ <i>cell array.</i> Liouvillian for the system in matrix product operator form.
<code>left</code>	$N \times 1$ <i>cell array.</i> Each cell n contains the contraction of the tensor network from site 1 to site $n - 1$ (the contraction from the ‘left’). The first cell simply contains a 1.
<code>right</code>	$N \times 1$ <i>cell array.</i> Each cell n contains the contraction of the tensor network from site N to site $n + 1$ (the contraction from the ‘right’). The last cell simply contains a 1.

<code>site</code>	<i>Double.</i> The site which is to be included in a contraction either from the left or right end of the system.
<code>direction</code>	<i>Character.</i> Either ‘L’ or ‘R’. Specifies whether the site should be included in a contraction from the left (from site 1), or the right (site N).

Testing `GrowBlockTest`. Checks that the return arrays are the correct class and are not empty, and that an error is thrown if a bad `direction` is supplied.

A.13 TrNorm

Docstring This mid-level function normalises a density matrix product operator by dividing it by its trace. This normalisation is physically relevant, but makes no difference to the calculation. This function depends on `DMPOTrace`, and `DMPOScalarDiv`.

```
function [normDMPO] = TrNorm(dmpo)
```

Return

`normDMPO` $N \times 1$ *cell array.* A trace normalised density matrix product operator, in the standard format.

Input

`dmpo` $N \times 1$ *cell array.* A density matrix product operator which is to be trace normalised, in the standard format.

Testing `TrNormTest`. Checks that `normDMPO` has the same class, size, and shape as `dmpo`, and checks that the trace is one.

A.14 ConvTest

Docstring This low-level function is used to determine whether or not the calculation has converged. It does this by finding the mean of the difference

APPENDIX A. STATIONARY STATE SEARCH IMPLEMENTATION

between sequential elements of the supplied vector, and testing it against some threshold. That is the following is calculated,

$$\bar{x} = \frac{1}{M-1} \sum_j^{M-1} |x_{j+1} - x_j|, \quad (\text{A.4})$$

and tested against some threshold value x_{th} , where M is the size of the data set supplied, and x is some vector. In the context of the stationary state search, the input vector contains the eigenvalues from the last M site updates, and convergence is tested against the user-defined convergence threshold.

```
function [convFlag, convergence] = ConvTest(data,  
THRESHOLD)
```

Return

convFlag	<i>Boolean.</i> True if the values supplied in data are deemed to have converged, otherwise false.
convergence	<i>Double.</i> The mean of the absolute value of the difference between neighbouring elements of the input vector – the value of \bar{x} . Returned for monitoring and debugging purposes.

Input

data	<i>1 dimensional complex double array.</i> A vector containing the values to be tested for convergence. The only assumption made about this vector is that successive elements are related, so that the difference $x_{j+1} - x_j$ is a meaningful measure of convergence.
THRESHOLD	<i>Double.</i> The value against which convergence is to be tested. If convergence < THRESHOLD , then convFlag is set to true.

Testing ConvTestTest. Checks that the function does not return true when the input vector contains **NaN** values, or is nearly (but not quite) converged,

and that it does correctly return a true value.

A.15 DMPOCompress

Docstring This low-level function compresses the virtual dimensions of a density matrix product operator, so that they do not exceed the limit χ_{\max} . A sparse singular value decomposition is performed at each site which needs to be compressed, and only χ_{\max} singular values retained. Only sites whose virtual dimension previously exceeded χ_{\max} are affected. This function is interfaced by `DMPOResize`.

```
function [compDMPO] = DMPOCompress(dmpo, COMPRESS,
HILBY, LENGTH)
```

Return	
<code>compDMPO</code>	$N \times 1$ <i>cell array</i> . A density matrix product operator whose virtual dimensions do not exceed the limit set by <code>COMPRESS</code> , in the standard format.
Input	
<code>dmpo</code>	$N \times 1$ <i>cell array</i> . A density matrix product operator, in the standard format.
<code>COMPRESS</code>	<i>Double</i> . The maximum size, χ_{\max} of the virtual dimensions of the density matrix product state site tensors, $A^{[n]}$. Should be a positive integer greater than or equal to d^2 .
<code>HILBY</code>	<i>Double</i> . The size of the local state space, d . Should be a positive integer, greater than one.
<code>LENGTH</code>	<i>Double</i> . The number of sites in the system, N . Should be a positive integer, greater than one.

Testing `DMPOCompressTest`. Checks that the type and size of `compDMPO` are correct, and checks that it is still possible to multiply through the chain of

site tensors. Checks that a set of easily representable states are not altered by light compression.

A.16 DMPOConj

Docstring This low-level function calculates the Hermitian conjugate density matrix product operator, by conjugating the matrices $A_{i,j}^{[n]}$, and swapping their physical indices.

```
function [conjDMPO] = DMPOConj(dmpo)
```

Return

conjDMPO	$N \times 1$ cell array. A density matrix product operator, in the standard format. Represents the density matrix ρ^\dagger , where ρ is the density matrix represented by the density matrix product operator, dmpo.
----------	---

Input

dmpo	$N \times 1$ cell array. A density matrix product operator, in the standard format. Represents the density matrix, ρ .
------	---

Testing `DMPOConjTest`. Checks the type, size, and shape of the returned density matrix product operator. Checks that its trace is unity, and by sampling elements, that it is the Hermitian conjugate of the input density matrix product operator.

A.17 DMPOEnlarge

Docstring This low-level function returns a copy of the input density matrix product operator with a larger maximum virtual dimension, χ_{\max} . Only sites where the virtual dimension was actually truncated by the previous value of χ_{\max} will be enlarged, and the additional rows and columns will be padded with zeros. This function is interfaced by `DMPOResize`.

```
function [bigDMPO] = DMPOEnlarge(dmpo, COMPRESS,
HILBY, LENGTH)
```

Return

bigDMPO	$N \times 1$ <i>cell array</i> . A density matrix product operator, in the standard format. Represents the same state as the input DMPO, but has a larger maximum virtual dimension.
----------------	--

Input

dmpo	$N \times 1$ <i>cell array</i> . A density matrix product operator, in the standard format.
COMPRESS	<i>Double</i> . The new maximum virtual dimension, χ_{\max} . Should be a positive integer greater than both d^2 and the current maximum virtual dimension of the input DMPO.
HILBY	<i>Double</i> . The size of the local state space, d . Should be a positive integer, greater than 1.
LENGTH	<i>Double</i> . The number of sites in the system, N . Should be a positive integer, greater than 1.

Testing `DMPOEnlargeTest`. Checks the size, shape, and class of `bigDMPO`. Checks that the function preserves the trace and state of the input.

A.18 DMPOExp

Docstring This low-level function calculates the expectation value of some set of locally acting operator \hat{O} , by calculating $\text{Tr}[\hat{O}\rho]$. The format of the operator here is that it should be a three dimensional complex double array, with the first two indices referencing the local physical state, and the third indexing the site.

```
function [expect] = DMPOExp(dmpo, op)
```

Return
expect <i>Complex double.</i> The expectation value corresponding to $\text{Tr}[\hat{O}\rho]$.
Input
dmpo $N \times 1$ <i>cell array.</i> Some density matrix product operator, in the standard format.
op <i>3 dimensional complex double array.</i> Some set of locally acting operators, in the format $\langle \text{braState} \hat{O}^{[n]} \text{ketState} \rangle =$ <code>op(braState, ketState, site)</code> . For example, if one wanted to calculate the expectation of the spin-flip operator acting on the first site in a spin chain, then <code>op(:, :, 1)</code> , would be the spin-flip operator $(\begin{smallmatrix} 0 & 1 \\ 1 & 0 \end{smallmatrix})$, while every other matrix in the array, <code>op(:, :, 2:end)</code> , would be the 2×2 identity matrix.

Testing `DMPOExpTest`. Checks the type of `expect`, the trace of a set of density matrix product operators, and the expectation value of \hat{n} on some product states.

A.19 DMPOScalarDiv

Docstring This low-level function divides a density matrix product operator by a scalar value. Currently it does so simply by dividing the first site tensor $A^{[1]}$ by the scalar.

```
function [divDMPO] = DMPOScalarDiv(dmpo, scalar)
```

Return

divDMP0	$N \times 1$ <i>cell array</i> . A density matrix product operator in the standard format which represents the density matrix, $\tilde{\rho} = \rho/a$, where ρ is the density matrix represented by dmpo , and a is the scalar value supplied as scalar .
<hr/>	
Input	
dmpo	$N \times 1$ <i>cell array</i> . Some density matrix product operator, in the standard format.
scalar	<i>Complex double</i> . Some complex (or real) number.

Testing `DMP0ScalarDivTest`. Checks the type, size, and shape of the returned density matrix product operator. Checks that $\text{Tr}[\tilde{\rho}] = \text{Tr}[\rho]/a$, and by sampling elements from the density matrix, that the division has been carried out correctly.

A.20 DMPOSum

Docstring This low-level function adds two density matrix product operators, which represent the same system, together. Given two density matrix product operators,

$$|\bar{\rho}_A\rangle = \sum_{i_1 \dots i_N} \sum_{j_1 \dots j_N} A_{i,j}^{[1]} A_{i,j}^{[2]} \dots A_{i,j}^{[N]} |j_1 j_2 \dots j_N\rangle \otimes |i_1 i_2 \dots i_N\rangle, \quad (\text{A.5})$$

$$|\bar{\rho}_B\rangle = \sum_{l_1 \dots l_N} \sum_{m_1 \dots m_N} B_{l,m}^{[1]} B_{l,m}^{[2]} \dots B_{l,m}^{[N]} |m_1 m_2 \dots m_N\rangle \otimes |l_1 l_2 \dots l_N\rangle, \quad (\text{A.6})$$

we perform the summation, $|\bar{\rho}_C\rangle = |\bar{\rho}_A\rangle + |\bar{\rho}_B\rangle$ with the following procedure. We form $C^{[1]}$ by concatenating $A^{[1]}$ and $B^{[1]}$ along the second virtual dimension, and we form $C^{[N]}$ by concatenating $A^{[N]}$ and $B^{[N]}$ along the first virtual dimension. For all the other sites, we create the block diagonal matrices,

$$C^{[n]} = \begin{pmatrix} A^{[n]} & 0 \\ 0 & B^{[n]} \end{pmatrix}, \quad (\text{A.7})$$

which we can see leads to $|\bar{\rho}_C\rangle$ having virtual dimensions which are the sum of those in $|\bar{\rho}_A\rangle$ and $|\bar{\rho}_B\rangle$. It is also not trace normalised. For this reason it is recommended that any use of `DMPOSum` is followed by `DMPOCompress` and `TrNorm`.

```
function [sumDMPO] = DMPOSum(rhoA, rhoB)
```

Return	
<code>sumDMPO</code>	$N \times 1$ <i>cell array</i> . An un-normalised density matrix product operator, in the standard format. Represents a density matrix which is the sum of those represented by the input density matrix product operators.
<hr/>	
Input	
<code>rhoA</code>	A density matrix product operator, in the standard format. If its size and physical dimensions do not match those of <code>rhoB</code> , an error will be thrown.
<code>rhoB</code>	A density matrix product operator, in the standard format. If its size and physical dimensions do not match those of <code>rhoA</code> , an error will be thrown.

Testing `DMPOSumTest`. Checks the type, size, and shape of `sumDMPO`. Checks that an error is thrown if the two input systems do not match. Checks that the trace of `sumDMPO` is the sum of the trace of `rhoA` and `rhoB`, and samples the density matrix to check the summation has been performed correctly.

A.21 DMPOTrace

Docstring This low-level function calculates the trace of a density matrix product operator. It uses the same contraction as `DMPOExp`, only it ignores non-diagonal terms.

```
function [trace] = DMPOTrace(dmpo)
```

Return	
<code>trace</code>	<i>Complex double.</i> The trace of the supplied density matrix product operator. Should always be exactly equal to one, with no imaginary component, but this will often not be the case.
Input	
<code>dmpo</code>	$N \times 1$ <i>cell array.</i> A density matrix product operator, in the standard format.

Testing Creates a ‘density matrix’ of all ones for various sizes of system, and then confirms that the trace is real, and equal to d^N .

A.22 EffLSparse

Docstring This low-level function returns the effective Liouvillian for a particular site, in sparse matrix format. This is the tensor network contraction shown in eq. (3.22) and fig. 3.4, and one of the most important tasks of the whole calculation. This function is interfaced by `EffL`.

```
function [effectiveLiouv] = EffLSparse(lBlock,
                                         siteMPO, rBlock, ROW_SIZE, COL_SIZE, HILBY)
```

Return	
<code>effectiveLiouv</code>	<i>2 dimensional sparse complex double array.</i> This very large sparse matrix is an effective Liouvillian for some site in the system. Its construction, and subsequent eigensolving places by far the greatest burden on available memory. This function sacrifices speed to some extent, in order to reduce memory consumption during array construction.
Input	

<code>lBlock</code>	<i>3 dimensional complex double array.</i> The contraction of the tensor network from site 1, up to the site on which the effective Liouvillian is being formed.
<code>siteMPO</code>	<i>6 dimensional complex double array.</i> The MPO tensor for the site on which the effective Liouvillian is being formed.
<code>rBlock</code>	<i>3 dimensional complex double array.</i> The contraction of the tensor network from the final site in the system N , up to the site on which the effective Liouvillian is being formed.
<code>ROW_SIZE</code>	<i>Double.</i> The size of the first virtual dimension of the site tensor for the site on which the effective Liouvillian is being formed. Should be a positive integer.
<code>COL_SIZE</code>	<i>Double.</i> The size of the second virtual dimension of the site tensor for the site on which the effective Liouvillian is being formed. Should be a positive integer.
<code>HILBY</code>	<i>Double.</i> The size of the local state space, d . Should be a positive integer, greater than 1.

Testing `EffLSparseTest`. Checks that the return is the right size, shape, and class. A test case is used where `effectiveLiouv` should be an identity matrix.

A.23 FWBase

Docstring This low-level function returns an array containing the big-endian, N -bit, base d representation of a decimal number. It is used by `ProdDMPO`, and extensively by test routines.

```
function [bits] = FWBase(n, BASE, WIDTH)
```

Return
bits <i>WIDTH</i> × 1 <i>double array</i> . Contains the big-endian, base <i>BASE</i> representation of <i>n</i> . Will be padded with zeros to ensure it reaches <i>WIDTH</i> .
Input
n <i>Double</i> . A decimal number. Should be a positive integer, if it is not, an error will be thrown.
BASE <i>Double</i> . The base into which n should be converted. Should be a positive integer.
WIDTH <i>Double</i> . The size of the bit string required. If it is longer than necessary for the chosen n and BASE , it will be padded with leading zeros. If it is not large enough, an error will be thrown.

Testing FWBaseTest. Checks that errors are thrown correctly, and that the right size arrays are created. Checks that decimal numbers are converted correctly.

A.24 GrowLeft

Docstring This low-level function returns the contraction of the system from site 1 up to and including the specified site. It is used to form and update the left block tensor, $L^{[n+1]}$, as described by eq. (3.17). This function is interfaced by GrowBlock.

```
function [updateBlock] = GrowLeft(siteTensor, mpo,  
leftBlock, ROW_SIZE, COL_SIZE, HILBY, OP_COL)
```

Return
updateBlock 3 dimensional complex double array. The rank-3 left block tensor for the site $n + 1$, $L^{[n+1]}$.

Input	
<code>siteTensor</code>	<i>4 dimensional complex double array.</i> The density matrix product operator tensor for the site n , in the standard format.
<code>mpo</code>	<i>6 dimensional complex double array.</i> The rank-6 tensor matrix product operator for the site n , $O^{[n]}$, in the standard format.
<code>leftBlock</code>	<i>3 dimensional complex double array.</i> The rank-3 left block tensor for the site n , $L^{[n]}$.
<code>ROW_SIZE</code>	<i>Double.</i> The size of the first virtual dimension of the density matrix product operator. Should be a positive integer.
<code>COL_SIZE</code>	<i>Double.</i> The size of the second virtual dimension of the density matrix product operator. Should be a positive integer.
<code>HILBY</code>	<i>Double.</i> The size of the local state space, d . Should be a positive integer, greater than 1.
<code>OP_COL</code>	<i>Double.</i> The size of the second virtual dimension of the matrix product operator. Should be a positive integer.

Testing `GrowLeftTest`. Checks the vector norm of the system, by calling `GrowLeft` on the last site.

A.25 GrowRight

Docstring This low-level function returns the contraction of the system from site N up to and including the specified site. It is used to form and update the right block tensor, $R^{[n-1]}$, as described by eq. (3.18). This function is interfaced by `GrowBlock`.

APPENDIX A. STATIONARY STATE SEARCH IMPLEMENTATION

```
function [updateBlock] = GrowRight(siteTensor, mpo,
rightBlock, ROW_SIZE, COL_SIZE, HILBY, OP_ROW)
```

Return

updateBlock *3 dimensional complex double array.* The rank-3 right block tensor for the site $n - 1$, $R^{[n-1]}$.

Input

siteTensor *4 dimensional complex double array.* The density matrix product operator tensor for the site n , in the standard format.

mpo *6 dimensional complex double array.* The rank-6 tensor matrix product operator for the site n , $O^{[n]}$, in the standard format.

rightBlock *3 dimensional complex double array.* The rank-3 right block tensor for the site n , $R^{[n]}$.

ROW_SIZE *Double.* The size of the first virtual dimension of the density matrix product operator. Should be a positive integer.

COL_SIZE *Double.* The size of the second virtual dimension of the density matrix product operator. Should be a positive integer.

HILBY *Double.* The size of the local state space, d . Should be a positive integer, greater than 1.

OP_ROW *Double.* The size of the first virtual dimension of the matrix product operator. Should be a positive integer.

Testing `GrowRightTest`. Checks the vector norm of the system, by calling `GrowRight` on the first site.

A.26 LCan

Docstring This low-level function returns a left-canonically normalised site tensor, and its now non-canonical following neighbour. This function is interfaced by `Can`.

```
function [canSite, SVNextSite] = LCan(siteTensor,
nextSiteTensor, HILBY, ROW_SIZE, COL_SIZE, NEXT_COL
)
```

Return	
<code>canSite</code>	<i>4 dimensional complex double array.</i> The left-canonically normalised density matrix product operator tensor for the site n , in the standard format.
<code>SVNextSite</code>	<i>4 dimensional complex double array.</i> The non-canonical density matrix product operator tensor for the site $n + 1$, in the standard format.

Input	
<code>siteTensor</code>	<i>4 dimensional complex double array.</i> The density matrix product operator tensor for the site n , in the standard format.
<code>nextSiteTensor</code>	<i>4 dimensional complex double array.</i> The density matrix product operator tensor for the site $n + 1$, in the standard format.
<code>HILBY</code>	<i>Double.</i> The size of the local state space, d . Should be a positive integer, greater than 1.
<code>ROW_SIZE</code>	<i>Double.</i> The size of the first virtual dimension of <code>siteTensor</code> . Should be a positive integer.
<code>COL_SIZE</code>	<i>Double.</i> The size of the second virtual dimension of <code>siteTensor</code> . Should be a positive integer.
<code>NEXT_COL</code>	<i>Double.</i> The size of the second virtual dimension of <code>nextSiteTensor</code> . Should be a positive integer.

Testing `LCanTest`. Checks the type, size, and shape of a density matrix product operator, operated on by `LCan`. Checks that the left-canonical normalisation condition holds. Checks that the function does not alter the trace, or a sample of the elements of the density matrix.

A.27 MPOHermProd

Docstring This low-level function returns an MPO representing the Hermitian product ($\mathcal{L}^\dagger \mathcal{L}$) of a Liouvillian supplied in MPO form. In this way the user can avoid having to explicitly formulate the MPO representation of the Hermitian product of the Liouvillian. For efficiency reasons this is never done automatically by a top-level function, so the user must always take care to supply the correct MPO.

```
function [hmpo] = MPOHermProd(mpo)
```

Return

<code>hmpo</code>	$N \times 1$ <i>cell array</i> . The Hermitian product of the input Liouvillian, in MPO form. Note that the virtual dimensions of this MPO are the square of those from the input.
-------------------	--

Input

<code>mpo</code>	$N \times 1$ <i>cell array</i> . Some Liouvillian, in matrix product operator form.
------------------	---

Testing `MPOHermProdTest`. Checks that the returned MPO is the right size and shape. Rebuilds the Liouvillian from the returned MPO, and checks that it is Hermitian, and that it is the Hermitian product of the input Liouvillian.

A.28 RCan

Docstring This low-level function returns a right-canonically normalised site tensor, and its now non-canonical following neighbour. This function is interfaced by `Can`.

```
function [canSite, nextSiteUS] = RCan(siteTensor,
    nextSiteTensor, HILBY, ROW_SIZE, COL_SIZE, NEXT_ROW
)
```

Return	
<code>canSite</code>	<i>4 dimensional complex double array.</i> The left-canonically normalised density matrix product operator tensor for the site n , in the standard format.
<code>nextSiteUS</code>	<i>4 dimensional complex double array.</i> The non-canonical density matrix product operator tensor for the site $n - 1$, in the standard format.

Input	
<code>siteTensor</code>	<i>4 dimensional complex double array.</i> The density matrix product operator tensor for the site n , in the standard format.
<code>nextSiteTensor</code>	<i>4 dimensional complex double array.</i> The density matrix product operator tensor for the site $n - 1$, in the standard format.
<code>HILBY</code>	<i>Double.</i> The size of the local state space, d . Should be a positive integer, greater than 1.
<code>ROW_SIZE</code>	<i>Double.</i> The size of the first virtual dimension of <code>siteTensor</code> . Should be a positive integer.
<code>COL_SIZE</code>	<i>Double.</i> The size of the second virtual dimension of <code>siteTensor</code> . Should be a positive integer.
<code>NEXT_ROW</code>	<i>Double.</i> The size of the first virtual dimension of <code>nextSiteTensor</code> . Should be a positive integer.

Testing `RCanTest`. Checks the type, size, and shape of a density matrix product operator, operated on by `RCan`. Checks that the right-canonical normalisation condition holds. Checks that the function does not alter the trace, or a sample of the elements of the density matrix.

A.29 SVDNorm

Docstring This function uses the SVD decomposition to vector normalise a density matrix product operator. Essentially the same as `LCan`, except it includes the last site in the system, and simply throws away the last V^\dagger matrix. Has no impact on the physicality of the density matrix product operator, so should only be used at initialisation. Thereafter the process of left and right normalising individual site tensors ensures that the density matrix product operator remains vector normalised.

```
function [normDMPO] = SVDNorm(dmpo)
```

Return

`normDMPO` $N \times 1$ *cell array*. A vector normalised density matrix product operator, in the standard format.

Input

`dmpo` $N \times 1$ *cell array*. A density matrix product operator, in the standard format.

Testing `SVDNormTest`. Checks the type, size, and shape of the returned density matrix product operator. Using a small system rebuilds the full vectorised density matrix, and confirms it has a vector norm of one.

Appendix B

Wannier basis MPO

I begin by stating the MPO in full. Due to the large size this is done in a sparse notation. The virtual dimension $\chi = 27$.

Row	Col	Value
1	1	$\mathbb{I} \otimes \mathbb{I}$
2	1	$W^\dagger W \otimes \mathbb{I}$
3	1	$\mathbb{I} \otimes W^\dagger W$
12	1	$\mathbb{I} \otimes W$
13	1	$W \otimes \mathbb{I}$
18	1	$\frac{\gamma-1}{2} (2W \otimes \mathbb{I} - \mathbb{I} \otimes W^\dagger)$
19	1	$-\frac{\gamma-1}{2} W^\dagger \otimes \mathbb{I}$
20	1	$W \otimes \mathbb{I}$
21	1	$W^\dagger \otimes \mathbb{I}$
22	1	$\mathbb{I} \otimes W^\dagger$
23	1	$\frac{\gamma-2}{2} (2W \otimes \mathbb{I} - \mathbb{I} \otimes W^\dagger)$
24	1	$-\frac{\gamma-2}{2} W^\dagger \otimes \mathbb{I}$
25	1	$\frac{\gamma-3}{2} (2W \otimes \mathbb{I} - \mathbb{I} \otimes W^\dagger)$
26	1	$-\frac{\gamma-3}{2} W^\dagger \otimes \mathbb{I}$
27	1	$iH_{\text{local}}^T \otimes \mathbb{I} - \mathbb{I} \otimes iH_{\text{local}}$ $+ \frac{\gamma_0}{2} (2W \otimes W - \mathbb{I} \otimes W^\dagger W - W^\dagger W \otimes \mathbb{I}),$ $H_{\text{local}} = U_{0,0,0}^{\text{eff},B} W^\dagger W^\dagger W W + \frac{\Omega_{W,i}}{2} W + \frac{\Omega_{W,i}^*}{2} W^\dagger$
27	2	$4iU_{1,1,0}^{\text{eff},B} W^\dagger W \otimes \mathbb{I}$

APPENDIX B. WANNIER BASIS MPO

27	3	$\mathbb{I} \otimes -4iU_{1,1,0}^{\text{eff},B}W^\dagger W$
27	4	$4iU_{2,2,0}^{\text{eff},B}W^\dagger W \otimes \mathbb{I}$
27	5	$\mathbb{I} \otimes -4iU_{2,2,0}^{\text{eff},B}W^\dagger W$
27	6	$iU_{2,1,0}^{\text{eff},B}W^\dagger W \otimes \mathbb{I}$
27	7	$\mathbb{I} \otimes -iU_{2,1,0}^{\text{eff},B}W^\dagger W$
27	8	$iW^\dagger \otimes \mathbb{I}$
27	9	$\mathbb{I} \otimes -iW^\dagger$
27	10	$iW \otimes \mathbb{I}$
27	11	$\mathbb{I} \otimes -iW$
27	12	$\frac{\gamma_1}{2} (2W \otimes \mathbb{I} - \mathbb{I} \otimes W^\dagger)$
27	13	$-\frac{\gamma_1}{2} W^\dagger \otimes \mathbb{I}$
27	14	$\frac{\gamma_2}{2} (2W \otimes \mathbb{I} - \mathbb{I} \otimes W^\dagger)$
27	15	$-\frac{\gamma_2}{2} W^\dagger \otimes \mathbb{I}$
27	16	$\frac{\gamma_3}{2} (2W \otimes \mathbb{I} - \mathbb{I} \otimes W^\dagger)$
27	17	$-\frac{\gamma_3}{2} W^\dagger \otimes \mathbb{I}$
27	18	$\mathbb{I} \otimes W$
27	19	$W \otimes \mathbb{I}$
27	27	$\mathbb{I} \otimes \mathbb{I}$
4	2	$\mathbb{I} \otimes \mathbb{I}$
5	3	$\mathbb{I} \otimes \mathbb{I}$
6	20	$W^\dagger \otimes \mathbb{I}$
6	21	$W \otimes \mathbb{I}$
7	12	$\mathbb{I} \otimes W^\dagger$
7	22	$\mathbb{I} \otimes W$
8	2	$U_{-2,-1,0}^{\text{eff},B}W \otimes \mathbb{I}$
8	20	$2U_{-1,0,1}^{\text{eff},B}W^\dagger W \otimes \mathbb{I}$
9	3	$\mathbb{I} \otimes U_{-2,-1,0}^{\text{eff},B}W$
9	12	$\mathbb{I} \otimes 2U_{-1,0,1}^{\text{eff},B}W^\dagger W$
10	2	$U_{-2,-1,0}^{\text{eff},B}W^\dagger \otimes \mathbb{I}$
10	21	$2U_{-1,0,1}^{\text{eff},B}W^\dagger W \otimes \mathbb{I}$
11	3	$\mathbb{I} \otimes U_{-2,-1,0}^{\text{eff},B}W^\dagger$
11	22	$\mathbb{I} \otimes 2U_{-1,0,1}^{\text{eff},B}W^\dagger W$
14	12	$\mathbb{I} \otimes \mathbb{I}$

APPENDIX B. WANNIER BASIS MPO

15	13	$\mathbb{I} \otimes \mathbb{I}$
16	14	$\mathbb{I} \otimes \mathbb{I}$
17	15	$\mathbb{I} \otimes \mathbb{I}$
18	23	$\mathbb{I} \otimes \mathbb{I}$
19	24	$\mathbb{I} \otimes \mathbb{I}$
23	25	$\mathbb{I} \otimes \mathbb{I}$
24	26	$\mathbb{I} \otimes \mathbb{I}$

Table B.1: The MPO for the strongly interacting frustrated lattice system, truncated to the single-excitation subspace in the Wannier basis. Listed in a sparse notation with the two virtual dimensions and the operator given. Note that to match the data structure for MPOs used in `mpostat`, the operator would need to be appropriately reshaped.

I will now discuss some features of the MPO in the hope that it is helpful to someone hoping to design one similar. First of all, note that as it is a Liouvillian MPO, all operators in the Hamiltonian are duplicated on both sides of the tensor space, to account for the commutator $\mathbb{I} \otimes -iH + iH^T \otimes \mathbb{I}$. I have broken from the previously stated convention that all coefficients would be placed in the bottom row, and the first column limited to dimensionless operators. This was done simply to keep the appearance of the dissipator terms consistent, which made the code cleaner during the actual implementation. Those dissipator terms in the first column all correspond to the ‘negative l ’ dissipator terms, however in practice they did not need unique coefficients as $\gamma_{-l} = \gamma_l$. Such practical considerations also explain the inclusion of a site index on the drive amplitude $\Omega_{W,i}$, although we know well that only site zero will be driven. The approach of including an array of such coefficients that is the length of the system, and pulling the correct element for each site allows more flexibility at almost no computational cost. The large gap in the first column from row 4 to row 11 (which I tend to refer to as a ‘passing lane’) facilitates nonlocal terms beyond nearest neighbours. Inspection of the bottom row will reveal that these elements are landing sites for nonlocal terms from the previous site, and they must be kept away from the first column until the operator chain is complete. It is a feature of MPO construction,

APPENDIX B. WANNIER BASIS MPO

that once an operator chain reaches a non-zero term in the first column of the following MPO site, it will thereafter only be multiplied by identities. It is the job of the interior elements of the MPO to correctly handle the nonlocal terms until an operator chain is completed. Consider for example the next-nearest neighbour cross-Kerr interaction. On some site j the chain begins with element $(27, 5)$ which contains $\mathbb{I}_j \otimes -4iU_{2,2,0}^{\text{eff},B}W_j^\dagger W_j$. Note that I have included the site index on the operators here to help illustrate my point, but the operators are still the strictly local W^\dagger , W , and \mathbb{I} – the tensor product between sites is handled by the way observables are calculated using matrix product states and operators. On multiplication in to the next site (again, something that never actually happens, but is notionally useful for MPO design) the operator encounters nothing but zeros until it reaches interior element $(5, 3)$ which contains the double identity $\mathbb{I}_{j+1} \otimes \mathbb{I}_{j+1}$ and the operator chain $\mathbb{I}_j \mathbb{I}_{j+1} \otimes -4iU_{2,2,0}^{\text{eff},B}W_j^\dagger W_j \mathbb{I}_{j+1}$ is formed. Next the operator chain finds the only non-zero value in element $(3, 1)$ of the following site, which contains $\mathbb{I}_{j+2} \otimes W_{j+2}^\dagger W_{j+2}$, resulting in the chain $\mathbb{I}_j \mathbb{I}_{j+1} \mathbb{I}_{j+2} \otimes -4iU_{2,2,0}^{\text{eff},B}W_j^\dagger W_j \mathbb{I}_{j+1} W_{j+2}^\dagger W_{j+2}$, and the next-nearest neighbour cross-Kerr interaction term is complete. Residing now in the first column, the operator chain will only encounter identities as it progresses through the rest of the system. This method of designing MPOs is described in detail in section 6 of Schollwöck's incomparable review article [2].

Appendix C

Rotating frame transformation

Here we transform the Hamiltonian for a driven nonlinear cavity array into a rotating frame. For simplicity we begin with only a single decoupled cavity, and then later introduce a second site to show the effect of the transformation on a hopping interaction.

C.1 Single cavity

In the reference frame, the Hamiltonian for a driven nonlinear cavity is,

$$\mathcal{H}_{\text{ref}} = \omega \hat{a}^\dagger \hat{a} + \frac{U}{2} \hat{a}^\dagger \hat{a}^\dagger \hat{a} \hat{a} + \Omega_\uparrow \hat{a}^\dagger \hat{a}^\dagger + \Omega_\downarrow \hat{a} \hat{a}, \quad (\text{C.1})$$

where,

$$\Omega_\downarrow = \frac{1}{\sqrt{2}} \left(\Omega^* e^{i\omega_L t} + \tilde{\Omega}^* e^{-i\omega_L t} \right), \quad (\text{C.2})$$

$$\Omega_\uparrow = \frac{1}{\sqrt{2}} \left(\Omega e^{-i\omega_L t} + \tilde{\Omega} e^{i\omega_L t} \right), \quad (\text{C.3})$$

ω is the cavity frequency, U is the interaction strength, ω_L is the frequency of the drive laser, and $\hbar = 1$. The drive amplitudes, Ω and $\tilde{\Omega}$, are derived by treating the two relevant energy levels as a dipole undergoing oscillations driven by an electromagnetic field [27]. Our aim is to transform this in to a rotating frame such that the time dependence of the drive terms is eliminated

APPENDIX C. ROTATING FRAME TRANSFORMATION

from the Hamiltonian.

To achieve this the frame must rotate at the frequency of the driving laser. The appropriate transformation is,

$$\mathcal{H}_{\text{RF}} = \hat{V}^\dagger \mathcal{H}_{\text{ref}} \hat{V} - \hat{A}, \quad (\text{C.4})$$

where,

$$\hat{V} = e^{-i\hat{A}t}, \quad (\text{C.5})$$

$$\hat{A} = \frac{\omega_L}{2} \hat{a}^\dagger \hat{a}, \quad (\text{C.6})$$

and where we note that since \hat{A} is Hermitian, \hat{V} is unitary.

Considering for now just the first term in eq. (C.4) we have,

$$\begin{aligned} \hat{V}^\dagger \mathcal{H}_{\text{ref}} \hat{V} &= \hat{V}^\dagger \left(\omega \hat{a}^\dagger \hat{a} + \frac{U}{2} \hat{a}^\dagger \hat{a}^\dagger \hat{a} \hat{a} + \Omega_\uparrow \hat{a}^\dagger \hat{a}^\dagger + \Omega_\downarrow \hat{a} \hat{a}, \right) \hat{V}, \\ &= \omega \hat{V}^\dagger \hat{a}^\dagger \hat{a} \hat{V} + \frac{U}{2} \hat{V}^\dagger \hat{a}^\dagger \hat{a}^\dagger \hat{a} \hat{a} \hat{V} + \Omega_\uparrow \hat{V}^\dagger \hat{a}^\dagger \hat{a}^\dagger \hat{V} + \Omega_\downarrow \hat{V}^\dagger \hat{a} \hat{a} \hat{V}, \end{aligned} \quad (\text{C.7})$$

where we will again choose to consider each term separately. In order to do so we must make use of the following relation,

$$e^{\xi B} A e^{-\xi B} = A + \sum_{n=1}^{\infty} \frac{\xi^n}{n!} [B, A]_n, \quad (\text{C.8})$$

where the notation $[B, A]_n$ implies the repeated commutator – for example $[B, A]_3 = [B, [B, [B, A]]]$. This relation is itself derived from the power series expansion of the exponential,

$$e^z = \sum_{k=0}^{\infty} \frac{z^k}{k!}, \quad (\text{C.9})$$

which we shall also make use of. Finally we also require the bosonic commutation relation,

$$[\hat{a}, \hat{a}^\dagger] = \mathbb{I}, \quad (\text{C.10})$$

APPENDIX C. ROTATING FRAME TRANSFORMATION

which implies that,

$$\hat{a}\hat{a}^\dagger = \hat{a}^\dagger\hat{a} + \mathbb{I}, \quad (\text{C.11})$$

$$\hat{a}^\dagger\hat{a} = \hat{a}\hat{a}^\dagger - \mathbb{I}, \quad (\text{C.12})$$

which is helpful for reordering operator chains.

Returning then to the first term in eq. (C.7) we find that,

$$\begin{aligned} \omega\hat{V}^\dagger\hat{a}^\dagger\hat{a}\hat{V} &= \omega\left(\hat{a}^\dagger\hat{a} + \frac{i\omega_L t}{2}[\hat{a}^\dagger\hat{a}, \hat{a}^\dagger\hat{a}] + \mathcal{O}(\omega^2 t^2)\right), \\ &= \omega\hat{a}^\dagger\hat{a}, \end{aligned} \quad (\text{C.13})$$

since $\hat{a}^\dagger\hat{a}$ trivially commutes with itself, and we note that if the term $[B, A]_n = 0$ then so does $[B, A]_m$ for all $m > n$. Considering then the second term we find,

$$\begin{aligned} \frac{U}{2}\hat{V}^\dagger\hat{a}^\dagger\hat{a}^\dagger\hat{a}\hat{a}\hat{V} &= \frac{U}{2}\left(\hat{a}^\dagger\hat{a}^\dagger\hat{a}\hat{a} + \frac{i\omega_L t}{2}[\hat{a}^\dagger\hat{a}, \hat{a}^\dagger\hat{a}^\dagger\hat{a}\hat{a}] + \mathcal{O}(\omega^2 t^2)\right), \\ &= \frac{U}{2}\left(\hat{a}^\dagger\hat{a}^\dagger\hat{a}\hat{a} + \frac{i\omega_L t}{2}[\hat{a}^\dagger\hat{a}\hat{a}^\dagger\hat{a}^\dagger\hat{a}\hat{a} - \hat{a}^\dagger\hat{a}^\dagger\hat{a}\hat{a}\hat{a}^\dagger\hat{a}] + \mathcal{O}(\omega^2 t^2)\right), \\ &= \frac{U}{2}\left(\hat{a}^\dagger\hat{a}^\dagger\hat{a}\hat{a} + \frac{i\omega_L t}{2}[\hat{a}^\dagger\hat{a}\hat{a}^\dagger\hat{a}^\dagger\hat{a}\hat{a} - \hat{a}^\dagger(\hat{a}\hat{a}^\dagger - \mathbb{I})\hat{a}\hat{a}^\dagger\hat{a}] + \mathcal{O}(\omega^2 t^2)\right), \\ &= \frac{U}{2}\left(\hat{a}^\dagger\hat{a}^\dagger\hat{a}\hat{a} + \frac{i\omega_L t}{2}[\hat{a}^\dagger\hat{a}\hat{a}^\dagger\hat{a}^\dagger\hat{a}\hat{a} - \hat{a}^\dagger\hat{a}\hat{a}^\dagger\hat{a}\hat{a}^\dagger\hat{a} + \hat{a}^\dagger\hat{a}\hat{a}^\dagger\hat{a}] \right. \\ &\quad \left. + \mathcal{O}(\omega^2 t^2)\right), \\ &= \frac{U}{2}\left(\hat{a}^\dagger\hat{a}^\dagger\hat{a}\hat{a} + \frac{i\omega_L t}{2}[\hat{a}^\dagger\hat{a}\hat{a}^\dagger\hat{a}^\dagger\hat{a}\hat{a} - \hat{a}^\dagger\hat{a}\hat{a}^\dagger(\hat{a}^\dagger\hat{a} + \mathbb{I})\hat{a} + \hat{a}^\dagger\hat{a}\hat{a}^\dagger\hat{a}] \right. \\ &\quad \left. + \mathcal{O}(\omega^2 t^2)\right), \\ &= \frac{U}{2}\left(\hat{a}^\dagger\hat{a}^\dagger\hat{a}\hat{a} + \frac{i\omega_L t}{2}[\hat{a}^\dagger\hat{a}\hat{a}^\dagger\hat{a}^\dagger\hat{a}\hat{a} - \hat{a}^\dagger\hat{a}\hat{a}^\dagger\hat{a}^\dagger\hat{a}\hat{a} - \hat{a}^\dagger\hat{a}\hat{a}^\dagger\hat{a} + \hat{a}^\dagger\hat{a}\hat{a}^\dagger\hat{a}] \right. \\ &\quad \left. + \mathcal{O}(\omega^2 t^2)\right), \\ &= \frac{U}{2}\hat{a}^\dagger\hat{a}^\dagger\hat{a}\hat{a}, \end{aligned} \quad (\text{C.14})$$

APPENDIX C. ROTATING FRAME TRANSFORMATION

so like the on-site energy, the interaction term commutes with the rotation operator. We now consider the coherent driving terms beginning with Ω_\uparrow . Using eq. (C.8) we have that,

$$\Omega_\uparrow \hat{V}^\dagger \hat{a}^\dagger \hat{a}^\dagger \hat{V} = \Omega_\uparrow \left(\hat{a}^\dagger \hat{a}^\dagger + \sum_{n=1}^{\infty} \frac{(i\omega_L t)^n}{2^n n!} [\hat{a}^\dagger \hat{a}, \hat{a}^\dagger \hat{a}^\dagger]_n \right), \quad (\text{C.15})$$

however unlike previous terms, we do not expect these terms to commute. As the situation is more complicated here we will first consider just the first order commutator,

$$\begin{aligned} [\hat{a}^\dagger \hat{a}, \hat{a}^\dagger \hat{a}^\dagger] &= \hat{a}^\dagger \hat{a} \hat{a}^\dagger \hat{a}^\dagger - \hat{a}^\dagger \hat{a}^\dagger \hat{a}^\dagger \hat{a}, \\ &= \hat{a}^\dagger \hat{a} \hat{a}^\dagger \hat{a}^\dagger - \hat{a}^\dagger \hat{a}^\dagger (\hat{a} \hat{a}^\dagger - \mathbb{I}), \\ &= \hat{a}^\dagger \hat{a} \hat{a}^\dagger \hat{a}^\dagger - \hat{a}^\dagger \hat{a}^\dagger \hat{a} \hat{a}^\dagger + \hat{a}^\dagger \hat{a}^\dagger, \\ &= \hat{a}^\dagger \hat{a} \hat{a}^\dagger \hat{a}^\dagger - \hat{a}^\dagger (\hat{a} \hat{a}^\dagger - \mathbb{I}) \hat{a}^\dagger + \hat{a}^\dagger \hat{a}^\dagger, \\ &= \hat{a}^\dagger \hat{a} \hat{a}^\dagger \hat{a}^\dagger - \hat{a}^\dagger \hat{a} \hat{a}^\dagger \hat{a}^\dagger + \hat{a}^\dagger \hat{a}^\dagger + \hat{a}^\dagger \hat{a}^\dagger, \\ &= 2\hat{a}^\dagger \hat{a}^\dagger, \end{aligned} \quad (\text{C.16})$$

which implies the repeated commutation relation,

$$[\hat{a}^\dagger \hat{a}, \hat{a}^\dagger \hat{a}^\dagger]_n = 2^n \hat{a}^\dagger \hat{a}^\dagger, \quad (\text{C.17})$$

which we can substitute back in to eq. (C.15). Doing so yields,

$$\begin{aligned} \Omega_\uparrow \hat{V}^\dagger \hat{a}^\dagger \hat{a}^\dagger \hat{V} &= \Omega_\uparrow \left[\hat{a}^\dagger \hat{a}^\dagger + \sum_{n=1}^{\infty} \frac{(i\omega_L t)^n}{2^n n!} (2^n \hat{a}^\dagger \hat{a}^\dagger) \right], \\ &= \Omega_\uparrow \left[\hat{a}^\dagger \hat{a}^\dagger + \sum_{n=1}^{\infty} \frac{(i\omega_L t)^n}{n!} \hat{a}^\dagger \hat{a}^\dagger \right], \\ &= \Omega_\uparrow \sum_{n=0}^{\infty} \frac{(i\omega_L t)^n}{n!} \hat{a}^\dagger \hat{a}^\dagger, \\ &= \Omega_\uparrow e^{i\omega_L t} \hat{a}^\dagger \hat{a}^\dagger, \end{aligned} \quad (\text{C.18})$$

indicating a rotation of the drive terms, as expected. Expanding the coefficient

APPENDIX C. ROTATING FRAME TRANSFORMATION

we get,

$$\begin{aligned}\Omega_{\uparrow} e^{i\omega_L t} \hat{a}^\dagger \hat{a}^\dagger &= \frac{1}{\sqrt{2}} \left(\Omega e^{-i\omega_L t} + \tilde{\Omega} e^{i\omega_L t} \right) e^{i\omega_L t} \hat{a}^\dagger \hat{a}^\dagger, \\ &= \frac{1}{\sqrt{2}} \left(\Omega + \tilde{\Omega} e^{2i\omega_L t} \right) \hat{a}^\dagger \hat{a}^\dagger.\end{aligned}\quad (\text{C.19})$$

It is here that we make the rotating wave approximation. We consider the term $\tilde{\Omega} e^{2i\omega_L t}$ to be a high frequency perturbation to the static term Ω , and thus neglect it. As a result, we are left with the rotated coherent drive term,

$$\Omega_{\uparrow} \hat{V}^\dagger \hat{a}^\dagger \hat{a}^\dagger \hat{V} = \frac{\Omega}{\sqrt{2}} \hat{a}^\dagger \hat{a}^\dagger, \quad (\text{C.20})$$

and since the annihilating coherent drive term must be the Hermitian conjugate of the creating term, we surmise it has the form,

$$\Omega_{\downarrow} e^{i\omega_L t} \hat{a} \hat{a} = \frac{\Omega^*}{\sqrt{2}} \hat{a} \hat{a}. \quad (\text{C.21})$$

We can now substitute eqs. (C.6), (C.13), (C.14), (C.20) and (C.21) in to eq. (C.4) to find the rotating frame Hamiltonian,

$$\begin{aligned}\mathcal{H}_{\text{RF}} &= \omega \hat{a}^\dagger \hat{a} + \frac{U}{2} \hat{a}^\dagger \hat{a}^\dagger \hat{a} \hat{a} + \frac{\Omega}{\sqrt{2}} \hat{a}^\dagger \hat{a}^\dagger + \frac{\Omega^*}{\sqrt{2}} \hat{a} \hat{a} - \frac{\omega_L}{2} \hat{a}^\dagger \hat{a}, \\ &= \left(\omega - \frac{\omega_L}{2} \right) \hat{a}^\dagger \hat{a} + \frac{U}{2} \hat{a}^\dagger \hat{a}^\dagger \hat{a} \hat{a} + \frac{\Omega}{\sqrt{2}} \hat{a}^\dagger \hat{a}^\dagger + \frac{\Omega^*}{\sqrt{2}} \hat{a} \hat{a}, \\ &= \Delta \hat{a}^\dagger \hat{a} + \frac{U}{2} \hat{a}^\dagger \hat{a}^\dagger \hat{a} \hat{a} + \frac{\Omega}{\sqrt{2}} \hat{a}^\dagger \hat{a}^\dagger + \frac{\Omega^*}{\sqrt{2}} \hat{a} \hat{a},\end{aligned}\quad (\text{C.22})$$

where $\Delta = \omega_L/2$ is the detuning.

C.2 Coupled cavities

Having found the rotating frame Hamiltonian for a single cavity, we now introduce a second site in order to determine the impact of the transformation on

APPENDIX C. ROTATING FRAME TRANSFORMATION

a hopping interaction. The reference Hamiltonian is now,

$$\mathcal{H}_{\text{ref}} = \sum_{j=1}^2 \left[\omega \hat{a}_j^\dagger \hat{a}_j + \frac{U}{2} \hat{a}_j^\dagger \hat{a}_j^\dagger \hat{a}_j \hat{a}_j + \Omega_\uparrow \hat{a}_j^\dagger \hat{a}_j^\dagger + \Omega_\downarrow \hat{a}_j \hat{a}_j - J (\hat{a}_j^\dagger \hat{a}_{j+1} + \hat{a}_j \hat{a}_{j+1}^\dagger) \right], \quad (\text{C.23})$$

where J is the hopping rate between sites. The rotating frame Hamiltonian is given by,

$$\mathcal{H}_{\text{RF}} = \sum_{j=1}^2 \left[\Delta \hat{a}_j^\dagger \hat{a}_j + \frac{U}{2} \hat{a}_j^\dagger \hat{a}_j^\dagger \hat{a}_j \hat{a}_j + \frac{\Omega}{\sqrt{2}} \hat{a}_j^\dagger \hat{a}_j^\dagger + \frac{\Omega^*}{\sqrt{2}} \hat{a}_j \hat{a}_j \right] + \mathcal{H}_{\text{RF},J}, \quad (\text{C.24})$$

where $\mathcal{H}_{\text{RF},J}$ is the rotating frame hopping term we have yet to find. It is determined using the same procedure as the local terms so,

$$\begin{aligned} \mathcal{H}_{\text{RF},J} &= -J \hat{V}^\dagger (\hat{a}_j^\dagger \hat{a}_{j+1} + \hat{a}_j \hat{a}_{j+1}^\dagger) \hat{V}, \\ &= -J \left(\hat{a}_j^\dagger \hat{a}_{j+1} + \hat{a}_j \hat{a}_{j+1}^\dagger \right. \\ &\quad \left. + \sum_{n=1}^{\infty} \frac{(i\omega_L t)}{2^n n!} [\hat{a}_j^\dagger \hat{a}_j + \hat{a}_{j+1}^\dagger \hat{a}_{j+1}, \hat{a}_j^\dagger \hat{a}_{j+1} + \hat{a}_j \hat{a}_{j+1}^\dagger]_n \right), \end{aligned} \quad (\text{C.25})$$

where we note that the only difference to the transform operator is that there is now a sum across sites, $\hat{A} = \sum_j (\omega_L/2) \hat{a}_j^\dagger \hat{a}_j$. To reduce this term we will need to make use of the many-body bosonic commutation relation,

$$[\hat{a}_j, \hat{a}_k^\dagger] = \delta_{j,k}, \quad (\text{C.26})$$

so that the operators commute unless they are acting on the same site ($j = k$), in which case the standard relations eqs. (C.10) to (C.12) apply. With this in

APPENDIX C. ROTATING FRAME TRANSFORMATION

mind, we will investigate the first order commutator,

$$\begin{aligned}
& \left[\hat{a}_j^\dagger \hat{a}_j + \hat{a}_{j+1}^\dagger \hat{a}_{j+1}, \hat{a}_j^\dagger \hat{a}_{j+1} + \hat{a}_j \hat{a}_{j+1}^\dagger \right] \\
&= \hat{a}_j^\dagger \hat{a}_j \hat{a}_j^\dagger \hat{a}_{j+1} + \hat{a}_j^\dagger \hat{a}_j \hat{a}_j \hat{a}_{j+1}^\dagger \\
&\quad + \hat{a}_{j+1}^\dagger \hat{a}_{j+1} \hat{a}_j^\dagger \hat{a}_{j+1} + \hat{a}_{j+1}^\dagger \hat{a}_{j+1} \hat{a}_j \hat{a}_{j+1}^\dagger \\
&\quad - \hat{a}_j^\dagger \hat{a}_{j+1} \hat{a}_j^\dagger \hat{a}_j - \hat{a}_j^\dagger \hat{a}_{j+1} \hat{a}_{j+1}^\dagger \hat{a}_{j+1} \\
&\quad - \hat{a}_j \hat{a}_{j+1}^\dagger \hat{a}_j^\dagger \hat{a}_j - \hat{a}_j \hat{a}_{j+1}^\dagger \hat{a}_{j+1}^\dagger \hat{a}_{j+1}, \\
&= \hat{a}_j^\dagger \hat{a}_j \hat{a}_j^\dagger \hat{a}_{j+1} - \hat{a}_j^\dagger \hat{a}_j^\dagger \hat{a}_j \hat{a}_{j+1} \\
&\quad + \hat{a}_j^\dagger \hat{a}_j \hat{a}_j \hat{a}_{j+1}^\dagger - \hat{a}_j \hat{a}_j^\dagger \hat{a}_j \hat{a}_{j+1}^\dagger \\
&\quad + \hat{a}_j^\dagger \hat{a}_{j+1}^\dagger \hat{a}_{j+1} \hat{a}_{j+1} - \hat{a}_j^\dagger \hat{a}_{j+1} \hat{a}_{j+1}^\dagger \hat{a}_{j+1} \\
&\quad + \hat{a}_j \hat{a}_{j+1}^\dagger \hat{a}_{j+1} \hat{a}_{j+1}^\dagger - \hat{a}_j \hat{a}_{j+1}^\dagger \hat{a}_{j+1}^\dagger \hat{a}_{j+1}, \\
&= \hat{a}_j^\dagger \hat{a}_j \hat{a}_j^\dagger \hat{a}_{j+1} - \hat{a}_j^\dagger (\hat{a}_j \hat{a}_j^\dagger - \mathbb{I}) \hat{a}_{j+1} \\
&\quad + \hat{a}_j^\dagger \hat{a}_j \hat{a}_j \hat{a}_{j+1}^\dagger - (\hat{a}_j^\dagger \hat{a}_j + \mathbb{I}) \hat{a}_j \hat{a}_{j+1}^\dagger \\
&\quad + \hat{a}_j^\dagger \hat{a}_{j+1}^\dagger \hat{a}_{j+1} \hat{a}_{j+1} - \hat{a}_j^\dagger (\hat{a}_{j+1}^\dagger \hat{a}_{j+1} + \mathbb{I}) \hat{a}_{j+1} \\
&\quad + \hat{a}_j \hat{a}_{j+1}^\dagger \hat{a}_{j+1} \hat{a}_{j+1}^\dagger - \hat{a}_j \hat{a}_{j+1}^\dagger (\hat{a}_{j+1} \hat{a}_{j+1}^\dagger - \mathbb{I}), \\
&= \hat{a}_j^\dagger \hat{a}_j \hat{a}_j^\dagger \hat{a}_{j+1} - \hat{a}_j^\dagger \hat{a}_j \hat{a}_j \hat{a}_{j+1}^\dagger + \hat{a}_j^\dagger \hat{a}_{j+1} \\
&\quad + \hat{a}_j^\dagger \hat{a}_j \hat{a}_j \hat{a}_{j+1}^\dagger - \hat{a}_j^\dagger \hat{a}_j \hat{a}_j \hat{a}_{j+1}^\dagger - \hat{a}_j \hat{a}_{j+1}^\dagger \\
&\quad + \hat{a}_j^\dagger \hat{a}_{j+1}^\dagger \hat{a}_{j+1} \hat{a}_{j+1} - \hat{a}_j^\dagger \hat{a}_{j+1}^\dagger \hat{a}_{j+1} \hat{a}_{j+1} - \hat{a}_j^\dagger \hat{a}_{j+1} \\
&\quad + \hat{a}_j \hat{a}_{j+1}^\dagger \hat{a}_{j+1} \hat{a}_{j+1}^\dagger - \hat{a}_j \hat{a}_{j+1}^\dagger \hat{a}_{j+1} \hat{a}_{j+1}^\dagger + \hat{a}_j \hat{a}_{j+1}^\dagger, \\
&= \hat{a}_j^\dagger \hat{a}_{j+1} - \hat{a}_j \hat{a}_{j+1}^\dagger - \hat{a}_j^\dagger \hat{a}_{j+1} + \hat{a}_j \hat{a}_{j+1}^\dagger, \\
&= 0,
\end{aligned} \tag{C.27}$$

which means that in the rotating frame the hopping term is given by,

$$\mathcal{H}_{\text{RF},J} = -J \left(\hat{a}_j^\dagger \hat{a}_{j+1} + \hat{a}_j \hat{a}_{j+1}^\dagger \right), \tag{C.28}$$

with no time dependency introduced by the transformation, as expected.

We can then write our full driven nonlinear cavity array Hamiltonian in

APPENDIX C. ROTATING FRAME TRANSFORMATION

the rotating frame, with the rotating wave approximation applied as,

$$\mathcal{H} = \sum_j \left[\Delta \hat{a}_j^\dagger \hat{a}_j + \frac{U}{2} \hat{a}_j^\dagger \hat{a}_j^\dagger \hat{a}_j \hat{a}_j + \frac{\Omega}{\sqrt{2}} \hat{a}_j^\dagger \hat{a}_j^\dagger + \frac{\Omega^*}{\sqrt{2}} \hat{a}_j \hat{a}_j - J (\hat{a}_j^\dagger \hat{a}_{j+1} + \hat{a}_j \hat{a}_{j+1}^\dagger) \right], \quad (\text{C.29})$$

which is the same form as that given in eqs. (5.1) to (5.4).

Appendix D

Two-level effective master equation

Here we perform an adiabatic elimination of the doubly-excited state from the master equation for a driven nonlinear cavity array, resulting in an effective model for the system truncated to the subspace of at most one excitation per site. To do this, we follow the prescription given in reference [127], beginning by separating our initial three-level master equation eq. (5.5) in to two components,

$$\mathcal{L}\rho = (\mathcal{L}_0 + \nu)\rho, \quad (\text{D.1})$$

where the subspace dynamics of interest takes place in the stationary states of \mathcal{L}_0 , and ν contains all other terms of the master equation. In our case,

$$\mathcal{L}_0\rho = D_1 [\rho], \quad (\text{D.2})$$

$$\nu\rho = -i [\mathcal{H}, \rho] + \mathcal{D}_0 [\rho], \quad (\text{D.3})$$

where,

$$\mathcal{H} = \sum_j \left[\frac{\Omega}{\sqrt{2}} \hat{a}_j^\dagger \hat{a}_j^\dagger + \frac{\Omega^*}{\sqrt{2}} \hat{a}_j \hat{a}_j - J \left(\hat{a}_j \hat{a}_{j+1}^\dagger + \hat{a}_j^\dagger \hat{a}_{j+1} \right) \right], \quad (\text{D.4})$$

$$\mathcal{D}_m [\rho] = \sum_{m,j} \frac{\gamma_m}{2} \left[2\kappa_{m,j} \rho \kappa_{m,j}^\dagger - \left\{ \kappa_{m,j}^\dagger \kappa_{m,j}, \rho \right\} \right], \quad (\text{D.5})$$

$\kappa_{m,j} = |m_j\rangle\langle m+1_j|$, and we have set the on-site energy and interaction terms in the Hamiltonian $\Delta = -U/2 = 0$ for simplicity. Those terms will only modify the energy of the two levels we retain, and we are primarily interested in seeing how the drive and dissipation interact in the two level approximation. We will treat ν as a perturbation to \mathcal{L}_0 , and project it on to the single excitation subspace. This approximation is valid in the limit where the fast decay rate γ_1 dominates ($\gamma_1 \gg \Omega, J, \gamma_0$).

D.1 Definitions

The truncated density matrix, which contains only the subspace we are interested in, is given by,

$$\rho_0 = Q_0 \rho_0 Q_0, \quad (\text{D.6})$$

where the projector,

$$Q_0 = q_0^{\otimes N}, \quad (\text{D.7})$$

and the subspace identity, $q_0 = (|0\rangle\langle 0| + |1\rangle\langle 1|)^{\otimes N}$. We then define a series of pseudo-projectors,

$$\mathcal{P}_0 X = Q_0 X Q_0 + \sum_j \kappa_{1,j} Q_1 X Q_1 \kappa_{1,j}^\dagger, \quad (\text{D.8})$$

$$\mathcal{P}_{1a} X = Q_1 X Q_0, \quad (\text{D.9})$$

$$\mathcal{P}_{1b} X = Q_0 X Q_1, \quad (\text{D.10})$$

where the projector,

$$Q_1 = \sum_j q_0^{\otimes j-1} \otimes |2\rangle\langle 2| \otimes q_0^{\otimes N-j}, \quad (\text{D.11})$$

so it is the sum of all configurations of the system, with one and only one doubly occupied site. To second order, the two-level effective master equation will be given by,

$$\dot{\rho} = (\mathcal{L}_1 + \mathcal{L}_2) \rho_0, \quad (\text{D.12})$$

where,

$$\mathcal{L}_1 = \mathcal{P}_0 \nu \mathcal{P}_0, \quad (\text{D.13})$$

$$\mathcal{L}_2 = \sum_{c \in \{1a, 1b\}} \frac{-1}{\lambda_c} \mathcal{P}_0 \nu \mathcal{P}_c \nu \mathcal{P}_0, \quad (\text{D.14})$$

and where $\lambda_c = -\gamma_1/2$. During the derivation, to make it obvious when we have truncated an operator we will replace it with,

$$\hat{\sigma} = Q_0 \hat{a} Q_0. \quad (\text{D.15})$$

D.2 First order

The first order term of the two-level effective master equation is given by,

$$\begin{aligned} \mathcal{L}_1 \rho_0 &= \mathcal{P}_0 \nu \mathcal{P}_0 \rho_0, \\ &= \mathcal{P}_0 \nu \left(Q_0 \rho_0 Q_0 + \sum_j \kappa_{1,j} Q_1 \rho_0 Q_1 \kappa_{1,j}^\dagger \right), \\ &= \mathcal{P}_0 \nu \rho_0, \\ &= Q_0 (\nu \rho_0) Q_0 + \sum_j \kappa_{1,j} Q_1 (\nu \rho_0) Q_1 \kappa_{1,j}^\dagger, \end{aligned} \quad (\text{D.16})$$

where we have used that $Q_0 Q_1 = 0$, and thus $Q_1 \rho_0 = 0$. We will consider each of these terms separately, starting with the simpler of the two,

$$Q_0 \nu \rho_0 Q_0 = Q_0 \left(-i [\mathcal{H}, \rho_0] + \frac{\gamma_0}{2} \sum_j \left[2\kappa_{0,j} \rho_0 \kappa_{0,j}^\dagger - \{\kappa_{0,j}^\dagger \kappa_{0,j}, \rho_0\} \right] \right) Q_0, \quad (\text{D.17})$$

APPENDIX D. TWO-LEVEL EFFECTIVE MASTER EQUATION

which we shall also treat separately, dealing first with the commutator. As such,

$$\begin{aligned} Q_0 (-i[\mathcal{H}, \rho_0]) Q_0 &= -iQ_0 \mathcal{H} \rho_0 Q_0 + iQ_0 \rho_0 \mathcal{H} Q_0, \\ &= -iQ_0 \mathcal{H} Q_0 \rho_0 + i\rho_0 Q_0 \mathcal{H} Q_0, \\ &= -i[\mathcal{H}_J, \rho_0], \end{aligned} \quad (\text{D.18})$$

where,

$$\mathcal{H}_J = -J \sum_j \left[\hat{\sigma}_j \hat{\sigma}_{j+1}^\dagger + \hat{\sigma}_j^\dagger \hat{\sigma}_{j+1} \right], \quad (\text{D.19})$$

since the coherent drive terms drive directly to the doubly excited subspace and are thus annihilated when braced by the single-excitation subspace identity. Considering next the dissipator from eq. (D.17),

$$\begin{aligned} Q_0 &\left(\frac{\gamma_0}{2} \sum_j \left[2\kappa_{0,j} \rho_0 \kappa_{0,j}^\dagger - \{\kappa_{0,j}^\dagger \kappa_{0,j}, \rho_0\} \right] \right) Q_0 \\ &= \frac{\gamma_0}{2} \sum_j \left[2Q_0 \kappa_{0,j} \rho_0 \kappa_{0,j}^\dagger Q_0 - Q_0 \kappa_{0,j}^\dagger \kappa_{0,j} \rho_0 Q_0 - Q_0 \rho_0 \kappa_{0,j}^\dagger \kappa_{0,j} Q_0 \right], \\ &= \frac{\gamma_0}{2} \sum_j \left[2Q_0 \kappa_{0,j} \rho_0 \kappa_{0,j}^\dagger Q_0 - Q_0 \kappa_{0,j}^\dagger \kappa_{0,j} Q_0 \rho_0 - \rho_0 Q_0 \kappa_{0,j}^\dagger \kappa_{0,j} Q_0 \right], \\ &= \frac{\gamma_0}{2} \sum_j \left[2\hat{\sigma}_j \rho_0 \hat{\sigma}_j^\dagger - \{\hat{\sigma}_j^\dagger \hat{\sigma}_j, \rho_0\} \right], \end{aligned} \quad (\text{D.20})$$

where we have used the fact that $\kappa_0 = |0\rangle\langle 1| = \hat{\sigma}$.

We now turn to the Q_1 term from eq. (D.16),

$$\begin{aligned} \sum_j \kappa_{1,j} Q_1 \nu \rho_0 Q_1 \kappa_{1,j}^\dagger \\ &= \sum_j \kappa_{1,j} Q_1 \left(-i[\mathcal{H}, \rho_0] + \frac{\gamma_0}{2} \sum_k \left[2\kappa_{0,k} \rho_0 \kappa_{0,k}^\dagger - \{\kappa_{0,k}^\dagger \kappa_{0,k}, \rho_0\} \right] \right) Q_1 \kappa_{1,j}^\dagger, \end{aligned} \quad (\text{D.21})$$

APPENDIX D. TWO-LEVEL EFFECTIVE MASTER EQUATION

where we will again consider the commutator first. As such,

$$\begin{aligned} \sum_j \kappa_{1,j} Q_1 (-i[\mathcal{H}, \rho_0]) Q_1 \kappa_{1,j}^\dagger &= -i \sum_j \kappa_{1,j} Q_1 \mathcal{H} \rho_0 Q_1 \kappa_{1,j}^\dagger \\ &\quad + i \sum_j \kappa_{1,j} Q_1 \rho_0 \mathcal{H} Q_1 \kappa_{1,j}^\dagger, \\ &= 0, \end{aligned} \tag{D.22}$$

where we have again used that $Q_0 Q_1 = Q_1 Q_0 = 0$. The dissipator,

$$\begin{aligned} &\sum_j \kappa_{1,j} Q_1 \left(\frac{\gamma_0}{2} \sum_k \left[2\kappa_{0,k} \rho_0 \kappa_{0,k}^\dagger - \{\kappa_{0,k}^\dagger \kappa_{0,k}, \rho_0\} \right] \right) Q_1 \kappa_{1,j}^\dagger \\ &= \sum_j \frac{\gamma_0}{2} \kappa_{1,j} \left(\sum_k [2Q_1 \kappa_{0,k} \rho_0 \kappa_{0,k}^\dagger Q_1 - Q_1 \kappa_{0,k}^\dagger \kappa_{0,k} \rho_0 Q_1 \right. \\ &\quad \left. - Q_1 \rho_0 \kappa_{0,k}^\dagger \kappa_{0,k} Q_1] \right) \kappa_{1,j}^\dagger, \\ &= \sum_j \frac{\gamma_0}{2} \kappa_{1,j} \left(\sum_k 2Q_1 \kappa_{0,k} \rho_0 \kappa_{0,k}^\dagger Q_1 \right) \kappa_{1,j}^\dagger, \\ &= \sum_j \frac{\gamma_0}{2} \kappa_{1,j} \left(\sum_k 2\kappa_{0,k} Q_1 \rho_0 Q_1 \kappa_{0,k}^\dagger \right) \kappa_{1,j}^\dagger, \\ &= 0, \end{aligned} \tag{D.23}$$

where we have used that $[Q_1, \kappa_{0,j}] = 0$.

We may now put together the results from eqs. (D.18), (D.20), (D.22) and (D.23) to write out the first order two-level effective master equation,

$$\mathcal{L}_1 \rho_0 = -i [\mathcal{H}_J, \rho_0] + \frac{\gamma_0}{2} \sum_j \left[2\hat{\sigma}_j \rho_0 \hat{\sigma}_j^\dagger - \{\hat{\sigma}_j^\dagger \hat{\sigma}_j, \rho_0\} \right], \tag{D.24}$$

where $\mathcal{H}_J = -J \sum_j [\hat{\sigma}_j \hat{\sigma}_{j+1}^\dagger + \hat{\sigma}_j^\dagger \hat{\sigma}_{j+1}]$ as in eq. (D.19).

D.3 Second order

The second order term of the two-level effective master equation is given by,

$$\begin{aligned}\mathcal{L}_2\rho_0 &= \sum_{c \in \{1a, 1b\}} \frac{-1}{\lambda_c} \mathcal{P}_0 \nu \mathcal{P}_c \nu \mathcal{P}_0 \rho_0, \\ &= \frac{2}{\gamma_1} (\mathcal{P}_0 \nu \mu_{1a} + \mathcal{P}_0 \nu \mu_{1b}),\end{aligned}\quad (\text{D.25})$$

where we have used that $\lambda_c = \gamma_1/2$, and defined,

$$\mu_{1a} = Q_1 \nu \rho_0 Q_0, \quad (\text{D.26})$$

$$\mu_{1b} = Q_0 \nu \rho_0 Q_1, \quad (\text{D.27})$$

which we shall find explicit forms for before continuing with eq. (D.25). The first term,

$$\begin{aligned}\mu_{1a} &= Q_1 \left(-i [\mathcal{H}, \rho_0] + \frac{\gamma_0}{2} \sum_j [2\kappa_{0,j} \rho_0 \kappa_{0,j}^\dagger - \kappa_{0,j}^\dagger \kappa_{0,j} \rho_0 - \rho_0 \kappa_{0,j}^\dagger \kappa_{0,j}] \right) Q_0, \\ &= -i Q_1 \mathcal{H} \rho_0 Q_0 + i Q_1 \rho_0 \mathcal{H} Q_0, \\ &= -i Q_1 \mathcal{H} \rho_0,\end{aligned}\quad (\text{D.28})$$

and the second,

$$\begin{aligned}\mu_{1b} &= Q_0 \left(-i [\mathcal{H}, \rho_0] + \frac{\gamma_0}{2} \sum_j [2\kappa_{0,j} \rho_0 \kappa_{0,j}^\dagger - \kappa_{0,j}^\dagger \kappa_{0,j} \rho_0 - \rho_0 \kappa_{0,j}^\dagger \kappa_{0,j}] \right) Q_1, \\ &= -i Q_0 \mathcal{H} \rho_0 Q_1 + i Q_0 \rho_0 \mathcal{H} Q_1, \\ &= i \rho_0 \mathcal{H} Q_1,\end{aligned}\quad (\text{D.29})$$

where we note that $\mu_{1b} = \mu_{1a}^\dagger$.

Returning to the first term in eq. (D.25),

$$\mathcal{P}_0 \nu \mu_{1a} = Q_0 \nu \mu_{1a} Q_0 + \sum_j \kappa_{1,j} Q_1 \nu \mu_{1a} Q_1 \kappa_{1,j}^\dagger, \quad (\text{D.30})$$

APPENDIX D. TWO-LEVEL EFFECTIVE MASTER EQUATION

and dealing with the Q_0 term first,

$$Q_0 \nu \mu_{1a} Q_0 = Q_0 \left(-i [\mathcal{H}, \mu_{1a}] + \frac{\gamma_0}{2} \sum_j \left[2\kappa_{0,j} \mu_{1a} \kappa_{0,j}^\dagger - \{\kappa_{0,j}^\dagger \kappa_{0,j}, \mu_{1a}\} \right] \right) Q_0, \quad (\text{D.31})$$

where we will, as before, consider the commutator first. As such,

$$\begin{aligned} -iQ_0 [\mathcal{H}, \mu_{1a}] Q_0 &= -iQ_0 \mathcal{H} \mu_{1a} Q_0 + iQ_0 \mu_{1a} \mathcal{H} Q_0, \\ &= -iQ_0 \mathcal{H} (-iQ_1 \mathcal{H} \rho_0) Q_0 + iQ_0 (-iQ_1 \mathcal{H} \rho_0) Q_0, \\ &= i^2 Q_0 \mathcal{H} Q_1 \mathcal{H} Q_0 \rho_0 - i^2 Q_0 Q_1 \mathcal{H} Q_0 \rho_0, \\ &= -Q_0 \mathcal{H} Q_1 \mathcal{H} Q_0 \rho_0, \\ &= - \left(\sum_j [|\Omega|^2 \hat{\sigma}_j \hat{\sigma}_j^\dagger - \sqrt{2} J \Omega^* \hat{\sigma}_j \hat{\sigma}_{j+1} - \sqrt{2} J \Omega^* \hat{\sigma}_{j-1} \hat{\sigma}_j \right. \\ &\quad \left. - \sqrt{2} J \Omega \hat{\sigma}_j^\dagger \hat{\sigma}_{j+1}^\dagger + 2 J^2 \hat{\sigma}_{j-1} \hat{\sigma}_j^\dagger \hat{\sigma}_j \hat{\sigma}_{j+1}^\dagger \right. \\ &\quad \left. + 2 J^2 \hat{\sigma}_j^\dagger \hat{\sigma}_j \hat{\sigma}_{j+1}^\dagger \hat{\sigma}_{j+1} - \sqrt{2} J \Omega \hat{\sigma}_{j-1}^\dagger \hat{\sigma}_j^\dagger \right. \\ &\quad \left. + 2 J^2 \hat{\sigma}_{j-1}^\dagger \hat{\sigma}_{j-1} \hat{\sigma}_j^\dagger \hat{\sigma}_j + 2 J^2 \hat{\sigma}_{j-1}^\dagger \hat{\sigma}_j^\dagger \hat{\sigma}_j \hat{\sigma}_{j+1}] \right) \rho_0, \\ &= -\frac{1}{2} \sum_j \alpha_j \alpha_j^\dagger \rho_0, \end{aligned} \quad (\text{D.32})$$

where we have defined,

$$\alpha_j = \sqrt{2} \Omega^* \hat{\sigma}_j - 2 J \hat{\sigma}_j^\dagger \hat{\sigma}_j \left(\hat{\sigma}_{j+1}^\dagger + \hat{\sigma}_{j-1}^\dagger \right). \quad (\text{D.33})$$

The explicit expansion of $Q_0 \mathcal{H} Q_1 \mathcal{H} Q_0$ in eq. (D.32) has been missed out, simply because even by the standards of this appendix it is lengthy, and furthermore it is quite trivial, requiring no special properties or assumptions.

APPENDIX D. TWO-LEVEL EFFECTIVE MASTER EQUATION

We next consider the dissipator from eq. (D.31),

$$\begin{aligned}
& Q_0 \left(\frac{\gamma_0}{2} \sum_j \left[2\kappa_{0,j} \mu_{1a} \kappa_{0,j}^\dagger - \{\kappa_{0,j}^\dagger \kappa_{0,j}, \mu_{1a}\} \right] \right) Q_0 \\
&= \frac{\gamma_0}{2} \sum_j [2\kappa_{0,j} Q_0 \mu_{1a} Q_0 \kappa_{0,j}^\dagger - \kappa_{0,j}^\dagger \kappa_{0,j} Q_0 \mu_{1a} Q_0 - Q_0 \mu_{1a} Q_0 \kappa_{0,j}^\dagger \kappa_{0,j}], \\
&= 0,
\end{aligned} \tag{D.34}$$

where we have used that $[Q_0, \kappa_{0,j}] = 0$.

Next, the Q_1 terms in eq. (D.30),

$$\begin{aligned}
& \sum_j \kappa_{1,j} Q_1 \nu \mu_{1a} Q_1 \kappa_{1,j}^\dagger \\
&= \sum_j \kappa_{1,j} Q_1 \left(-i [\mathcal{H}, \mu_{1a}] + \frac{\gamma_0}{2} \sum_k \left[2\kappa_{0,k} \mu_{1a} \kappa_{0,k}^\dagger - \{\kappa_{0,k}^\dagger \kappa_{0,k}, \mu_{1a}\} \right] \right) Q_1 \kappa_{1,j}^\dagger,
\end{aligned} \tag{D.35}$$

where it should come as no surprise that we will consider the commutator first. It is,

$$\begin{aligned}
& \sum_j \kappa_{1,j} Q_1 (-i [\mathcal{H}, \mu_{1a}]) Q_1 \kappa_{1,j}^\dagger \\
&= \sum_j \left[-i \kappa_{1,j} Q_1 \mathcal{H} \mu_{1a} Q_1 \kappa_{1,j}^\dagger + i \kappa_{1,j} Q_1 \mu_{1a} \mathcal{H} Q_1 \kappa_{1,j}^\dagger \right], \\
&= \sum_j \left[-i \kappa_{1,j} Q_1 \mathcal{H} (-i Q_1 \mathcal{H} \rho_0) Q_1 \kappa_{1,j}^\dagger + i \kappa_{1,j} Q_1 (-i Q_1 \mathcal{H} \rho_0) \mathcal{H} Q_1 \kappa_{1,j}^\dagger \right], \\
&= \sum_j \left[i^2 \kappa_{1,j} Q_1 \mathcal{H} Q_1 \mathcal{H} \rho_0 Q_1 \kappa_{1,j}^\dagger - i^2 \kappa_{1,j} Q_1 \mathcal{H} \rho_0 \mathcal{H} Q_1 \kappa_{1,j}^\dagger \right], \\
&= \sum_j \kappa_{1,j} Q_1 \mathcal{H} Q_0 \rho_0 Q_0 \mathcal{H} Q_1 \kappa_{1,j}^\dagger, \\
&= \sum_j \left[\left(\frac{1}{\sqrt{2}} \alpha_j^\dagger \right) \rho_0 \left(\frac{1}{\sqrt{2}} \alpha_j \right) \right], \\
&= \frac{1}{2} \sum_j \alpha_j^\dagger \rho_0 \alpha_j,
\end{aligned} \tag{D.36}$$

APPENDIX D. TWO-LEVEL EFFECTIVE MASTER EQUATION

where we have again neglected to show the full expansion of terms, however we note that the fact that $\kappa_{1,j}Q_1\mathcal{H}Q_0 = (Q_0\mathcal{H}Q_1\kappa_{1,j}^\dagger)^\dagger$ saves some time here.

Next the dissipator from eq. (D.35),

$$\begin{aligned} & \sum_j \kappa_{1,j}Q_1 \left(\frac{\gamma_0}{2} \sum_k \left[2\kappa_{0,k}\mu_{1a}\kappa_{0,k}^\dagger - \{\kappa_{0,k}^\dagger\kappa_{0,k}, \mu_{1a}\} \right] \right) Q_1\kappa_{1,j}^\dagger \\ &= \sum_j \frac{\gamma_0}{2} \kappa_{1,j} \left(\sum_k \left[2\kappa_0 Q_1 \mu_{1a} Q_1 \kappa_{0,k}^\dagger - \kappa_{0,k}^\dagger \kappa_{0,k} Q_1 \mu_{1a} Q_1 \right. \right. \\ &\quad \left. \left. - Q_1 \mu_{1a} Q_1 \kappa_{0,k}^\dagger \kappa_{0,k} \right] \right) \kappa_{1,j}^\dagger, \\ &= 0, \end{aligned} \tag{D.37}$$

where we have again used that $[Q_1, \kappa_{0,j}] = 0$ and $Q_0Q_1 = 0$.

We are now able to piece together the results from eqs. (D.32), (D.34), (D.36) and (D.37), and substitute them in to eq. (D.30) to find,

$$\mathcal{P}_0\nu\mu_{1a} = \sum_j \left[\frac{1}{2}\alpha_j^\dagger\rho_0\alpha_j - \frac{1}{2}\alpha_j\alpha_j^\dagger\rho_0 \right]. \tag{D.38}$$

Furthermore, since $\mu_{1b} = \mu_{1a}^\dagger$ we may surmise that,

$$\mathcal{P}_0\nu\mu_{1b} = \sum_j \left[\frac{1}{2}\alpha_j^\dagger\rho_0\alpha_j - \frac{1}{2}\rho_0\alpha_j\alpha_j^\dagger \right]. \tag{D.39}$$

Finally, we may substitute the results from eqs. (D.38) and (D.39) back in to eq. (D.25) and state the form of the second-order Liouvillian,

$$\begin{aligned} \mathcal{L}_2\rho_0 &= \frac{2}{\gamma_1} \left(\sum_j \left[\frac{1}{2}\alpha_j^\dagger\rho_0\alpha_j - \frac{1}{2}\alpha_j\alpha_j^\dagger\rho_0 \right] + \sum_j \left[\frac{1}{2}\alpha_j^\dagger\rho_0\alpha_j - \frac{1}{2}\rho_0\alpha_j\alpha_j^\dagger \right] \right), \\ &= \frac{2}{\gamma_1} \sum_j \left[\alpha_j^\dagger\rho_0\alpha_j - \frac{1}{2}\alpha_j\alpha_j^\dagger\rho_0 - \frac{1}{2}\rho_0\alpha_j\alpha_j^\dagger \right], \\ &= \frac{1}{\gamma_1} \sum_j \left[2\alpha_j^\dagger\rho_0\alpha_j - \{\alpha_j\alpha_j^\dagger, \rho_0\} \right]. \end{aligned} \tag{D.40}$$

D.4 Effective master equation

Combining results from eqs. (D.24) and (D.40) we find the form of the two-level effective master equation to second order is,

$$\begin{aligned}\dot{\rho} = & -i [\mathcal{H}_J, \rho] + \frac{\gamma_0}{2} \sum_j \left[2\hat{\sigma}_j \rho \hat{\sigma}_j^\dagger - \{\hat{\sigma}_j^\dagger \hat{\sigma}_j, \rho\} \right] \\ & + \frac{1}{\gamma_1} \sum_j \left[2\alpha_j^\dagger \rho \alpha_j - \{\alpha_j \alpha_j^\dagger, \rho\} \right],\end{aligned}\quad (\text{D.41})$$

where,

$$\mathcal{H}_J = -J \sum_j \left[\hat{\sigma}_j \hat{\sigma}_{j+1}^\dagger + \hat{\sigma}_j^\dagger \hat{\sigma}_{j+1} \right], \quad (\text{D.42})$$

$$\alpha_j = \sqrt{2}\Omega^* \hat{\sigma}_j - 2J\hat{\sigma}_j^\dagger \hat{\sigma}_j \left(\hat{\sigma}_{j+1}^\dagger + \hat{\sigma}_{j-1}^\dagger \right). \quad (\text{D.43})$$

We note that in this model the drive term now appears as an incoherent pump, and hopping transitions between upper level on neighbouring sites appear as a density activated nonlocal dissipation.

References

- [1] G. Vidal, “Efficient simulation of one-dimensional quantum many-body systems,” Physical Review Letters **93**, 040502 (2004).
- [2] U. Schollwöck, “The density-matrix renormalization group in the age of matrix product states,” Annals of Physics **326**, 96 (2011).
- [3] J. Cui, J. I. Cirac, and M. C. Bañuls, “Variational Matrix Product Operators for the Steady State of Dissipative Quantum Systems,” Physical Review Letters **114**, 220601 (2015).
- [4] E. Mascarenhas, H. Flayac, and V. Savona, “Matrix-product-operator approach to the nonequilibrium steady state of driven-dissipative quantum arrays,” Physical Review A **92**, 022116 (2015).
- [5] O. T. Brown, “mpostat-matlab,”, <https://github.com/otbrown/mpostat-matlab> (2016), Accessed: 2018-01-24.
- [6] MathWorks, “MATLAB Release 2017b,”, <http://uk.mathworks.com/> (2017), ©1994—2018 The MathWorks, Inc.
- [7] E. T. Owen, O. T. Brown, and M. J. Hartmann, “Dissipation-induced mobility and coherence in frustrated lattices,” Physical Review A **95**, 063851 (2017).
- [8] O. T. Brown and M. J. Hartmann, “Localization to delocalization crossover in a driven nonlinear cavity array,” New Journal of Physics **20**, 055004 (2018).

REFERENCES

- [9] G. Vidal, “Efficient Classical Simulation of Slightly Entangled Quantum Computations,” Physical Review Letters **91**, 147902 (2003).
- [10] S. R. White, “Density matrix formulation for quantum renormalization groups,” Physical Review Letters **69**, 2863 (1992).
- [11] S. R. White, “Density-matrix algorithms for quantum renormalization groups,” Physical Review B **48**, 10345 (1993).
- [12] I. Affleck, T. Kennedy, E. H. Lieb, and H. Tasaki, “Rigorous results on valence-bond ground states in antiferromagnets,” Physical Review Letters **59**, 799 (1987).
- [13] A. Fruchtmann, R. Gómez-Bombarelli, B. W. Lovett, and E. M. Gauger, “Photocell optimization using dark state protection,” Physical Review Letters **117**, 203603 (2016).
- [14] N. D. Mermin, “What’s Wrong with this Pillow?,” Physics Today **42**, 9 (1989).
- [15] S. M. Barnett, *Quantum Information* (Oxford University Press, 2009), (Section 2.2, pp.37–43).
- [16] M. A. Nielsen and I. L. Chuang, *Quantum Computation and Quantum Information* (Cambridge University Press, 2010), (Section 2.2.8, pp.93–96).
- [17] P. W. Anderson, “More Is Different,” Science **177**, 393 (1972).
- [18] J. Hubbard, “Electron Correlations in Narrow Energy Bands,” Proceedings of the Royal Society A: Mathematical, Physical and Engineering Sciences **276**, 238 (1963).
- [19] M. P. Fisher, P. B. Weichman, G. Grinstein, and D. S. Fisher, “Boson localization and the superfluid-insulator transition,” Physical Review B **40**, 546 (1989).

REFERENCES

- [20] A. Pérot and C. Fabry, “On the Application of Interference Phenomena to the Solution of Various Problems of Spectroscopy and Metrology,” *Astrophysical Journal* **9**, 87 (1899).
- [21] M. Fox, *Quantum Optics: An Introduction* (Oxford University Press, 2006), (Section 10.1, pp.194–197).
- [22] A. E. Siegman, *Lasers* (University Science Books, 1986), (Section 11.4, pp.428–432).
- [23] K. Yang, D. Oh, S. Lee, Q.-F. Yang, X. Yi, and K. Vahala, “Bridging ultra-high-Q devices and photonic circuits,” arXiv (2017), 1702.05076.
- [24] E. M. Purcell, “Spontaneous Emission Probabilities at Radio Frequencies,” *Proceedings of the American Physical Society* **69**, 681 (1946).
- [25] M. Fox, *Quantum Optics: An Introduction* (Oxford University Press, 2006), (Section 10.3.3, pp.202–204).
- [26] J. Gérard, B. Sermage, B. Gayral, B. Legrand, E. Costard, and V. Thierry-Mieg, “Enhanced Spontaneous Emission by Quantum Boxes in a Monolithic Optical Microcavity,” *Physical Review Letters* **81**, 1110 (1998).
- [27] M. Fox, *Quantum Optics: An Introduction* (Oxford University Press, 2006), (Section 9.3, pp.172–174).
- [28] M. J. Hartmann, F. G. S. L. Brandão, and M. B. Plenio, “Strongly interacting polaritons in coupled arrays of cavities,” *Nature Physics* **2**, 849 (2006).
- [29] M. J. Hartmann, F. G. S. L. Brandão, and M. B. Plenio, “Quantum many-body phenomena in coupled cavity arrays,” *Laser and Photonics Reviews* **2**, 527 (2008).
- [30] M. Kitagawa and Y. Yamamoto, “Number-phase minimum-uncertainty state with reduced number uncertainty in a Kerr nonlinear interferometer,” *Physical Review A* **34**, 3974 (1986).

REFERENCES

- [31] R. W. Boyd, *Nonlinear Optics* (Academic Press, 2008), 3rd ed., (Section 4.1, pp.207–211).
- [32] H. Schmidt and A. Imamoglu, “Giant Kerr nonlinearities obtained by electromagnetically induced transparency,” *Optics Letters* **21**, 1936 (1996).
- [33] U. Vool and M. Devoret, “Introduction to quantum electromagnetic circuits,” *International Journal of Circuit Theory and Applications* **45**, 897 (2017).
- [34] L. N. Cooper, “Bound electron pairs in a degenerate Fermi gas,” *Physical Review* **104**, 1189 (1956).
- [35] B. D. Josephson, “Possible new effects in superconductive tunnelling,” *Physics Letters* **1**, 251 (1962).
- [36] R. J. Schoelkopf and S. M. Girvin, “Wiring up quantum systems,” *Nature* **451**, 664 (2008).
- [37] P. W. Anderson and J. M. Rowell, “Probable observation of the Josephson superconducting tunneling effect,” *Physical Review Letters* **10**, 230 (1963).
- [38] G. Wendin, “Quantum information processing with superconducting circuits: A review,” *Reports on Progress in Physics* **80**, 106001 (2017).
- [39] J. Koch, T. M. Yu, J. Gambetta, A. A. Houck, D. I. Schuster, J. Majer, A. Blais, M. H. Devoret, S. M. Girvin, and R. J. Schoelkopf, “Charge-insensitive qubit design derived from the Cooper pair box,” *Physical Review A* **76**, 042319 (2007).
- [40] G. Wendin and V. S. Shumeiko, “Quantum bits with Josephson junctions,” *Low Temperature Physics* **33**, 724 (2007).
- [41] J. Majer, J. M. Chow, J. M. Gambetta, J. Koch, B. R. Johnson, J. A. Schreier, L. Frunzio, D. I. Schuster, A. A. Houck, A. Wallraff, et al.,

REFERENCES

- “Coupling superconducting qubits via a cavity bus,” *Nature* **449**, 443 (2007).
- [42] Y. Chen, C. Neill, P. Roushan, N. Leung, M. Fang, R. Barends, J. Kelly, B. Campbell, Z. Chen, B. Chiaro, et al., “Qubit architecture with high coherence and fast tunable coupling,” *Physical Review Letters* **113**, 220502 (2014).
 - [43] M. A. Nielsen and I. L. Chuang, *Quantum Computation and Quantum Information* (Cambridge University Press, 2010), (Section 2.4, pp.98–108).
 - [44] H.-P. Breuer and F. Petruccione, *The Theory of Open Quantum Systems* (Oxford University Press, 2002), (Section 3.2.2, pp.115–120).
 - [45] H. Carmichael, *An Open Systems Approach to Quantum Optics* (Springer-Verlag Berlin Heidelberg, 1993).
 - [46] G. Lindblad, “On the generators of quantum dynamical semigroups,” *Communications in Mathematical Physics* **48**, 119 (1976).
 - [47] V. Gorini, A. Kossakowski, and E. C. G. Sudarshan, “Completely positive dynamical semigroups of N-level systems,” *Journal of Mathematical Physics* **17**, 821 (1976).
 - [48] H.-P. Breuer and F. Petruccione, *The Theory of Open Quantum Systems* (Oxford University Press, 2002), (Section 3.1.1, pp.106–107).
 - [49] M. Hartmann (2016), *Open Quantum Systems* (SUPAQOS Lecture notes, Section 3.2, pp.14–16).
 - [50] H.-P. Breuer and F. Petruccione, *The Theory of Open Quantum Systems* (Oxford University Press, 2002), (Section 3.3.1, pp.126–131).
 - [51] H. D. Macedo and J. N. Oliveira, “Typing linear algebra: A biproduct-oriented approach,” *Science of Computer Programming* **78**, 2160 (2013).
 - [52] W. E. Roth, “On direct product matrices,” *Bulletin of the American Mathematical Society* **40**, 461 (1934).

REFERENCES

- [53] R. Orús, “A practical introduction to tensor networks: Matrix product states and projected entangled pair states,” *Annals of Physics* **349**, 117 (2014).
- [54] F. Verstraete, D. Porras, and J. I. Cirac, “Density Matrix Renormalization Group and Periodic Boundary Conditions: A Quantum Information Perspective,” *Physical Review Letters* **93**, 227205 (2004).
- [55] I. P. McCulloch, “From density-matrix renormalization group to matrix product states,” *Journal of Statistical Mechanics: Theory and Experiment* **2007**, P10014 (2007).
- [56] G. M. Crosswhite and D. Bacon, “Finite automata for caching in matrix product algorithms,” *Physical Review A* **78**, 012356 (2008).
- [57] F. Fröwis, V. Nebendahl, and W. Dür, “Tensor operators: Constructions and applications for long-range interaction systems,” *Physical Review A* **81**, 062337 (2010).
- [58] B. Pirvu, V. Murg, J. I. Cirac, and F. Verstraete, “Matrix product operator representations,” *New Journal of Physics* **12**, 25012 (2010).
- [59] G. B. Arfken and H. J. Weber, *Mathematical Methods for Physicists* (Elsevier Academic Press, 2005), 6th ed., (Section 17.8, pp.1072—1073).
- [60] S. Gasiorowicz, *Quantum Physics* (John Wiley & Sons, 2003), 3rd ed., (Section 14-4, pp.224—226).
- [61] M. Suzuki, “Generalized Trotter’s formula and systematic approximants of exponential operators and inner derivations with applications to many-body problems,” *Communications in Mathematical Physics* **51**, 183 (1976).
- [62] M. P. Zaletel, R. S. Mong, C. Karrasch, J. E. Moore, and F. Pollmann, “Time-evolving a matrix product state with long-ranged interactions,” *Physical Review B* **91**, 165112 (2015).

REFERENCES

- [63] J. Haegeman, C. Lubich, I. Oseledets, B. Vandereycken, and F. Verstraete, “Unifying time evolution and optimization with matrix product states,” *Physical Review B* **94**, 165116 (2016).
- [64] P. W. Anderson, “Absence of diffusion in certain random lattices,” *Physical Review* **109**, 1492 (1958).
- [65] P. A. Lee and T. V. Ramakrishnan, “Disordered electronic systems,” *Reviews of Modern Physics* **57**, 287 (1985).
- [66] M. Segev, Y. Silberberg, and D. N. Christodoulides, “Anderson localization of light,” *Nature Photonics* **7**, 197 (2013).
- [67] D. Guzmán-Silva, C. Mejía-Cortés, M. A. Bandres, M. C. Rechtsman, S. Weimann, S. Nolte, M. Segev, A. Szameit, and R. A. Vicencio, “Experimental observation of bulk and edge transport in photonic Lieb lattices,” *New Journal of Physics* **16**, 063061 (2014).
- [68] R. A. Vicencio, C. Cantillano, L. Morales-Inostroza, B. Real, C. Mejía-Cortés, S. Weimann, A. Szameit, and M. I. Molina, “Observation of Localized States in Lieb Photonic Lattices,” *Physical Review Letters* **114**, 245503 (2015).
- [69] S. Mukherjee, A. Spracklen, D. Choudhury, N. Goldman, P. Öhberg, E. Andersson, and R. R. Thomson, “Observation of a Localized Flat-Band State in a Photonic Lieb Lattice,” *Physical Review Letters* **114**, 245504 (2015).
- [70] S. Mukherjee and R. R. Thomson, “Observation of localized flat-band modes in a one-dimensional photonic rhombic lattice,” *Optics Letters* **40**, 5443 (2015).
- [71] T. Jacqmin, I. Carusotto, I. Sagnes, M. Abbarchi, D. D. Solnyshkov, G. Malpuech, E. Galopin, A. Lemaître, J. Bloch, and A. Amo, “Direct observation of Dirac cones and a flatband in a honeycomb lattice for polaritons,” *Physical Review Letters* **112**, 116402 (2014).

REFERENCES

- [72] F. Baboux, L. Ge, T. Jacqmin, M. Biondi, E. Galopin, A. Lemaître, L. Le Gratiet, I. Sagnes, S. Schmidt, H. E. Türeci, et al., “Bosonic condensation and disorder-induced localization in a flat band,” Physical Review Letters **116**, 066402 (2016).
- [73] S. Taie, H. Ozawa, T. Ichinose, T. Nishio, S. Nakajima, and Y. Takahashi, “Coherent driving and freezing of bosonic matter wave in an optical Lieb lattice,” Science Advances **1**, e1500854 (2015).
- [74] Y. Nakata, T. Okada, T. Nakanishi, and M. Kitano, “Observation of flat band for terahertz spoof plasmons in a metallic kagomé lattice,” Physical Review B **85**, 205128 (2012).
- [75] S. Kajiwara, Y. Urade, Y. Nakata, T. Nakanishi, and M. Kitano, “Observation of a nonradiative flat band for spoof surface plasmons in a metallic Lieb lattice,” Physical Review B **93**, 075126 (2016).
- [76] Z. H. Yang, Y. P. Wang, Z. Y. Xue, W. L. Yang, Y. Hu, J. H. Gao, and Y. Wu, “Circuit quantum electrodynamics simulator of flat band physics in a Lieb lattice,” Physical Review A **93** (2016).
- [77] G. H. Wannier, “The structure of electronic excitation levels in insulating crystals,” Physical Review **52**, 191 (1937).
- [78] P. Ehrenfest, “Bemerkung über die angenäherte Gültigkeit der klassischen Mechanik innerhalb der Quantenmechanik,” Zeitschrift für Physik **45**, 455 (1927).
- [79] H.-P. Breuer and F. Petruccione, *The Theory of Open Quantum Systems* (Oxford University Press, 2002), (Section 3.1.2, pp.108–110).
- [80] S. D. Huber and E. Altman, “Bose condensation in flat bands,” Physical Review B **82**, 184502 (2010).
- [81] M. Tovmasyan, E. P. Van Nieuwenburg, and S. D. Huber, “Geometry-induced pair condensation,” Physical Review B **88**, 220510 (2013).

REFERENCES

- [82] S. Takayoshi, H. Katsura, N. Watanabe, and H. Aoki, “Phase diagram and pair Tomonaga-Luttinger liquid in a Bose-Hubbard model with flat bands,” *Physical Review A* **88**, 063613 (2013).
- [83] L. G. Phillips, G. De Chiara, P. Öhberg, and M. Valiente, “Low-energy behavior of strongly interacting bosons on a flat-band lattice above the critical filling factor,” *Physical Review B* **91**, 054103 (2015).
- [84] P. Pudleiner and A. Mielke, “Interacting bosons in two-dimensional flat band systems,” *European Physical Journal B* **88**, 207 (2015).
- [85] P. D. Drummond and D. F. Walls, “Quantum theory of optical bistability. I. Nonlinear polarisability model,” *Journal of Physics A: Mathematical and General* **13**, 725 (1980).
- [86] A. Le Boité, G. Orso, and C. Ciuti, “Steady-state phases and tunneling-induced instabilities in the driven dissipative Bose-Hubbard model,” *Physical Review Letters* **110**, 233601 (2013).
- [87] S. Mukherjee, D. Mogilevtsev, G. Y. Slepyan, T. H. Doherty, R. R. Thomson, and N. Korolkova, “Dissipatively coupled waveguide networks for coherent diffusive photonics,” *Nature Communications* **8**, 1909 (2017).
- [88] P. Würfel, “The chemical potential of radiation,” *Journal of Physics C: Solid State Physics* **15**, 3967 (1982).
- [89] J. Keeling, F. M. Marchetti, M. H. Szymanska, and P. B. Littlewood, “Collective coherence in planar semiconductor microcavities,” *Semiconductor Science and Technology* **22**, 46 (2007).
- [90] P. R. Eastham and P. B. Littlewood, “Bose condensation of cavity polaritons beyond the linear regime: The thermal equilibrium of a model microcavity,” *Physical Review B* **64**, 235101 (2001).
- [91] I. Carusotto and C. Ciuti, “Quantum fluids of light,” *Reviews of Modern Physics* **85**, 299 (2013).

REFERENCES

- [92] J. Kasprzak, M. Richard, S. Kundermann, A. Baas, P. Jeambrun, J. M. J. Keeling, F. M. Marchetti, M. H. Szymańska, R. André, J. L. Staehli, et al., “Bose-Einstein condensation of exciton polaritons,” *Nature* **443**, 409 (2006).
- [93] J. Klaers, J. Schmitt, F. Vewinger, and M. Weitz, “Bose-Einstein condensation of photons in an optical microcavity,” *Nature* **468**, 545 (2010).
- [94] D. Vocke, T. Roger, F. Marino, E. M. Wright, I. Carusotto, M. Clerici, and D. Faccio, “Experimental characterization of nonlocal photon fluids,” *Optica* **2**, 484 (2015).
- [95] M. J. Hartmann, “Quantum simulation with interacting photons,” *Journal of Optics* **18**, 104005 (2016).
- [96] C. Noh and D. G. Angelakis, “Quantum simulations and many-body physics with light,” *Reports on Progress in Physics* **80**, 16401 (2017).
- [97] M. J. Hartmann and M. B. Plenio, “Strong photon nonlinearities and photonic mott insulators,” *Physical Review Letters* **99**, 103601 (2007).
- [98] D. Jaksch, C. Bruder, J. I. Cirac, C. W. Gardiner, and P. Zoller, “Cold bosonic atoms in optical lattices,” *Physical Review Letters* **81**, 3108 (1998).
- [99] M. Greiner, O. Mandel, T. Esslinger, T. W. Hänsch, and I. Bloch, “Quantum phase transition from a superfluid to a mott insulator in a gas of ultracold atoms,” *Nature* **415**, 39 (2002).
- [100] A. D. Greentree, C. Tahan, J. H. Cole, and L. C. L. Hollenberg, “Quantum phase transitions of light,” *Nature Physics* **2**, 856 (2006).
- [101] J. Koch and K. Le Hur, “Superfluid-Mott-insulator transition of light in the Jaynes-Cummings lattice,” *Physical Review A* **80**, 023811 (2009).
- [102] A.-W. de Leeuw, O. Onishchenko, R. A. Duine, and H. T. C. Stoof, “Effects of dissipation on the superfluid-Mott-insulator transition of photons,” *Physical Review A* **91**, 033609 (2015).

REFERENCES

- [103] D. Marcos, A. Tomadin, S. Diehl, and P. Rabl, “Photon condensation in circuit quantum electrodynamics by engineered dissipation,” *New Journal of Physics* **14**, 055005 (2012).
- [104] M. Hafezi, P. Adhikari, and J. M. Taylor, “Chemical potential for light by parametric coupling,” *Physical Review B* **92**, 174305 (2015).
- [105] R. Ma, C. Owens, A. Houck, D. I. Schuster, and J. Simon, “Autonomous stabilizer for incompressible photon fluids and solids,” *Physical Review A* **95**, 043811 (2017).
- [106] J. Lebreuilly, A. Biella, F. Storme, D. Rossini, R. Fazio, C. Ciuti, and I. Carusotto, “Stabilizing strongly correlated photon fluids with non-Markovian reservoirs,” *Physical Review A* **96**, 033828 (2017).
- [107] A. Biella, F. Storme, J. Lebreuilly, D. Rossini, R. Fazio, I. Carusotto, and C. Ciuti, “Phase diagram of incoherently driven strongly correlated photonic lattices,” *Physical Review A* **96**, 023839 (2017).
- [108] M. J. Hartmann, “Polariton crystallization in driven arrays of lossy nonlinear resonators,” *Physical Review Letters* **104**, 113601 (2010).
- [109] J. Jin, D. Rossini, R. Fazio, M. Leib, and M. J. Hartmann, “Photon solid phases in driven arrays of nonlinearly coupled cavities,” *Physical Review Letters* **110**, 163605 (2013).
- [110] M. Abbarchi, A. Amo, V. G. Sala, D. D. Solnyshkov, H. Flayac, L. Ferrier, I. Sagnes, E. Galopin, A. Lemaître, G. Malpuech, et al., “Macroscopic quantum self-trapping and Josephson oscillations of exciton polaritons,” *Nature Physics* **9**, 275 (2013).
- [111] J. Raftery, D. Sadri, S. Schmidt, H. E. Türeci, and A. A. Houck, “Observation of a dissipation-induced classical to quantum transition,” *Physical Review X* **4**, 031043 (2014).
- [112] E. Altman, L. M. Sieberer, L. Chen, S. Diehl, and J. Toner, “Two-dimensional superfluidity of exciton polaritons requires strong anisotropy,” *Physical Review X* **5**, 011017 (2015).

REFERENCES

- [113] G. Dagvadorj, J. M. Fellows, S. Matyjaśkiewicz, F. M. Marchetti, I. Carusotto, and M. H. Szymańska, “Nonequilibrium Phase Transition in a Two-Dimensional Driven Open Quantum System,” Physical Review X **5**, 041028 (2015).
- [114] J. Ruiz-Rivas, E. Del Valle, C. Gies, P. Gartner, and M. J. Hartmann, “Spontaneous collective coherence in driven dissipative cavity arrays,” Physical Review A **90**, 033808 (2014).
- [115] V. Savona, “Spontaneous symmetry breaking in a quadratically driven nonlinear photonic lattice,” Physical Review A **96**, 033826 (2017).
- [116] A. Bienfait, J. J. Pla, Y. Kubo, X. Zhou, M. Stern, C. C. Lo, C. D. Weis, T. Schenkel, D. Vion, D. Esteve, et al., “Controlling spin relaxation with a cavity,” Nature **531**, 74 (2016).
- [117] D. Rossini and R. Fazio, “Mott-insulating and glassy phases of polaritons in 1D arrays of coupled cavities,” Physical Review Letters **99**, 186401 (2007).
- [118] N. F. Mott and R. Peierls, “Discussion of the paper by de Boer and Verwey,” Proceedings of the Physical Society **49**, 72 (1937).
- [119] J. H. De Boer and E. J. W. Verwey, “Semi-conductors with partially and with completely filled 3 d-lattice bands,” Proc. Phys. Soc **49**, 59 (1937).
- [120] I. Bloch, J. Dalibard, and W. Zwerger, “Many-body physics with ultracold gases,” Reviews of Modern Physics **80**, 885 (2008).
- [121] K. E. Dorfman, D. V. Voronine, S. Mukamel, and M. O. Scully, “Photosynthetic reaction center as a quantum heat engine,” Proceedings of the National Academy of Sciences of the United States of America **110**, 2746 (2013).
- [122] F. Beaudoin, J. M. Gambetta, and A. Blais, “Dissipation and ultrastrong coupling in circuit QED,” Physical Review A **84**, 043832 (2011).

REFERENCES

- [123] S. Al-Assam, S. R. Clark, D. Jaksch, and T. D. Team, “Tensor network theory library, beta version 1.2.0,” <http://www.tensornetworktheory.org/> (2016).
- [124] S. Al-Assam, S. R. Clark, and D. Jaksch, “The tensor network theory library,” *Journal of Statistical Mechanics: Theory and Experiment* **2017**, 093102 (2017).
- [125] A. Stathopoulos and J. R. McCombs, “PRIMME: PReconditioned Iterative MultiMethod Eigensolver - Methods and Software Description,” *ACM Transactions on Mathematical Software* **37**, 21 (2010).
- [126] L. Wu, E. Romero, and A. Stathopoulos, “PRIMME_SVDS: A High-Performance Preconditioned SVD Solver for Accurate Large-Scale Computations,” *SIAM Journal on Scientific Computing* **39**, S248 (2017).
- [127] J. J. García-Ripoll, S. Dürr, N. Syassen, D. M. Bauer, M. Lettner, G. Rempe, and J. I. Cirac, “Dissipation-induced hard-core boson gas in an optical lattice,” *New Journal of Physics* **11**, 013053 (2009).